

DESIGN AND APPLICATIONS OF AN IMPROVED CAPILLARY
ELECTROPHORESIS-ELECTROSPRAY IONIZATION-MASS
SPECTROMETRY INTERFACE

by

Xuefei Zhong

B.Sc., Peking University, 2006

A THESIS SUBMITTED IN PARTIAL FULFILMENT
OF THE REQUIREMENTS FOR THE DEGREE

DOCTOR OF PHILOSOPHY

in

The Faculty of Graduate Studies

(Chemistry)

THE UNIVERSITY OF BRITISH COLUMBIA

(Vancouver)

August 2012

© Xuefei Zhong, 2012

ABSTRACT

A novel capillary electrophoresis – electrospray ionization – mass spectrometry (CE-ESI-MS) interface has been developed to provide a robust, user-friendly and more sensitive alternative interface strategy. The new interface uses a flow-through microvial design and a bevelled sprayer tip geometry. The capillary column terminus is surrounded by a tapered stainless steel hollow needle, and the interior of the needle tip acts as the CE outlet while its exterior tip surface provides the electrode surface for electrospray ionization. A chemical modifier is supplied to the open-ended microvial at the CE outlet through a standard tee union, serving the purpose of maintaining electrical continuity, and supporting a stable electrospray. The chemical modifier supplied through the flow-through microvial can also be used to improve the compatibility of CE effluent with electrospray ionization. The bevelled sprayer tip design extends the optimal flow rate range for ESI and requires lower flow rate compared to conventional blunt tips or symmetrically tapered sprayer tips. This feature leads to reduced dilution effect caused by the chemical modifier solution and improves the detection sensitivity.

The mass transport process in the flow-through microvial was investigated by numerical simulation and experimental comparison of on-column and post-column detection. Both approaches demonstrated that the laminar flow profile inside the microvial does not significantly distort the peak shape and the major characteristics of the eluted peaks are maintained when the modifier flow rate is properly adjusted.

The chemical modifier solution in the flow-through microvial enables CE separation without electroosmotic flow (EOF). One useful application of this feature is interfacing online capillary isoelectric focusing (cIEF) with ESI-MS detection, which could be a

potential replacement in many applications of two-dimensional gel electrophoresis (2DE) for protein analysis in the future.

The final part of the thesis elucidates the electric field distribution in the ESI source with an atmospheric ion lens, which could be incorporated in the CE-ESI-MS interface to improve the ionization and sampling efficiency in the future.

PREFACE

The majority of the research included in this dissertation was conducted by the author, Xuefei Zhong. The contributions of other researchers and collaborations are detailed below.

Contributions from other researchers:

- Chapter 2: The images of electrospray plume were captured by Jane Maxwell. The separation method for angiotensin I and II was also optimized by Jane Maxwell.
- Chapter 4: The calibration of basic drugs on triple quadrupole mass spectrometer was performed collaboratively with John Hudson in the labs of Beckman Coulter, Canada. The samples were provided by John Hudson.
- Chapter 5: The cIEF separation with NCHO coated capillary shown in this chapter was performed collaboratively with Jane Maxwell. She also contributed to writing of this part of experiment results. The cIEF materials, including proteins and carrier ampholytes and coated capillaries were provided by Beckman Coulter (Brea, CA).
- Chapter 6: The data in Figure 6.5 was collected by Rong Yi.

Publications arising from work presented in the dissertation:

E. Jane Maxwell, Xuefei Zhong, Hong Zhang, Nikita van Zeijl, and David D.Y. Chen. Decoupling capillary electrophoresis and electrospray ionization for a more robust interface with mass spectrometry. *Electrophoresis* (2010) 31, 1130-1137.

Material from this article is included in Chapter 2. Reused with permission. Copyright (2010) John Wiley and Sons.

Xuefei Zhong, E. Jane Maxwell and David D. Y. Chen. Mass transport in a micro flow-through vial of a junction-at-the-tip capillary electrophoresis-mass spectrometry interface. *Analytical Chemistry* (2011) 83, 4916-4923.

Material from this article is included in Chapter 3. Reused with permission. Copyright (2011) American Chemical Society.

Xuefei Zhong, E. Jane Maxwell, Chitra Ratnayake, Scott Mack and David D. Y. Chen. Flow-Through microvial facilitating interface of capillary isoelectric focusing and electrospray ionization mass spectrometry. *Analytical Chemistry* (2011), 83, 8748-8755.

Material from this article is included in Chapter 5. Reused with permission. Copyright (2011) American Chemical Society.

Xuefei Zhong, Rong Yi, Alison E. Holliday and David D.Y. Chen. Field distribution in an electrospray ionization source determined by finite element method. *Rapid Communications in Mass Spectrometry* (2009), 23, 689-697

Material from this article is included in Chapter 6. Reused with permission. Copyright (2009) John Wiley and Sons.

TABLE OF CONTENTS

Abstract.....	ii
Preface.....	iv
Table of contents	vi
List of tables.....	ix
List of figures.....	x
List of terms and abbreviation.....	xii
Acknowledgements	xiii
Chapter 1: Introduction to capillary electrophoresis and mass spectrometry interfacing.....	1
1.1 CAPILLARY ELECTROPHORESIS – SEPARATION OF CHARGED SPECIES IN LIQUID PHASE.....	2
1.1.1 Capillary zone electrophoresis.....	2
1.1.2 Capillary isoelectric focusing.....	7
1.2 MASS SPECTROMETRY – SEPARATION OF CHARGED SPECIES IN GAS PHASE.....	11
1.2.1 Quadrupole mass analyzer.....	11
1.2.2 3D ion trap mass analyzer.....	14
1.2.3 Time of flight mass analyzer.....	18
1.3 ELECTROSPRAY IONIZATION – GENERATING GASEOUS IONS FROM A LIQUID SOLUTION.....	20
1.4 INTERFACING OF CE AND MS	23
1.4.1 General concerns on CE-ESI-MS interfaces.....	24
1.4.2 Sheath liquid CE–ESI–MS interfaces.....	25
1.4.3 Sheathless CE-ESI-MS interfaces.....	27
1.5 RESEARCH OBJECTIVES	29
1.5.1 Design and characterization of a novel CE-ESI-MS coupling strategy.....	29
1.5.2 Applications of the interface in different capillary electrophoresis modes	29
1.5.3 Improvements on ESI sensitivity in reduced flow region.....	30
Chapter 2: Decoupling CE and ESI for a more robust interface with mass spectrometry.....	31
2.1 INTRODUCTION	32

2.2	MATERIALS AND METHODS.....	34
2.2.1	Chemicals and materials	34
2.2.2	Instrumentation	35
2.2.3	Separation methods.....	37
2.2.4	Simulation.....	38
2.3	RESULTS AND DISCUSSION.....	39
2.3.1	Design rationale	39
2.3.2	Sprayer tip geometry.....	40
2.3.3	Comparison of the flow-through microvial interface and sheath flow interface.....	44
2.3.4	CE-MS separation without EOF or with reversed EOF.....	48
2.3.5	CE-UV-ESI-MS analysis of catecholamines and HPLC peptide calibration standards	52
2.3.6	Automated CE-ESI-MS system	56
2.4	CONCLUSIONS.....	57
	Chapter 3: Mass transport in the flow-through microvial of a capillary electrophoresis-mass spectrometry interface	59
3.1	INTRODUCTION	60
3.2	THEORY	62
3.3	MODELING	63
3.3.1	Geometry.....	64
3.3.2	Physical conditions	65
3.4	MATERIALS AND METHODS.....	67
3.4.1	Chemicals and materials	67
3.4.2	Instrumentation	68
3.5	RESULTS AND DISSCUSSION.....	69
3.5.1	Simulation of steady-state flow patterns in the flow-through microvial	69
3.5.2	Simulation of band broadening for a transient analyte peak.....	72
3.5.3	Experimental verification of modeling results.....	74
3.6	CONCLUSIONS.....	79
	Chapter 4: Basic compounds of drugs of abuse analyzed by capillary zone electrophoresis – electrospray – mass spectrometry.....	80
4.1	INTRODUCTION	81
4.2	MATERIALS AND METHODS.....	83
4.2.1	Chemicals and materials	83

4.2.2	Instrument and method	83
4.3	RESULTS AND DISCUSSION	87
4.4	CONCLUDING REMARKS	92
	Chapter 5: Flow-through microvial facilitates interface of capillary isoelectric focusing with electrospray ionization mass spectrometry	93
5.1	INTRODUCTION	94
5.2	MATERIALS AND METHODS	98
5.2.1	Chemicals and materials	98
5.2.2	Capillary isoelectric focusing	99
5.2.3	Electrospray ionization-mass spectrometry	102
5.3	RESULTS AND DISCUSSION	102
5.3.1	Suitability of the interface for cIEF-MS interfacing	102
5.3.2	cIEF in bare fused silica capillaries using a partial filling technique	104
5.3.3	cIEF with electroosmotic and electrophoretic mobilization	106
5.3.4	Optimization of experimental conditions and reproducibility	111
5.3.5	cIEF-MS in a neutral coated capillary with electrophoretic mobilization	116
5.4	CONCLUSIONS	118
	Chapter 6: Field distribution in an electrospray ionization source determined by finite element method	120
6.1	INTRODUCTION	121
6.2	THEORY OF ELECTRIC FIELD CALCULATION	122
6.3	MATERIALS AND METHODS	127
6.3.1	Chemicals	127
6.3.2	Instrumentation	128
6.4	MODELING	130
6.5	RESULTS AND DISCUSSION	131
6.6	CONCLUSIONS	142
	Chapter 7: Concluding remarks and future work	144
7.1	CONCLUDING REMARKS	145
7.2	FUTURE WORK	147
7.2.1	Further optimization on cIEF-ESI-MS strategies	147
7.2.2	Incorporation of atmospheric ion lens into the CE-ESI-MS interface	148
	Bibliography	149

LIST OF TABLES

Table 2.1: Amino acids calibration with sheath flow interface and the built-in-house interface.....	47
Table 2.2: Calibration curve linearity and LOD of the catecholamines.	54
Table 3.1: Comparison of peak widths (in seconds) of UV detected peaks, COMSOL simulated peaks and MS detected peaks of tryptophan, DOPA and epinephrine.	77
Table 4.1: MRM detection conditions, linear quantitation range and correlation coefficient of drug mixture I.	92
Table 5.1: Migration times of RNase A (pI 9.4) and CCK peptide (pI 3.6) of repeated cIEF-MS runs under different conditions.	113
Table 6.1: Field strength at the sprayer tip for onset of signal under various conditions.	140
Table 6.2: Field strength at the sprayer tip for optimum signal under various conditions.	140

LIST OF FIGURES

Figure 1.1: Schematic diagram of a capillary electrophoresis system with optical detection.	2
Figure 1.2: (A) Structure of the electrical double layer. (B) Potential profile from the capillary surface to the bulk solution.	5
Figure 1.3: Quadrupole with hyperbolic rods and applied potential.	12
Figure 1.4: The First stability region of quadrupole with an operation line.	13
Figure 1.5: (A) Photograph of an ion trap cut in half along the axis of cylindrical symmetry. (B) Schematic diagram of the cross section of an ion trap showing the asymptotes.	15
Figure 1.6: First stability region of 3D ion trap.	17
Figure 1.7: Schematic illustration of a TOF mass analyzer with reflectron.	19
Figure 1.8: Schematic of the electrospray ionization process.	21
Figure 1.9: Common sheath-liquid interface arrangements.	26
Figure 1.10: Methods for creating electrical contact in sheathless interfaces.	28
Figure 2.1: CE-ESI-MS apparatus (A) and the interface assembly (B).	40
Figure 2.2: Simulated electric field lines for the blunt tapered (A) and beveled (B) stainless steel emitters.	43
Figure 2.3: Photograph of an electrospray plume from a beveled stainless steel emitter.	44
Figure 2.4: Extracted ion electropherograms for a mixture of 18 amino acids.	45
Figure 2.5: Total ion electropherogram (A) and mass spectra (B) of three basic proteins separated under positive polarity with a neutral-coated capillary.	49
Figure 2.6: Total ion electropherogram and mass spectra of continuous CE infusion of (A) SDS and (B) 1, 2, 4-Benzenetricarboxylic acid.	51
Figure 2.7: Chemical structures of the catecholamines and their analog tyrosine.	53
Figure 2.8: CE-UV-ESI-MS analysis of catecholamines and tyrosine standard mixture.	53
Figure 2.9: CE-UV-ESI-MS of HPLC peptide standard mixture.	55
Figure 2.10: Total ion electropherograms of 15 successive programmed sequence runs of Angiotensin I&II.	57
Figure 3.1: (A) Schematic of the flow-through microvial of a junction-at-the-tip capillary electrophoresis mass spectrometry interface. (B) Geometry of the flow-through microvial established in COMSOL where the electro osmotic flow mixes with the modifier solution.	62
Figure 3.2: Illustration of the physical modeling process and boundary conditions.	67
Figure 3.3: (A-C) Simulated velocity field and (D-F) concentration distribution when analyte is constantly infused into the microvial under different conditions.	71
Figure 3.4: Simulation of peaks eluted from the microvial if a transient Gaussian profile peak (peak height 1 mM, peak centre 12 s, standard deviation 4 s) is injected into the microvial.	73
Figure 3.5: Simulated time progress of analyte concentration distribution in the microvial.	74
Figure 3.6: Comparison of UV detected peaks, COMSOL simulated peaks, and MS detected peaks of tryptophan, DOPA, and epinephrine under different modifier flow rate.	76
Figure 4.1: Chemical structures of drug mixture I.	85

Figure 4.2: Chemical structures of drug mixture II.	86
Figure 4.3: Summed extracted ion electropherograms of separation of drug mixture I under different conditions.	88
Figure 4.4: Extracted ion electropherograms of separation of drug mixture I.	89
Figure 4.5: Summed extracted ion electropherograms of separation of drug mixture II under different conditions.	90
Figure 4.6: Extracted ion electropherograms of separation of drug mixture II.	91
Figure 5.1: Injection techniques for automated cIEF-MS.	101
Figure 5.2: Schematic illustration of cIEF-MS process with the bare fused silica capillary.	106
Figure 5.3: Separation of protein mixtures in bare fused silica capillary with pressure (A), and without pressure (B-D) applied at the capillary inlet.	109
Figure 5.4: Total ion electropherogram of separation of protein mixture in bare fused silica capillary with different ratio of catholyte/sample/anolyte injection length.	112
Figure 5.5: Current profile of replicates of cIEF-MS runs with bare fused silica capillary under different conditions.	114
Figure 5.6: Total ion electropherogram for a protein mixture separated by cIEF with electrophoretic mobilization in a neutral coated capillary.	117
Figure 6.1: Schematic diagram of the ESI source with the atmospheric pressure ion lens.	129
Figure 6.2: COMSOL Multiphysics configurations of the ESI source with ion lens.	131
Figure 6.3: Voltage distribution (A) and magnitude of electric field strength (B) from the center of the sprayer tip to the center of curtain plate at different ion lens voltage.	133
Figure 6.4: Simulation results of model A (left, sprayer 5000V, no ion lens) and model B (right, sprayer 5000 V, ion lens 3000 V).	136
Figure 6.5: Signal intensity as a function of sprayer voltage at different ion lens voltages.	138
Figure 6.6: Equipotential surfaces for various voltage combinations of the sprayer and ion lens that result in maximum signal intensity.	141
Figure 6.7: Field line distributions for various voltage combinations of the sprayer and ion lens.	142

LIST OF TERMS AND ABBREVIATION

amu	atomic mass unit
APCI	atmospheric pressure chemical ionization
APPI	atmospheric pressure photoionization
BGE	background electrolyte
CA II	carbonic anhydrase II
CD	cyclodextrin
CE	capillary electrophoresis
cIEF	capillary isoelectric focusing
Cyt C	cytochrome C
DC	direct current
2DE	two-dimensional gel electrophoresis
EOF	electroosmotic flow
ESI	electrospray ionization
HPLC	high performance liquid chromatography
ICP	inductively coupled plasma
ID	inner diameter
LC	liquid chromatography
LOD	limit of detection
Lys	lysozyme
MALDI	matrix-assisted laser desorption ionization
MRM	multiple reaction monitoring
MS	mass spectrometry
Myo	myoglobin
OD	outer diameter
PDA	photodiode array
PEEK	polyethyl ether ketone
PEI	polyethyleneimine
ppb	parts per billion
PVA	polyvinyl alcohol
RF	radio frequency
RNase A	ribonuclease A
SRN	signal-to-noise ratio
s.s.	stainless steel
TIE	total ion electropherogram
TOF	time of flight
UV	ultra-violet
β -lac	β -lactoglobulin

ACKNOWLEDGEMENTS

It is difficult to overstate my gratitude to my Ph.D. supervisor, Dr. David Chen. I am indebted to him for the continuous support and guidance of my Ph.D. study and research, for his patient attitude, persistent encouragement, thoughtful approach, and immense knowledge. I would have been lost without him. His great personality has also influenced me deeply beyond research – the courage to face difficulties, the optimistic attitude towards life, and the open mind to listen to different opinions.

My sincere thanks also go to my fellow group mates, who have accompanied me throughout my graduate school years. I would like to particularly express my gratitude to Dr. Jane Maxwell, who collaborated with me in the CE-MS project during the past several years. She shared a lot of ideas with me and helped revise the manuscripts. This thesis could not be completed without her contribution. Thank Dr. Allison Holiday for teaching me the COMSOL software and Dr. Hong Zhang for initiating the CE-MS project with two high voltage power supplies. Sharon, Joe, Koen, Chang, Sherry, Roxana, Cai, Alexis, Laiel, Akram, thank you all for creating a friendly and supportive community in the lab. Chang, thank you for always giving me helpful advice; Sherry, thank you for being a wonderful friend to me during the last two years and carrying on the CE-MS project.

This research would not have been possible without financial support from Beckman Coulter. I particularly would like to acknowledge Chitra Ratnayake, John Hudson and Scott Mack for their dedication.

Lastly, and most importantly, I appreciate my entire extended family for giving me wholehearted support from the other side of the planet. I am grateful for my dearest grandfather has lived his life to witness my growth.

Chapter 1: Introduction to capillary electrophoresis and mass spectrometry interfacing

1.1 CAPILLARY ELECTROPHORESIS – SEPARATION OF CHARGED SPECIES IN LIQUID PHASE

1.1.1 Capillary zone electrophoresis

First demonstrated by Jorgenson and Lukacs in 1981¹, capillary electrophoresis (CE) has become a widely used separation technique for ionic substances in the liquid phase, especially biomolecules. This technique involves applying a very large electric potential across a narrow-bore fused silica capillary, and the ionic species migrate in a conductive medium under the electric field in the capillary. Figure 1.1 shows a typical CE apparatus using online optical detection. Conventionally, a standard setup involves a high voltage power supply, a polyimide-coated capillary with inner diameter (ID) smaller than 200 μm , two buffer vials that host both the capillary ends and the electrodes connected to the power supply, and a detector².

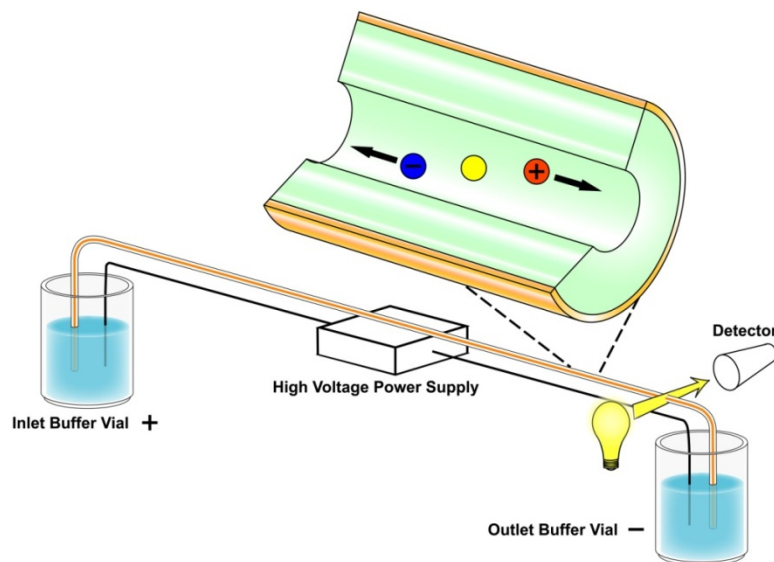


Figure 1.1: Schematic diagram of a capillary electrophoresis system with optical detection.

Capillary zone electrophoresis is the most popular mode of application, which separates charged analytes based on their charge-to-size ratio². To perform this experiment, the capillary is first filled with background electrolyte (BGE), and then a small plug of sample is introduced into the capillary by pressure or electrokinetic pumping. After that, both ends of the capillary and two electrodes are immersed in the BGE, and a high direct current (DC) voltage up to 30 kV is applied across the capillary. Upon application of high voltage, the ions in the solution experience an electrostatic force \vec{F}_e (1-1) and start to accelerate. However, the drag force from the solution \vec{F}_D (1-2) that is proportional to velocity soon balances the electrostatic force $q\vec{E}$ (1-3), and the ions travel at a constant electrophoretic velocity \vec{v}_{ep} (1-4) determined by the electric field in the capillary \vec{E} , the hydrated radius of the ion R , net charge carried by the ion q , and the viscosity of the medium η .

$$\vec{F}_e = q\vec{E} \quad (1-1)$$

$$\vec{F}_D = 6\pi\eta R\vec{v} \quad (1-2)$$

$$q\vec{E} = 6\pi\eta R\vec{v} \quad (1-3)$$

$$\vec{v}_{ep} = \frac{q\vec{E}}{6\pi\eta R} \quad (1-4)$$

To describe the electromigration behaviour independent of electric field, \vec{E} , the electrophoretic mobility, μ_{ep} , is defined as

$$\bar{\mu}_{ep} \equiv \frac{\vec{v}_{ep}}{\vec{E}} = \frac{q}{6\pi\eta R} \quad (1-5)$$

From Eq (1-5), it is clear that in free solution, electrophoretic mobility only depends on the charge-to-size ratio of the ionic species, which is the fundamental variable that differentiates the analytes in the separation.

In addition to electrophoretic mobility, electroosmotic flow (EOF) is another transport mechanism that can mobilize the analyte towards the capillary outlet. EOF is a type of bulk flow caused by the movement of the diffuse layer near the charged inner surface wall. Figure 1.2A depicts the structure of the electrical double layer, diffuse layer and bulk solution adjacent to a bare fused silica capillary surface. When the pH of buffer is greater than 3, the capillary surface is negatively-charged due to the dissociation of the silanol groups. These negatively-charged silanol groups attract counter ions in the solution to the wall. The counterions are almost bound to the surface due to the strong electrostatic force. Thus, a fixed layer, also called Stern layer, is formed on the capillary surface. The amount of positive charges in the electrical double layer are not enough to neutralize all the negative charges on the capillary surface, so that a second layer of cation-rich solution is formed next to the fixed layer. This second layer, which is called the diffuse layer, contains more positive ions than negative ions. The electrical potential decreases linearly within the fixed layer, exponentially in the diffuse layer, and approaches zero in the bulk solution (Figure 1.2B). The potential at the interface of the fixed layer and the diffuse layer is called zeta potential (ζ). When voltage is applied across the length of the capillary, the diffuse layer moves towards the cathode as the ions in this layer are only loosely bound to the capillary surface. Because the ID of the capillary is very small, the bulk solution is dragged by the diffuse layer to be moved at the same velocity. The

magnitude of electroosmotic flow is determined by Eq(1-6), where ε is the dielectric constant of the fluid, ζ is the zeta potential, and η is the viscosity of the fluid.

$$\bar{\mu}_{eo} = \frac{\bar{v}_{eo}}{E} = \frac{\varepsilon\zeta}{4\pi\eta} \quad (1-6)$$

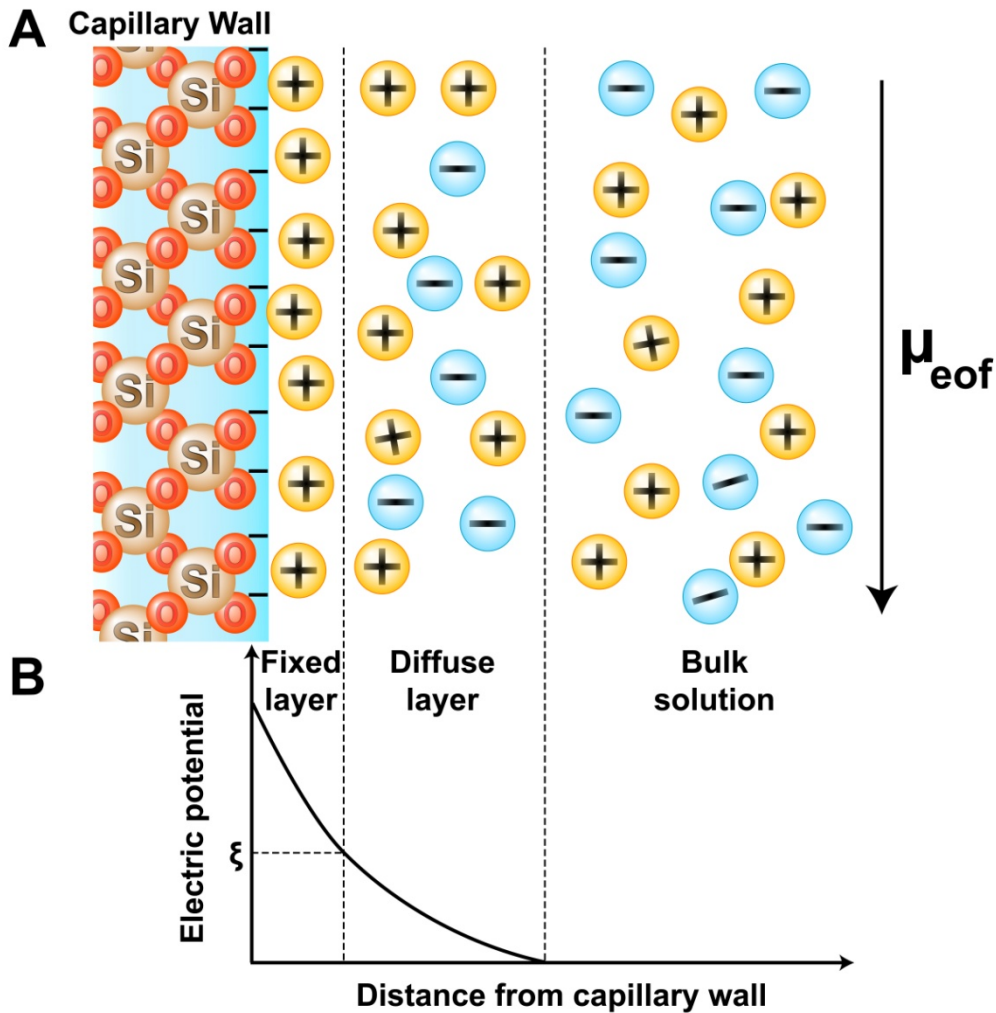


Figure 1.2: (A) Structure of the electrical double layer. (B) Potential profile from the capillary surface to the bulk solution.

Zeta potential is proportional to the charge density on the capillary wall, which is affected by the buffer pH. EOF mobility is the strongest above pH 10, because the silanol groups are fully dissociated; below pH 3, EOF is insignificant since the degree of silanol

deprotonation is minimal. The ionic strength of the buffer also has an impact on the zeta potential: as buffers with high ionic strength have more counter ions to be attracted to the capillary wall in the electrical double layer, the larger potential drop within the electrical double layer results in decreased zeta potential. Therefore, increasing the ionic strength decreases the magnitude of electroosmotic flow.

The apparent electrophoretic mobility is the sum of electroosmotic mobility and electrophoretic mobility as shown in Eq (1-7).

$$\bar{\mu}_{app} = \bar{\mu}_{ep} + \bar{\mu}_{eo} \quad (1-7)$$

The most appreciated feature of CE is its exceptional resolving power and separation efficiency. Assuming that the peak width in CE separations is mainly governed by diffusion, the resolution of two adjacent peaks can be approximated by Eq (1-8)^{1,3}, where $\Delta\mu_{ep}$ is the difference of electrophoretic mobility of two analytes, $\bar{\mu}_{ep}$ is the average electrophoretic mobility, μ_{eo} is the electroosmotic mobility, V is the voltage applied across the capillary, and D is the average diffusion constants of the two analytes. From this equation, it can be concluded that maximizing the difference of electrophoretic mobility and increasing the voltage applied are the major means to improve the resolving power of CE.

$$Re = \frac{\Delta\mu_{ep} \sqrt{V}}{4\sqrt{2D(\bar{\mu}_{ep} + \mu_{eo})}} \quad (1-8)$$

For on-column detection in CE, the band broadening is mainly influenced by factors including injection length of the sample, longitudinal diffusion, Joule heating, wall adsorption, and width of the detection window⁴⁻⁶. The total variance σ^2 of the peak is

expressed as the sum of the variance caused by each individual factor (1-9)⁷. Although the variance caused by the injection length and longitudinal diffusion are well understood and easy to calculate^{4,6}, research on the band broadening induced by other factors needs more complicated mathematical modeling and experimental design.

$$\sigma^2_{\text{total}} = \sigma^2_{\text{injection}} + \sigma^2_{\text{diffusion}} + \sigma^2_{\text{Joule heating}} + \sigma^2_{\text{adsorption}} + \sigma^2_{\text{other}} \quad (1-9)$$

1.1.2 Capillary isoelectric focusing

Capillary isoelectric focusing (cIEF) is another popular mode of application for CE. Twenty years after the development of polyacrylamide gel-based IEF (gIEF) was developed in the 1960s⁸, Hjerten and coworkers adapted this technique to high performance capillary electrophoresis⁹. As the separation is based on the difference among isoelectric points of amphoteric compounds, cIEF can have many applications in both pharmaceutical industry and academic research, including purity analysis, post translational modification, and charge heterogeneity of proteins and peptides¹⁰.

Generally, cIEF involves three steps: sample loading, focusing, and mobilization, although the mobilization step is unnecessary if whole column imaging is used for detection. The capillary surface is usually modified with a neutral coating to reduce protein-wall interactions and ampholyte-wall interactions. The whole capillary column is first filled with a mixture of analyte proteins and carrier ampholytes which are dissolved in aqueous gel solution. An acidic solution with a pH value lower than the ampholytes pI range (anolyte) is placed at the anodic side of the capillary, while a basic solution with a pH value higher than the ampholytes pI range (catholyte) is placed at the cathodic side of the capillary. Upon application of high voltage across the capillary, the protons and hydroxide ions enter the capillary from the anolyte and catholyte reservoir respectively,

and change the pH along the capillary. Meanwhile, the positively-charged ampholytes and proteins, which possess pI values higher than the local pH, migrate towards the cathode; the negatively-charged ampholytes and proteins, which possess pI values lower than the local pH, move towards the anode. Eventually, a pH gradient is established from the anode to the cathode along the capillary by the carrier ampholytes and each amphoteric species is focused to a narrow band where the local pH matches its pI value. At this time, the net charges on the amphoteric compounds are zero, and the current decreases to almost zero.

There are two common methods to mobilize the focused pH gradient through a single point detector. The easier way is to apply pressure at the inlet while keeping the high potential across the capillary. It preserves the formed pH gradient, however, the pressure induces laminar flow which broadens the peak width and often results in reduced resolution. An alternative means of mobilization is called chemical mobilization or electrophoretic mobilization. By replacing the catholyte solution with another solution that contains anions other than hydroxide ions, the newly introduced anions can disturb the local charge balance and acid-base equilibrium. Subsequently, the amphoteric species gain positive charges and migrate towards the cathode. Chemical mobilization can also be achieved by changing the anolyte solution to another solution that contains cations other than protons. Although laminar flow is avoided in chemical mobilization, the electrophoretic migration might alter the relative spacing of the separated bands formed in the focusing stage, as the analyte velocity depends on charge-to-size ratio during the mobilization stage.

Harry Rilbe derived equations to describe the resolving power of isoelectric focusing by simplifying the physical phenomena with a few assumptions in the early stage of IEF development¹¹. His theory can still be applied in cIEF if we do not take into account the band broadening caused by the mobilization. The mobility of amphoteric compounds changes drastically around the pI value. After the amphoteric compounds are completely focused, if a protein or ampholytes molecule diffuses too far away from the focused zone, it gains charge again and the electrostatic force will pull it back. At this stage, the mass transport equation describing the concentration distribution of a specific protein along the capillary (1-10) can be simplified to Eq (1-11), which reflects the balance of electrostatic force and molecular diffusion.

$$\frac{\partial c}{\partial t} = -\bar{v} \bullet \frac{\partial c}{\partial x} + D \frac{\partial^2 c}{\partial x^2} \quad (1-10)$$

$$\mu \bar{E} \bullet \frac{dc}{dx} = D \frac{d^2c}{dx^2} \quad (1-11)$$

Here, c is the concentration of a certain species, t is time, x is the position along the column, \bar{v} is the velocity of convective flow, D is the diffusion constant, \bar{E} is the electric field, and μ is the apparent electrophoretic mobility.

Assuming that the protein's mobility is proportional to the distance deviated from the centre of the focused band, where the pH equals to its pI value, solution to the equation above (1-12) gives a Gaussian profile of the concentration in Eq (1-12) below.

$$c(x) = \frac{m}{A} \sqrt{\frac{pE}{2\pi D}} e^{-\frac{pEx^2}{2D}} \quad (1-12)$$

Here, x is the distance deviated from the centre of the focused band, and the concentration of the protein reaches a maximum when $x = 0$. A is the cross sectional area

of the capillary, m is the total mass of this protein in the zone, and p is the slope of mobility near $x = 0$. If resolving two adjacent peaks requires that the distance of the band centers is at least three times of the standard deviation of the peak, then the minimal pI difference that can be differentiated is expressed by Eq (1-13).

$$\begin{aligned} (\Delta pI)_{\min} &= \Delta x \frac{dpH}{dx} = 3\sigma \frac{dpH}{dx} \\ &= 3 \sqrt{\frac{D (dpH / dx)}{E(-d\mu / dpH)_{pI}}} \end{aligned} \quad (1-13)$$

In an ideal case when the pH gradient in the whole capillary is linear, dpH/dx can be simplified as $(\Delta pH)_{\text{total}}/L$, where $(\Delta pH)_{\text{total}}$ is the entire pI range of the ampholytes used. Therefore, Eq (1-13) can be further simplified as (1-14) below¹².

$$(\Delta pI)_{\min} = 3 \sqrt{\frac{D \cdot (\Delta pH)_{\text{total}}}{V \cdot (-d\mu / dpH)_{pI}}} \quad (1-14)$$

Except for $(-d\mu/dpH)_{pI}$, which is the intrinsic property of the protein analyte, other factors determining the resolving power of the IEF can be optimized experimentally. Better resolution can be achieved by applying higher voltage, decreasing the diffusion coefficient using inert neutral polymer solutions as the focusing medium, and using narrow pI range ampholytes. It is important to notice that increasing the length of the capillary alone does not improve the resolution, because the increase of distance between band centres is accompanied by broadening of each band, due to the smaller field strength counteracting the molecular diffusion.

If the peak width is approximated as four times the standard deviation of the Gaussian peak, the maximum number of peaks that can be accommodated in a capillary, which has

a length of L , is calculated by Eq (1-15). Higher voltage, smaller diffusion coefficient and larger ampholyte pI range will increase the peak capacity. Still, the capillary length itself does not play an important role in determining the peak capacity.

$$\begin{aligned}
 n_{pc} &= \frac{L}{4\sigma} = \frac{L}{4} \sqrt{\frac{E}{D} \cdot \left(-\frac{d\mu}{dpH}\right)_{pI} \cdot \frac{dpH}{dx}} \\
 &= \frac{1}{4} \sqrt{\frac{V}{D} \cdot \left(-\frac{d\mu}{dpH}\right)_{pI} \cdot (\Delta pH)_{total}}
 \end{aligned}
 \tag{1-15}$$

Although these conclusions above only apply to cIEF without mobilization, they still provide some guidelines for optimizing the separation efficiency cIEF.

1.2 MASS SPECTROMETRY – SEPARATION OF CHARGED SPECIES IN GAS PHASE

Mass spectrometry separates and detects charged species, such as metal ions, organic molecular ions, polymer ions, protein ions, or their fragment ions, in the gas phase under vacuum. Its high sensitivity, high speed, and low detection limit lead to many applications that have raised this technology to an unrivalled position among analytical technologies. At the heart of a mass spectrometer is the mass analyzer, which differentiates the ions based on their mass-to-charge ratio. The discussion below is focused on three types of mass analyzers involved in later applications of this thesis, namely, linear quadrupole, 3D ion trap, and time of flight mass analyzers.

1.2.1 Quadrupole mass analyzer¹³

The linear quadrupole mass analyzer is composed of four parallel electrodes ideally with hyperbolic surfaces, though round rods are sometimes used for approximation. The cross sections of the rods and electric potential applied on each rod are shown in Figure

1.3. The applied potential, ϕ_0 , contains both direct current (DC) and radio frequency (RF) components, and is given by Eq(1-16),

$$\phi_0 = U - V_{RF} \cos \Omega t \quad (1-16)$$

where U is a DC voltage applied pole to ground, V_{RF} is a zero to peak alternating voltage applied pole to ground, and Ω is the angular frequency of the RF voltage. By solving the Laplace equation, $\nabla^2 \phi = 0$, with boundary conditions shown in Figure 1.3, the potential among the four rods is expressed as Eq (1-17), where x and y are Cartesian co-ordinates, with the origin at the centre of the four rods, and where r_0 is the shortest distance from the centre to the rod surface.

$$\phi(x, y, t) = \left(\frac{x^2 - y^2}{r_0^2} \right) \times (U - V_{RF} \cos \Omega t) \quad (1-17)$$

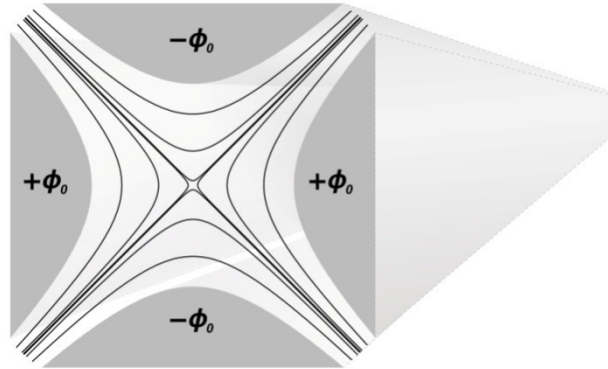


Figure 1.3: Quadrupole with hyperbolic rods and applied potential.

The centre point $(0, 0)$ is a saddle point and its potential is maintained at zero no matter how the potential on the electrodes vary with time. The charged ions travelling through the quadrupole experience oscillating electric field generated by the potential applied on the rods, and the ion motions in the x and y directions are subjected to

Newton's law shown in Eq (1-18), where m is the mass of the ion, and ze is the charge carried by the ion.

$$F_x = m \frac{d^2x}{dt^2} = -ze \frac{\delta\phi}{\delta x}, \quad F_y = m \frac{d^2y}{dt^2} = -ze \frac{\delta\phi}{\delta y} \quad (1-18)$$

The ion trajectories determined by Eq (1-18) are difficult to solve analytically; however, the stability diagram can be used to judge whether an ion with a specific m/z will hit on the rods as a result of its displacement in either x or y direction being greater than r_0 . The most frequently used stability region is shown in Figure 1.4. The parameters a and q in the diagram are given by Eq (1-19).

$$a = \frac{8zeU}{m\Omega^2 r_0^2}, \quad q = \frac{4zeV_{RF}}{m\Omega^2 r_0^2} \quad (1-19)$$

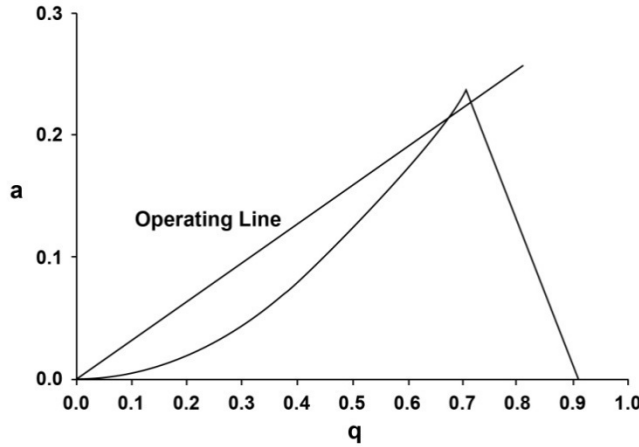


Figure 1.4: The First stability region of quadrupole with an operation line.

Under given conditions, if the point (a, q) for an ion with a specific mass-to-charge ratio falls within the triangular stability region, then the ion will pass through the quadrupole and be detected. Otherwise, it will collide with the quadrupole surface without reaching the detector. For a commercial quadrupole mass spectrometer, r_0 is a constant and Ω is usually fixed, so the U and V are variables that determine whether an

ion has a stable trajectory. By increasing U and V simultaneously, ions can be brought into and pushed out of the stability region sequentially, so that the ions in the order of increasing mass-to-charge ratio can pass through the linear quadrupole region and reach the detector. Thus, a mass spectrum is generated by scanning the DC and RF voltage simultaneously, and the resolution depends on the slope of the operation line. If the slope of the operation line is zero, the quadrupole serves as a low molecular weight cut-off ion guide that lets all the ions pass through.

Operated in scanning mode, the duty cycle of the quadrupole mass analyzer is determined by the ratio of dwell time on each small mass window over time spent on the whole scan range. If the mass-to-charge ratios of the target ions are known, the quadrupole can be operated in single ion monitoring or multiple ion monitoring mode. In this case, U and V are fixed or hopping among several pairs of settings for the specific mass-to-charge ratio, and the duty cycle is significantly improved.

1.2.2 3D ion trap mass analyzer

3D ion trap is another type of mass analyzer which makes use of the quadrupole field. It is composed of two cap electrodes and a ring electrode, and the inner surfaces of all the electrodes have a hyperbolic contour (Figure 1.5). When the cap electrodes are grounded, and a combined DC and RF voltage ϕ_0 (1-16) is applied on the ring electrode, a near ideal quadrupole field is produced within this specifically designed geometry.

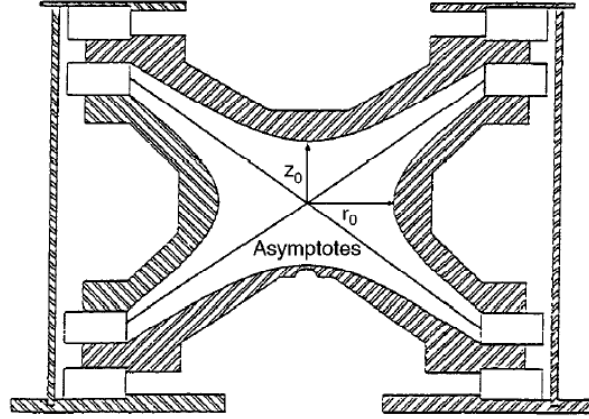
A**B**

Figure 1.5: (A) Photograph of an ion trap cut in half along the axis of cylindrical symmetry. (B) Schematic diagram of the cross section of an ion trap showing the asymptotes. $(r_0^2 = 2z_0^2)$ ¹⁴

Reprinted from *Journal of Mass Spectrometry*, 32, R.E. March, An Introduction to Quadrupole Ion Trap Mass Spectrometry, 351, Copyright (1998), with permission from John Wiley & Sons.

Using the Laplace equation, the potential in the ion trap can be expressed as Eq (1-20), where r and z are the cylindrical coordinates with the origin at the intersection of the two asymptotes, r_0 is the nearest distance from the origin to the ring electrode surface, and z_0 is the nearest distance from the origin to the cap electrode surface.

$$\phi(r, z, t) = \frac{r^2 - 2z^2 - r_0^2}{2r_0^2} \times (U - V_{RF} \cos \Omega t) \quad (1-20)$$

From Eq (1-20), the potential at the centre is $\phi_0/2$, which oscillates with the potential applied on the ring electrode. By applying Newton's Law in the r and z directions respectively, the ion motions inside the ion trap can be treated the same way as inside the linear quadrupole. Again, the complexity of solving the differential equations for the trajectories is reduced to the stability diagram, which predicts a range of stable mass-to-

charge ratios depending on simple variables. Figure 1.6 shows the first stability region for a 3D ion trap. The parameters a_z and q_z in the diagram are determined by Eq (1-21). If the calculated (a_z, q_z) under given conditions for a specific ion is within this stability region, the oscillation of the ions will be confined within the 3D ion trap.

$$a_z = -\frac{16zeU}{m\Omega^2(r_0^2 + 2z_0^2)}, \quad q_z = \frac{8zeV_{RF}}{m\Omega^2(r_0^2 + 2z_0^2)} \quad (1-21)$$

For the 3D ion trap to function as a mass analyzer, the ions are first injected into the ion trap through the gating lens and the orifice on one of the cap electrodes. From Eq (1-21), the adjustable variables that determine the stability of specific ions are U and V_{RF} , since r_0 and z_0 are decided by the trap geometry and the RF voltage frequency Ω is usually fixed. The simplest way to sequentially eject ions through the orifice on the other cap electrode is to set the DC voltage on the ring electrode zero and ramp up V_{RF} gradually. While scanning the RF voltage, the (a_z, q_z) of the stored ions will eventually approach the point (0, 0.908) in increasing mass-to-charge ratio. According to the stability diagram, when U equals to zero, q_z must be smaller than 0.908 for an ion to be stored in the trap. Thus, the lower mass-to-charge ratio cut-off value of this ejection method is determined by Eq(1-22),

$$\frac{m}{ze} \geq \frac{8V_{RF}}{0.908\Omega^2(r_0^2 + 2z_0^2)} \quad (1-22)$$

The upper mass-to-charge ratio limit of this ejection method is determined by the highest V_{RF} that could be applied on the ring electrode. For the first series of LCQ ion trap mass spectrometers with $r_0=7.07$ mm, $z_0=7.83$ mm, $\Omega= 2\pi \times 20.76$ MHz, and V_{RF} is variable up to a maximum of 8500V, the calculated upper mass limit is 1837.6 Th¹⁵.

To increase the mass analysis range of ion trap mass spectrometer, resonant ejection at smaller q_z value, also known as ‘axial modulation’, is used¹⁶. The stored ions oscillate in the z direction at secular frequency f_z , which can be approximated by Eq (1-23), when a_z is zero and q_z is smaller than 0.4.

$$f_z \approx \frac{q_z \Omega}{2\sqrt{2}} \quad (1-23)$$

If a small AC voltage at the frequency f_z is applied on the cap electrodes, the ions at this q_z value will resonate along the z -axis, and the oscillation amplitudes will increase until the ions are ejected through the end cap. By applying AC voltage on the end cap electrode while scanning the V_{RF} on the ring electrode, ions of increasing mass-to-charge ratio are brought to a desired q_z value, that is smaller than 0.4, excited and then ejected. In this way, the required V_{RF} for ejection can be reduced and the mass analysis range of the ion trap analyzer is extended.

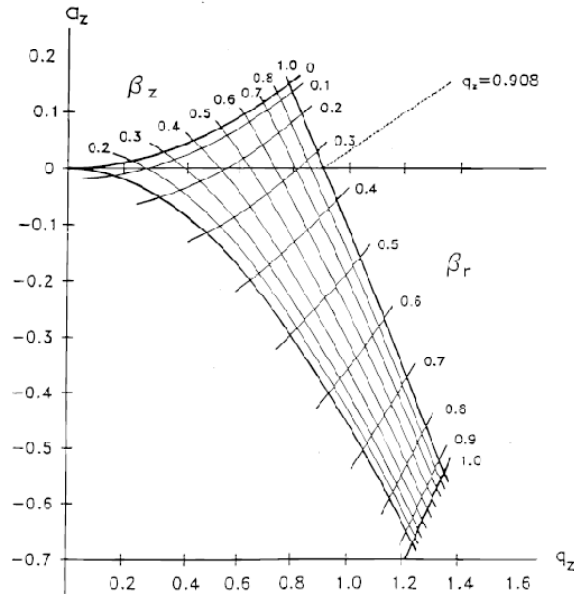


Figure 1.6: First stability region of 3D ion trap.¹⁴

Reprinted from *Journal of Mass Spectrometry*, 32, R.E. March, An Introduction to Quadrupole Ion Trap Mass Spectrometry, 351, Copyright (1998), with permission from John Wiley & Sons.

As the ions have to be stored in the ion trap before they are ejected, the electric field induced by charged ions will modify the original field applied by the electrodes. The resulting field is the sum of the original external field and the field induced by the ion clouds. When there are too many ions trapped, the stability diagram will be shifted, resulting in problems on the mass accuracy and resolution. Although increasing the ion injection time improves the detection sensitivity, a balance between sensitivity and space charge effect should be maintained.

If the ions are generated continuously in the ion source, only those ions injected into the ion trap can be analyzed, and the rest are repelled by the gating lens while the ion trap is scanning. The duty cycle of a trap analyzer is calculated by Eq (1-24), where t_{inj} is the time for ion injection, and t_{ana} is the time for mass analysis. It was estimated that more than 98% of the ions from the ion source are discarded without entering the 3D trap¹⁷.

$$\text{Duty Cycle} = \frac{t_{inj}}{t_{inj} + t_{ana}} \quad (1-24)$$

1.2.3 Time of flight mass analyzer

The time of flight (TOF) analyzer employs a very simple concept to separate ions of different mass-to-charge ratio in field-free vacuum. All the ions are accelerated through an electric field to gain the same kinetic energy, and then they drift in a field-free region. The time of flight in the drift tube is related to mass-to-charge ratio by Eq (1-25), where U is the acceleration potential, t is the drift time, and L is the length of the drift tube.

$$\frac{m}{z} = \frac{2eUt^2}{L^2} \quad (1-25)$$

As larger mass-to-charge ratio simply results in longer flight time, a TOF instrument does not have an upper mass limit in principle. This feature makes it ideal for analyzing large molecules such as proteins and protein complexes. Another advantage of TOF is the fast analysis speed. A broad mass range spectrum can be obtained on a time scale of about one hundred microseconds.

In order to correct the kinetic energy dispersion of the ions with the same mass-to-charge ratio coming from the source, a reflectron composed of a series of equally spaced grid electrodes is usually added at one end of field free region, and the detector is placed at the other end of the drift tube opposing the reflectron, as shown in Figure 1.7. When the ions enter the reflectron region, the electric field will decelerate the ions and reverse their travel direction. Given identical mass-to-charge ratio, ions with higher kinetic energy in the source will penetrate the reflectron region further, and the total traveling distance would be longer than that of the ions with lower initial kinetic energy. The longer time that the ions with excess energy spend in the reflectron region will compensate for the shorter time they spent in the field-free region, resulting in identical flight time regardless of the initial kinetic energy. Mass resolution of a reflectron TOF mass spectrometer can reach as high as 20,000¹⁵.

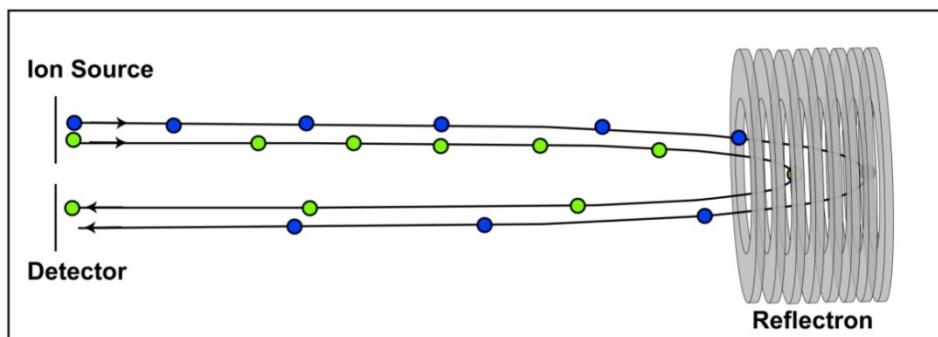


Figure 1.7: Schematic illustration of a TOF mass analyzer with reflectron.

The blue and green circles represent ions of the same mass-to-charge ratio but different initial kinetic energy.

1.3 ELECTROSPRAY IONIZATION – GENERATING GASEOUS IONS FROM A LIQUID SOLUTION

Electrospray ionization (ESI) is a soft ionization technique that converts charged species in liquid phase to gas phase under atmospheric pressure. Dispersion of liquid into small charged droplets in an electrostatic field was observed as early as two centuries ago¹⁸. Since then, electrospray as a method for generating fine aerosols has found a wide range of industrial applications, including crop spraying, paint spraying, and ink-jet printing¹⁸. In 1968, Malcolm Dole¹⁹ first attempted to use electrospray as a means to produce gas phase ions of macromolecules from a liquid solution for analysis by mass spectrometry. However, this technique did not prove to be an effective ionization method for MS until two decades later, when Fenn and Yamashita²⁰ successfully coupled ESI to a quadrupole mass spectrometer. Since these pioneering studies, ESI has demonstrated its analytical prowess in analyzing many classes of chemical compounds, from small molecules to large polymers. Its contribution is especially significant in the study of biomolecules, in the fields such as metabolomics²¹, lipidomics²², and proteomics²³, and the non-covalent complexation of biomolecules²⁴. Furthermore, ESI owes its increasing popularity to the ease of online coupling to separation techniques such as liquid chromatography and capillary electrophoresis.

A schematic of the positive electrospray process²⁵ is illustrated in Figure 1.8. A voltage of 2–5kV is applied to a metal capillary whose outer diameter is usually several hundred micrometers and is located several centimetres away from the counter electrode (in this case, the MS inlet). The counter electrode is grounded or has a potential several

kilovolts lower than the metal capillary. It might be a plate with an aperture leading to the mass spectrometer sampling system, or a sampling capillary or cone mounted on a plate, which serves as the entrance of mass spectrometer. Due to the large voltage difference between the two electrodes, a strong electric field, typically $\sim 10^6$ V/m, can be generated at the capillary tip. A solution of polar and volatile solvent in which electrolytes are soluble is usually delivered to the capillary tip by a syringe pump, liquid chromatography or capillary electrophoresis. Typical flow rate of the solution is from $1\mu\text{L}/\text{min}$ to $20\mu\text{L}/\text{min}$.

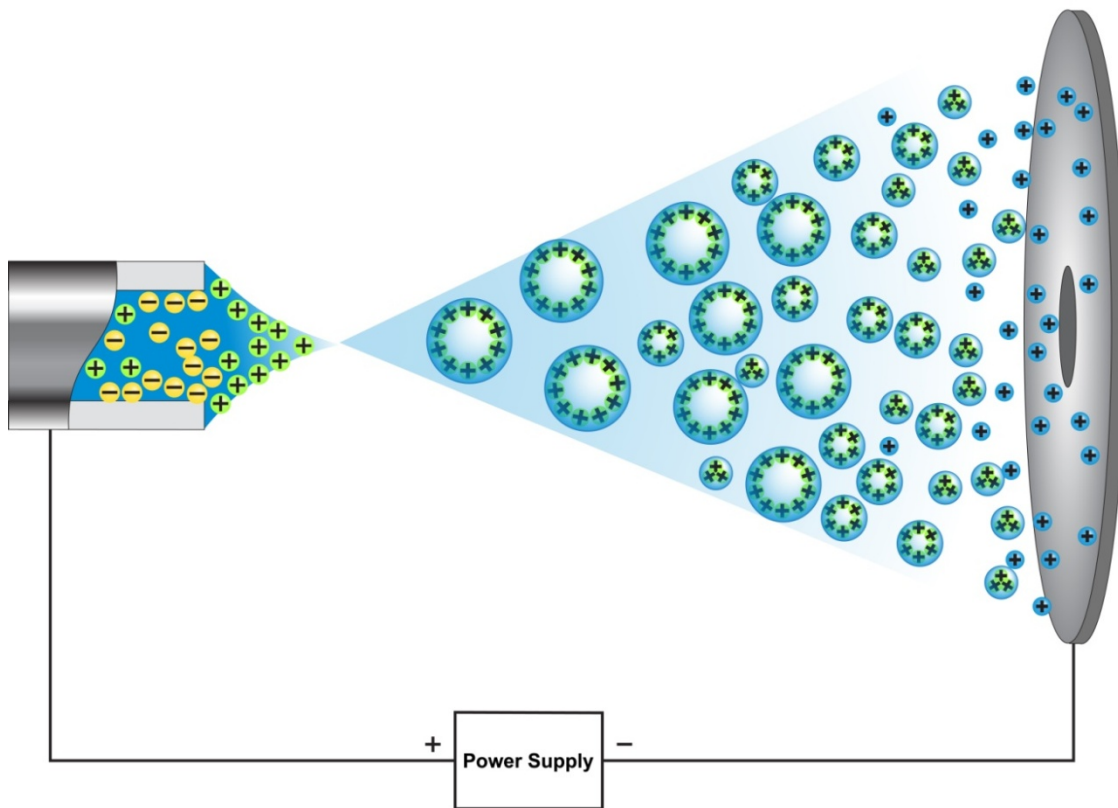


Figure 1.8: Schematic of the electrospray ionization process.

The analyte solution is pumped through a needle to which a high voltage is applied. A Taylor cone with an excess of positive charge on its surface forms as a result of the electric field gradient between the ESI needle and the counter electrode. Charged droplets are formed from the tip of the Taylor cone, and these droplets evaporate and burst into smaller droplets as they move towards the entrance to the mass spectrometer. Eventually,

free, charged analyte molecules are generated to be analyzed by their mass-to-charge ratio.

Three major steps are involved in the production of gas-phase ions from electrolyte ions in the solution^{26,27}: (1) formation of charged droplets at the electrospray capillary tip; (2) shrinkage of the charged droplets by solvent evaporation and disintegration of the droplets; and (3) production of gas-phase ions from high charge density droplets. When the voltage is turned on, the large electric field penetrates the solution at the capillary tip. The electrostatic pressure on the solution surface induced by this large electric field makes the solution stretch downfield. A liquid cone (also known as Taylor cone) forms at the tip of the capillary as the result of the surface tension generated to oppose the electrostatic pressure. Meanwhile, under the influence of the electric field, charges in the solution are redistributed to counteract the external field: positive ions migrate towards the meniscus of the solution while negative ions drift upfield in the solution. Due to electrophoresis of the electrolytes, excess positive ions accumulate at the surface of the liquid. The mutual repulsion among the positive ions soon overcomes the surface tension and the surface begins to expand, allowing the positive charges and liquid to move downfield. If the electric field at the capillary tip is high enough to overcome the surface tension of the liquid, a fine jet emerges from the liquid cone tip, which breaks up into small charged droplets.

The droplets emitted at the cone jet are positively-charged because of excess positive electrolytes. These charged droplets then move in the air towards the counter electrode and shrink in size due to solvent evaporation. Shrinkage of the droplets with constant charge leads to an increased electric field normal to the surface of the droplet. At a certain radius, the mutual Coulombic repulsion of the positive ions on the droplet surface

finally overcomes the surface tension, resulting in Coulombic fission. During Coulombic fission, smaller offspring droplets are generated. Further fissions of the charged droplets produce progressively smaller and more highly charged droplets.

Two mechanisms have been proposed to account for the formation of gas-phase ions from very small and highly charged droplets. The first one, developed by Dole¹⁹, is commonly called the charged residue mechanism (CRM). It is suggested that when the solution is dilute enough, successive Coulombic fission will produce droplets so small that each one would contain only one solute molecule. With continuing evaporation of the solvent, single gas phase ions could be eventually set free, bearing one or more excess charges. Iribarne and Thomson^{28,29} proposed another mechanism: ion evaporation mechanism (IEM). It predicts that after the radii of the droplets decrease to a certain size, direct ion emission from the droplets becomes possible. In fact, it is proposed that direct ion emission dominates over Coulombic fission for droplets of radii smaller than 10 nm. Merits of each mechanism are still under debate.

1.4 INTERFACING OF CE AND MS

Since capillary electrophoresis and mass spectrometry are both techniques for separation of charged species, combining of the two would create an extremely powerful tool for two dimensional separations. Techniques for combining CE and MS have been developed for many ionization methods, including electrospray ionization(ESI)³⁰, inductively coupled plasma (ICP)³¹, matrix assisted laser desorption ionization (MALDI)³², atmospheric pressure chemical ionization (APCI)³³, and atmospheric pressure photoionization (APPI)³⁴. However, most of them are limited to a specific category of analytes. The extremely high temperature of the ICP torch restricts its

application to ionization of metal elements; MALDI requires extra efforts of collecting the fractions from CE separation, and conversion of analytes in liquid phase to solid phase; APCI and APPI are only suitable for small nonpolar organic compounds. ESI has become the most popular CE-MS ionization technique because it is relatively easy to operate and can be adapted to many different types of compounds, especially large biomolecules.

1.4.1 General concerns on CE-ESI-MS interfaces

CE and ESI share many common properties which heighten their compatibility: for example, they both enjoy simple DC circuits, and are suitable for large biomolecules. However, several fundamental issues still need to be addressed for successful online coupling of CE and ESI-MS. First of all, consolidation of the CE and ESI circuits poses several concerns. While the inlet electrode of the CE apparatus can be preserved, the outlet electrode needs to be modified to function as an electrospray emitter, capable of generating intense electric field for electrospray. Stable electrical contact at this shared electrode is important for continuous CE current and electrospray. Furthermore, CE is usually operated at currents around tens to hundreds of microamperes. In contrast, the spray current is confined to under one microampere.

Secondly, participation of the CE electrolytes in the electrospray ionization process requires modification of the CE effluents. The highly conductive and polar background electrolytes in CE are in direct contrast to the properties of an ideal electrospray solvent which has low conductivity, low surface tension and polarity. Thirdly, the bulk flow rate of CE, within hundreds of nanoliters per minute, is not high enough to support a stable

electrospray from an emitter with typical dimension of several hundreds of micrometers in diameter.

1.4.2 Sheath liquid CE–ESI–MS interfaces

In the last twenty years, a variety of CE-ESI-MS interfaces have been developed to address some of the concerns mentioned above. They can be divided into two categories: sheath liquid interfaces and sheathless interfaces. Three major configurations of the sheath liquid interface design³⁵ are summarized in Figure 1.9. These interfaces employ additional sheath liquid to supplement the flow rate of CE and to modify the surface tension and polarity of the BGE before electrospray. The most common type is the coaxial sheath liquid interface shown in Figure 1.9A, which has been commercially available for years³⁶. In this interface, the capillary terminus is inserted into a coaxial metal sheath tube and slightly extrudes out of it. The sheath liquid, which usually contains organic solvents to facilitate electrospray ionization, flows between the capillary and the metal sheath tube and mixes with the CE effluent outside the capillary tip. A third tube delivers a coaxial sheath gas to help with solvent evaporation and improve ionization efficiency. A major drawback of this interface is analyte dilution caused by the sheath flow liquid³⁷.

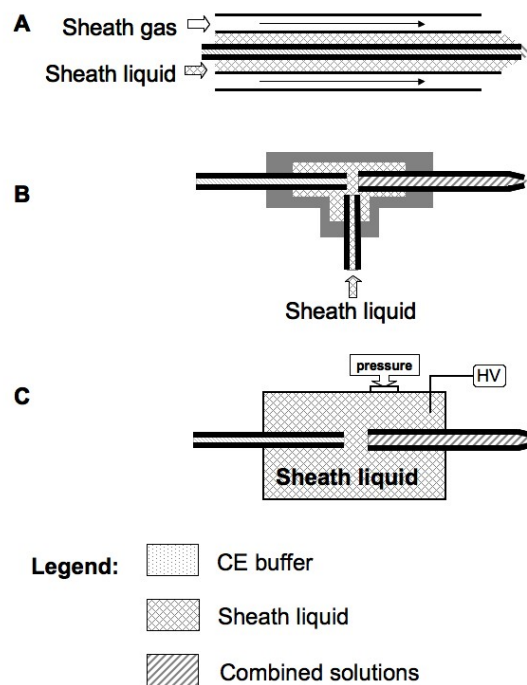


Figure 1.9: Common sheath-liquid interface arrangements.

(A) Coaxial sheath-liquid interface with sheath gas, (B) liquid junction interface, and (C) pressurized liquid junction interface.³⁵

Reprinted from *Analytica Chimica Acta*, 627, E. J. Maxwell and D.D.Y. Chen, Twenty years of interface development for capillary electrophoresis-electrospray ionization-mass spectrometry, 25, Copyright (2008), with permission from Elsevier.

Liquid junction interfaces, which employ a metal sprayer or silica capillary connected to the capillary terminus via sheath liquid as electrospray emitter³⁸⁻⁴¹, as illustrated in Figure 1.9B and C, were designed to reduce dilution effect from the sheath liquid. The sheath liquid is either delivered through another capillary (Figure 1.9B) or provided by the pressurized sheath liquid reservoir (Figure 1.9C), to be mixed with the CE effluent at the gap between the capillary terminus and the metal emitter. The difficulty of aligning the emitter with the capillary and controlling the gap distance between the two hinder wider application of this interface. Another disadvantage of the liquid junction interfaces is the peak broadening caused by the large post-column dead volume.

1.4.3 Sheathless CE-ESI-MS interfaces

To improve detection sensitivity, researchers have modified the CE column terminus to adapt the inherent CE flow rate to match the required flow rate for stable electrospray, instead of using another piece of tubing as electrospray emitter. A fused silica capillary tip is pulled or etched into a very thin emitter, with an OD of several to ten microns to eliminate the need for sheath flow liquid. In the nanospray regime, the initial liquid droplet sizes are so small that gas phase ions can be generated fast and efficiently in the ion source. Therefore, the ionization efficiency of sheathless interfaces is usually much higher compared to that of sheath flow interfaces. Despite these merits, establishing a stable electric contact at the CE terminus remains a tricky problem. Various solutions have been proposed to solve this problem, as shown in Figure 1.10. The most widely used one is to apply a thin layer of conductive coating, such as gold^{42,43}, silver⁴⁴, copper⁴⁵, nickel⁴⁶ or graphite⁴⁷⁻⁴⁹, to the outer surface of the silica capillary tip and attach this coating to high voltage power supply (Figure 1.11A). However, quick deterioration of the coating materials makes lifetime of these CE columns as short as a few days. Other methods of creating electric contact include inserting a wire into the capillary through the opening at the tip⁵⁰(Figure 1.10B) or creating a hole or crack near the tip⁵¹ (Figure 1.10C); splitting the liquid flow inside the capillary by drilling a small hole near the capillary tip so that the portion flow outside of the capillary contacts an electrode⁵² (Figure 1.11D); etching silica capillary tip to make it thin and porous and inserting the porous tip into a metal tube filled with conductive liquid^{53,54,55} (Figure 1.10E).

As the small size nanospray tips are prone to getting clogged or damaged, it is desirable to have disposable emitters connected to the CE column to prolong the lifetime

of the capillary. There have been several reports of this type of sheathless interface. With silica emitters, metal sleeve⁵⁶ (Figure 1.10F) or micro dialysis tubing⁵⁷ (Figure 1.10G) are used to align the two pieces of capillaries and make the electric contact. With stainless steel emitters (Figure 1.10H), high voltage for ESI can be applied directly on the emitter⁵⁸.

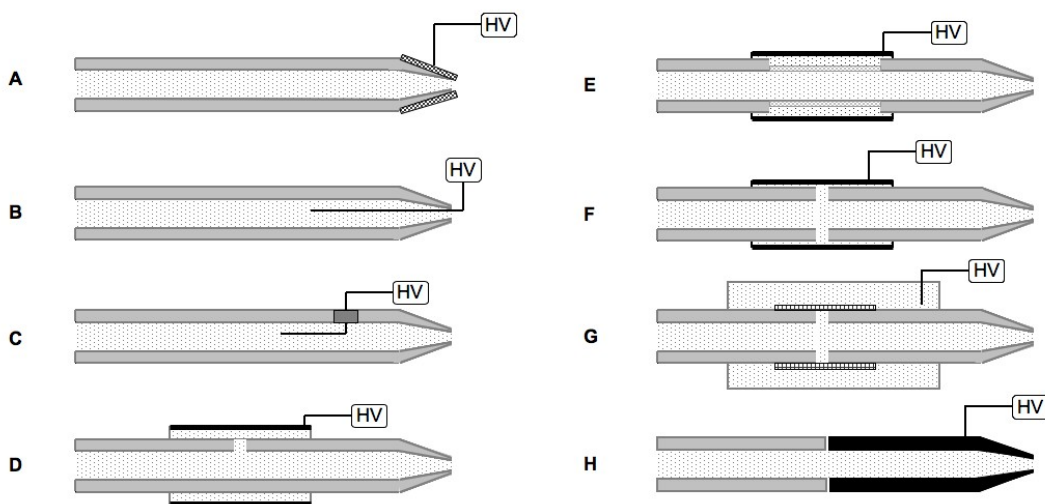


Figure 1.10: Methods for creating electrical contact in sheathless interfaces. (A) Conductive coating applied to the emitter tip, (B) wire inserted at tip, (C) wire inserted through hole, (D) split-flow interface with a metal sheath, (E) porous, etched capillary walls in metal sleeve, (F) junction with metal sleeve, (G) microdialysis junction, and (H) junction with conductive emitter tip.³⁵

Reprinted from *Analytica Chimica Acta*, 627, E. J. Maxwell and D.D.Y. Chen, Twenty years of interface development for capillary electrophoresis-electrospray ionization-mass spectrometry, 25, Copyright (2008), with permission from Elsevier.

Some common problems of the sheathless interfaces include complicated fabrication process, fragility and reproducibility. As the electrospray solution comes only from the bulk flow in the CE column, the choice of buffer solution is more restricted by the requirement of electrospray, and pressure has to be applied at the CE inlet to support electrospray when the EOF rate is not large enough.

1.5 RESEARCH OBJECTIVES

1.5.1 Design and characterization of a novel CE-ESI-MS coupling strategy

The first section of this thesis focuses on the design, rationale, and characterization of a novel CE-ESI-MS interface using a flow-through microvial. Although the current commercial sheath liquid interface has brought CE-MS applications to a wide audience, demands on improving sensitivity for biological samples pushed us to explore new solutions for CE-MS interfaces. In addition to increased sensitivity, the new interface should be robust, easy to fabricate, compatible with different types of CE columns and separation modes, and offer excellent reproducibility for routine analysis. Chapter 2 discusses these features of the novel CE-ESI-MS interfacing strategy. As MS is a post-column detector, band broadening caused by the flow-through microvial CE-MS interface is a concern. Chapter 3 is devoted to describing the mass transport process in the interface region and its influence on peak shape.

1.5.2 Applications of the interface in different capillary electrophoresis modes

Although CE-ESI-MS interfacing technologies are not as mature as liquid chromatography (LC)-ESI-MS interfacing, its vast potential in drug analysis⁵⁹, metabolite profiling^{60,61}, peptide and protein characterization⁶²⁻⁶⁵, carbohydrate identification⁶⁶⁻⁶⁸, and biomarker discovery^{69,70} has been demonstrated. To evaluate performance of this novel CE-ESI-MS interface for small molecule characterization, Chapter 4 presents the results of separation and quantification of two groups of basic compounds that are of drugs of abuse. In addition, this interface also facilitates online coupling of cIEF and ESI-MS. Chapter 5 demonstrates the strategy of online cIEF-MS with both uncoated and coated capillaries using pI markers and protein standards.

1.5.3 Improvements on ESI sensitivity in reduced flow region

To further enhance the performance of the CE-ESI-MS interface, it is crucial to improve spray stability, ionization efficiency and sampling efficiency of the electrospray ionization source in the reduced flow region (lower than a couple of microlitre per minute). Chapter 6 explains how an atmospheric ion lens modifies the electric field distribution in the ion source and improves the detection sensitivity.

Chapter 2: Decoupling CE and ESI for a more robust interface with mass spectrometry

2.1 INTRODUCTION

Since first demonstrated in 1987³⁰, the strategy of interfacing the highly efficient separation technology capillary electrophoresis to highly sensitive detection technology of mass spectrometry via electrospray ionization has been modified and improved by many researchers. Over the past twenty years, a variety of interfacing techniques have emerged³⁵, among which the sheath liquid, sheathless and liquid junction are the most frequently employed methods. As the sheath liquid interfaces³⁶ are relatively rugged and easy to adapt to the existing LC-ESI-MS interface, they have been incorporated into commercial CE-MS systems and found lots of applications in analysis of biomolecules, such as metabolites, peptides, proteins and carbohydrates. However, the sheath liquid interfaces always suffer from the sacrificed sensitivity caused by dilution from the high sheath liquid flow with a volume rate of 1~10 $\mu\text{L}/\text{min}$ ³⁷. While showing higher sensitivity, use of the sheathless interfaces generally involves lengthy and complicated fabrication work, such as coating the silica capillary tip with various conductive materials^{42,45-49,71-73}, drilling a hole on the capillary to split the liquid flow in the capillary⁵², inserting an electrode into the capillary^{50,51}, or etching the tip of silica capillary to make it porous⁵³. Due to electrolysis of the metal coating or the poor mechanical strength of the capillary tips, these sheathless interfaces usually do not last for long time; sometimes reproducibility is also a problem due to the fabrication process. In addition, as only the bulk flow from CE supports the electrospray, the choices for BGE are more limited, and the sheathless interfaces cannot accommodate coated capillaries that suppress EOF unless pressure is applied at the inlet buffer vial. As to the liquid junction^{38,40,41,74} interfaces, the

large dead volume of the junction and difficulty to align the separation capillary with the ESI emitter remained to be resolved.

Another type of CE-MS interface design uses the ‘junction-at-the-tip’ concept⁷⁵⁻⁸¹. The end of the CE column is surrounded by a tapered outer tubing and does not extrude out of it, and the CE effluent and sheath liquid or make-up flow mix inside the tapered emitter tip. The dimensions of emitter tips are usually smaller than those of the typical sheath flow interfaces, so that the ‘junction-at-the-tip’ interfaces require lower make-up flow compared to the traditional sheath flow interfaces. In addition, the coaxial alignment also makes assembly of this kind of interface easy. However, the emitter material used by most researchers was silica or glass capillaries, which requires extra effort to build electric contact at the CE outlet. To obtain both the ruggedness and sensitivity, our group has recently designed a robust, easy-to-build, improved ‘junction-at-the-tip’ type CE-ESI-MS interface⁸², which uses a stainless steel (s.s.) needle as both the ESI emitter and the CE terminal electrode. The capillary column is inserted as far as possible into a tapered ending of the s.s. needle tubing, and the space enclosed by the end of CE column and s.s. tip inner surface forms an open flow-through microvial for the CE outlet. A grounded, pressurized reservoir supplies a low flow modifier to the very end of the capillary to regulate the effluent flow rate and sustain stable electrospray. This low make-up flow pushes the products generated by electrochemical reactions, such as oxygen bubbles, out of the s.s. needle, making the electric contact stable by constantly filling the space in the open flow through outlet vial. The grounded reservoir is also responsible for sinking part of the current from CE.

Previous studies by other researchers have shown the geometry and dimensions of the sprayer tip play a critical role in the electrospray ionization process⁸³ and the shape of the geometry of the tip does not have to be symmetrical. Her and co-workers found the optimal flow rate of a 75 μm ID, 90 μm OD bevelled, tapered and carbon coated silica capillary tip was similar to that of a conventional flat silica capillary tip with a 25 μm OD⁷³. To further improve the performance of the CE-MS emitter, our s.s. emitter tip was 35 degree bevelled to adapt to a wider flow rate range for stable electrospray. Due to the lower volume flow rate of the modifier (less than 1 $\mu\text{L}/\text{min}$), the sensitivity of this interface is improved compared to the conventional sheath liquid interface.

In this chapter, incorporation of our home-built interface into commercial instruments with UV detection is demonstrated. Amino acids, protein standards, peptides, and catecholamines were chosen as the analytes because of their biological importance and previous extensive studies on these samples. The capability of accommodating different types of capillaries for analyzing different samples promises a wide application area for this CE-ESI-MS system in the future.

2.2 MATERIALS AND METHODS

2.2.1 Chemicals and materials

Individual amino acids, hydroxyl-proline, catecholamines, thymol, sodium dodecyl sulfate (SDS) and 1, 2, 4-benzenetricarboxylic acid (BCA) were purchased from Sigma Chemical Co. (St. Louis, MO, USA). A HPLC peptide standard mixture composed of angiotensin II (DRVYIHPF, M.W. 1046.2), Gly-Tyr (M.W. 238.3), Val-Tyr-Val (M.W. 379.5), Leu enkephalin (YGGFL, M.W. 555.6) and Met enkephalin (YGGFM, M.W. 573.6) was also purchased from Sigma. Angiotensin I&II peptide mixture and a protein

standard test mix containing cytochrome C (Cyt C), lysozyme (Lys) and ribonuclease A (RNase A) were obtained from Beckman Coulter (Brea, CA). Methanol (HPLC grade), acetonitrile (HPLC grade), ammonium hydroxide (A.C.S. reagent), 88% formic acid (Certified A.C.S.), hydrochloric acid (A.C.S. reagent) were from Fisher Scientific (Nepean, ON, Canada). The deionized water was generated from a Milli-Q purification system (Millipore, Bedford, MA). To prevent decomposition of the amino acid mixture, the 1 mM stock solution was prepared in 50% methanol and stored at -20 °C. In order to dissolve the catecholamines and its analog tyrosine, the 1 mM stock solution was prepared in 0.1 M HCl solution. The HPLC peptide standard mixture, angiotensin I&II mixture, and protein standard mixture were dissolved in deionized water to produce a 1 mg/ mL stock solution, and aliquots were stored at -20 °C and diluted before use.

Bare fused silica capillary (75 and 50 µm ID, 365 µm OD) was purchased from Polymicro Technologies (Phoenix, AZ). Neutral coated capillary with double layer polyacrylamide-based hydrophilic wall coating (50 µm ID, 365 µm OD, 67 cm long) was obtained from Beckman Coulter. A polyethylenimine (PEI) capillary coating solution was obtained from Gelest, Inc. (Morrisville, PA).

2.2.2 Instrumentation

All the CE-MS experiments were performed on a P/ACE MDQ capillary electrophoresis system from Beckman Coulter Instruments (Brea, CA), and a Finnigan LCQ Duo mass spectrometer (Thermo Scientific, Waltham MA) or Waters Q-TOF1E mass spectrometer (Waters Corporation, Milford MA). Figure 2.1A illustrates the CE-ESI-MS setup with our built-in-house CE-ESI-MS interface. Both the separation and modifier capillaries are hosted by a modified cartridge designed for external detection

(Beckman Coulter Instruments, Brea, CA). The CE buffer vial and the chemical modifier vial are placed on the two separate buffer trays of the MDQ system. Standard stainless steel (s.s.) tee unions and polyethyl ether ketone (PEEK) fittings purchased from Upchurch Scientific (Oak Harbor, WA) are used to secure the separation capillary, modifier delivery capillary, and stainless steel sprayer (Figure 2.1B). The two opposing ports of the tee are used to connect the separation column and the s.s. sprayer. The orthogonal port of the tee union is attached to the modifier capillary through a PEEK nut, which delivers a low flow solution to the sprayer tip when a small pressure is applied to the chemical modifier vial. The s.s. sprayers were fabricated from approximately 2 inch long hollow stainless steel tubings (OD 0.028", ID 0.016") according to customer design (Popper & Sons, Inc, New Hyde Park, NY). One end of the s.s tube was laser welded to 1/16" OD stainless steel tubing for connection with the standard fittings. The other end, which was tapered both internally and externally, was used as electrospray emitter. The emitter outlet surface has an OD of 305 μm and ID of 75 μm . To improve the stability of electrospray ionization, the emitter tip was bevelled, such that the face of the tip forms a 55° angle with the central axis of the electrode. Inset of Figure 2.1A gives these details of the sprayer tip geometry. Because of the gradual tapering of the internal surface of the sprayer tip, the CE separation column is inserted all the way through the s. s. needle to the very end but does not extrude out of the end of the s. s. needle. The CE effluent and the modifier converge and mix at the microvial enclosed by the tapered inner surface of the s. s. emitter and the end of the separation column. The tee union was mounted on an XYZ micro-positioning stage in the ion source of the mass spectrometer. The s. s. emitter is directly aimed at the orifice of the heated transfer capillary of the LCQ mass

spectrometer or the orifice of the sample cone of the Q-TOF mass spectrometer, and the distance from the sprayer tip to the inlet was approximately 0.5~1 cm.

Images of the electrospray process were captured on a CCD camera (Watec, Middletown, NY) with an 8×20 lens (Specwell, Tokyo, Japan). The electrospray plume was illuminated by a 12 mW diode laser (Power technology Inc, Little Rock, AR). The mass spectrometer inlet was approximated using a conducting rod connected through a picoammeter (Kiethley, Cleveland, OH) to ground. A syringe pump (Harvard apparatus, Holliston, MA) was used to infuse the solution for electrospray.

2.2.3 Separation methods

Separations of amino acids, catecholamines and HPLC peptide mixture standard were carried out using 75 μm ID \times 360 μm OD bare fused-silica capillaries (Polymicro Technologies, Phoenix, AZ). Another 75 μm ID capillary was used for chemical modifier delivery. Before each run, the capillary was flushed with methanol, 2% formic acid, and run buffer for 5 minutes each. The BGE and chemical modifier were methanol/water/formic acid (v/v/v) 50:50:0.2 for amino acid and catecholamine separations, acetonitrile/water/formic acid (v/v/v) 50:50:0.2 for HPLC peptide mixture standard separation. During the separation, positive 30 kV was applied at the CE inlet vial and 4.3 kV was applied at the s. s. electrospray emitter. The Finnigan LCQ ion trap mass spectrometer was operated in positive ESI and full scan mode. The scan range was set at m/z 70 ~250 for the amino acids mixture, 145 ~ 210 for catecholamines and 200~600 for the HPLC peptide standard mixture. The heated transfer capillary was set at 200 °C. The MS data were collected and processed by the Xcalibur 2.0 software (Thermo Scientific, Waltham, MA).

Separations of the angiotensin peptide mixture were carried out using a polyethylenimine (PEI) coated capillary. The PEI coating protocol was as described in U.S. Patent 6,923,895 B2. The BGE was methanol/water/formic acid (v/v/v) 25:74:1, and the modifier solution was isopropanol/water/formic acid (v/v/v) 75:24.9:0.1. The capillary was rinsed with BGE for 3 min before each run. MS detection was performed by Waters Q-ToF mass spectrometer in positive ESI and full scan mode. A negative 30 kV voltage was applied at the CE inlet vial and a positive 4.3 kV voltage was applied at the electrospray emitter. The sample cone of the mass spectrometer was set at 30 V, 150°C, and the scan range was m/z 410~550. Data were collected and processed by the MassLynx 4.0 software (Waters, Milford MA).

Basic protein standard separations were performed by using 'Neutral' coated capillary (Beckman Coulter, CA). The BGE was 100 mM pH 3.1NH₄Ac /MeOH (v/v) 9:1, and the modifier solution was 0.2% formic acid, 90% methanol. Deionized water and BGE solution were used to rinse the capillary before each run. During separation, positive 30 kV was applied at the CE inlet vial and positive 4.0 kV was applied at the electrospray emitter. The Finnigan LCQ ion trap mass spectrometer was operated in positive ESI and full scan mode. The scan range was set at m/z 800~2000.

2.2.4 Simulation

Simulations of the electric field strength in the electrospray ion source were carried out by solving the Laplace equation using the Electromagnetics - Electrostatics module of COMSOL Multiphysics 3.4 software (COMSOL Inc., Los Angeles CA). The interface features were drawn according to their actual dimensions. An 'extra-fine' finite element mesh was used in order to accurately calculate the field lines around the sharp features of

the needle tips. Further description of the fundamentals of electric field modelling will be provided in Chapter 6.

2.3 RESULTS AND DISCUSSION

2.3.1 Design rationale

For an ideal electrospray emitter, it should be inert, inexpensive, robust, easy to fabricate, and adapted to a wide range of flow rates. Stainless steel is chosen as the material for electrospray emitter for the mentioned advantages as well as its conductivity. For online CE-ESI coupling, the ESI emitter functions as a shared electrode for both CE and ESI to complete the circuit. The stainless needle shown in Figure 2.1 serves as an ESI emitter and a CE terminal electrode. The space enclosed by the end of CE column and the inner surface of the tapered stainless steel tip acts as an open flow-through microvial at the CE outlet. The small volume of the microvial, estimated to be approximately 15~ 20 nL, does not contribute to the peak distortion significantly (Details will be discussed in Chapter 3). A grounded, pressurized solution vial supplies a low flow modifier to the very end of the microvial to regulate the pH, surface tension and flow rate of the effluent from CE column. By filling the open space in the microvial continuously, this low make-up flow maintains the electric contact between the CE terminal electrode and the BGE, refreshes the electrolyte around the electrode, and pushes the products generated by electrochemical reactions, such as oxygen bubbles, out of the s.s. needle. Due to the low volume flow rate of the modifier (less than 1 $\mu\text{L}/\text{min}$), the sensitivity of this interface is improved from the conventional sheath liquid method. Part of the current from CE can sink through the grounded modifier vial.

pH, ionic strength and viscosity of run buffer. A stable spray could be sustained only when the supplying rate of the effluent matches the emission rate of the liquid on the Taylor cone⁸⁴. When high voltage is applied on the emitter, the competition between the Coulombic force, which pulls charge out of the bulk solution, and surface tension, which keeps the solvent molecules together, determines the shape and vibration frequency of the Taylor cone seated on the sprayer tip. For a certain flow rate, there is an onset voltage to generate strong enough field to pull the charged droplets out from the bulk solution; if the applied voltage is too high, the Taylor cone tip breaks down too frequently so that the relatively small flow rate cannot sustain the volume of the Taylor cone. On the other hand, at a fixed ESI voltage, there is a threshold of solution infusion rate above which a stable spray could form. The ion signals increase with the infusion rate until a plateau is reached. The existence of this plateau is due to the limited desolvation efficiency and the current of electrospray³⁵. In order to use the mass spectrometer as a concentration detector, the optimal flow rate should be chosen in the plateau region. When the flow rate is higher than a certain value, the droplets produced by electrospray will be too large to evaporate in the ion source region without auxiliary means, such as extremely high temperature or nebulizer gas.

To evaluate the performance of sprayer tips in different geometries, we have conducted a series of comparisons by plotting the signal noise ratio (SNR) as a function of electrospray voltage and flow rate⁸⁵. It has been demonstrated that (1) emitter tips with smaller OD can tolerate lower flow rate, but are more easily clogged; (2) a bevelled emitter tip can accommodate a wider flow rate range compared to blunt tips of similar dimension. Considering that the magnitude of electroosmotic flow rate from CE column

can vary over a large range, and that the combined flow rate of EOF and modifier is typically lower than $1\ \mu\text{L}/\text{min}$, a 35 degree bevelled tip was chosen for later application. It is found that this tip performs best in the flow rate range of $0.1\sim 0.6\ \mu\text{L}/\text{min}$ (the upper limit could be improved by increasing the temperature in the ion source), while other blunt tips of similar dimensions have a narrower stable operational region. In a CE-ESI-MS experiment, the electroosmotic flow rate depends on a variety of parameters mentioned above; the operational stable flow rate is determined by the tip geometry, voltage applied on the tip and the surface tension of the liquid. The difference between the EOF rate and the required stable flow rate for a specific sprayer can be adjusted by the modifier flow. However, as the modifier flow causes dilution of the sample concentration, the flow rate of modifier should be kept as low as possible to maximize the detection sensitivity.

Figure 2.2 AB compares the electric field generated by a s.s. blunt tapered tip and a bevelled tapered tip in the ion source. Under the same conditions, the bevelled tip generates higher electric field intensity compared to a flat tip of the same dimension when an identical voltage is applied. For a symmetrical blunt tip, the electric field strength around the circumference of the tip surface is identical, so the Taylor cone is usually based on the whole tip outlet surface. However, for an asymmetrical bevelled tip, the strongest field intensity point lies at the sharpest point of the tip surface and draws solution there. In this way, a smaller Taylor cone could reside at this point instead of covering the whole outlet surface. This assumption was demonstrated by photographing the electrospray plume from a bevelled stainless steel emitter. As shown in Figure 2.3,

due to the low wettability of the metal surface and the strongest field strength at the sharpest point, the base of the Taylor cone covers the sharpest edge of the bevel.

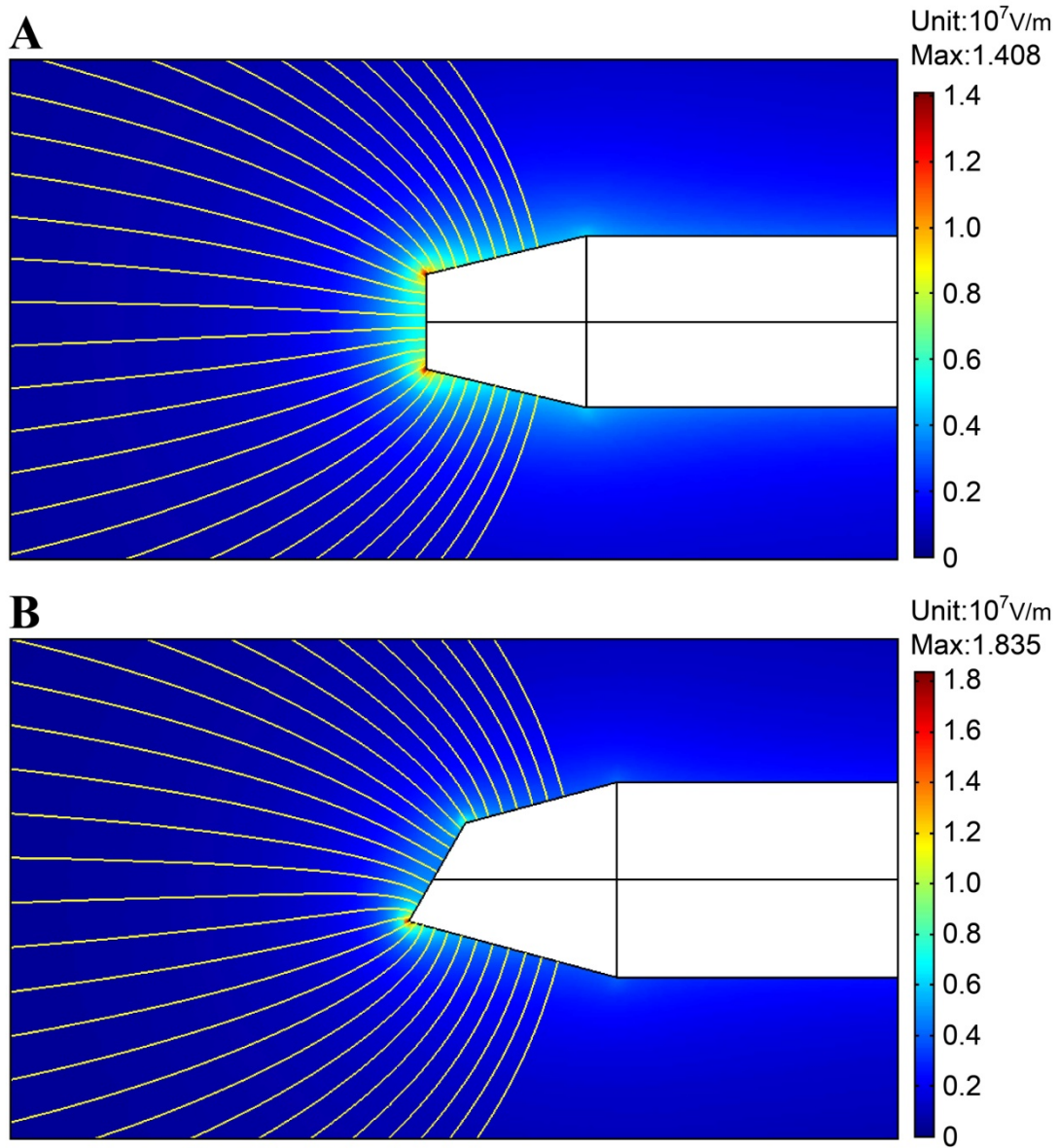


Figure 2.2: Simulated electric field lines for the blunt tapered (A) and beveled (B) stainless steel emitters.

The voltage applied on the tapered blunt tip is 3.8 kV, and the voltage applied on the 35 degree bevelled tip is 3.2 kV Color legend is coded for the intensity of the field.

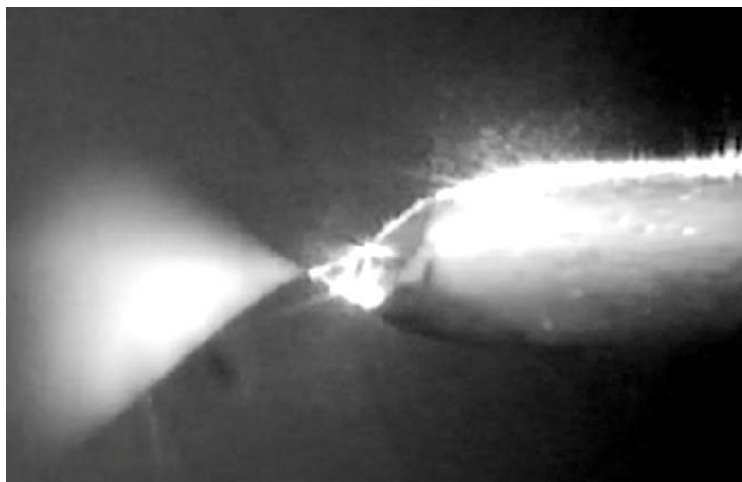


Figure 2.3: Photograph of an electro spray plume from a beveled stainless steel emitter.

2.3.3 Comparison of the flow-through microvial interface and sheath flow interface

A group of 18 protein amino acids was chosen to study the performance of our CE-ESI-MS interface because it involves a variety of chemicals with different properties: hydrophobic and hydrophilic, acidic and basic, aliphatic and aromatic. Since the isoelectric points of these amino acids range from 2.8 to 11.1, a volatile organic acid must be used as electrolyte to charge all of them under positive CE and positive ESI mode. After a series of comparisons, 0.2% formic acid in 50% methanol was chosen to be the run buffer. The 50% methanol was added into the background electrolyte (BGE) to serve three purposes: reduce the surface tension of water to facilitate the electro spray; decrease the conductivity so that the CE current is suppressed to match the ESI current; and minimize the pH change of the BGE and bubble formation due to electrolysis of water. Although the BGE does not have strong buffer capacity, the small current does not change the composition of BGE significantly. To calibrate the MS signal fluctuation from run to run, 50 μ M hydroxyl-proline was used to spike the sample as the internal standard. As shown in Figure 2.4, all the 18 amino acids were separated into three large groups, basic, acidic

and neutral. Due to different ionization and transmission efficiency, the signal responses of these amino acids span two orders of magnitude. The observed signal from cysteine was at m/z 241 (Cys-Cys) instead of the protonated molecular ion because of oxidation under high temperature in the heated capillary region.

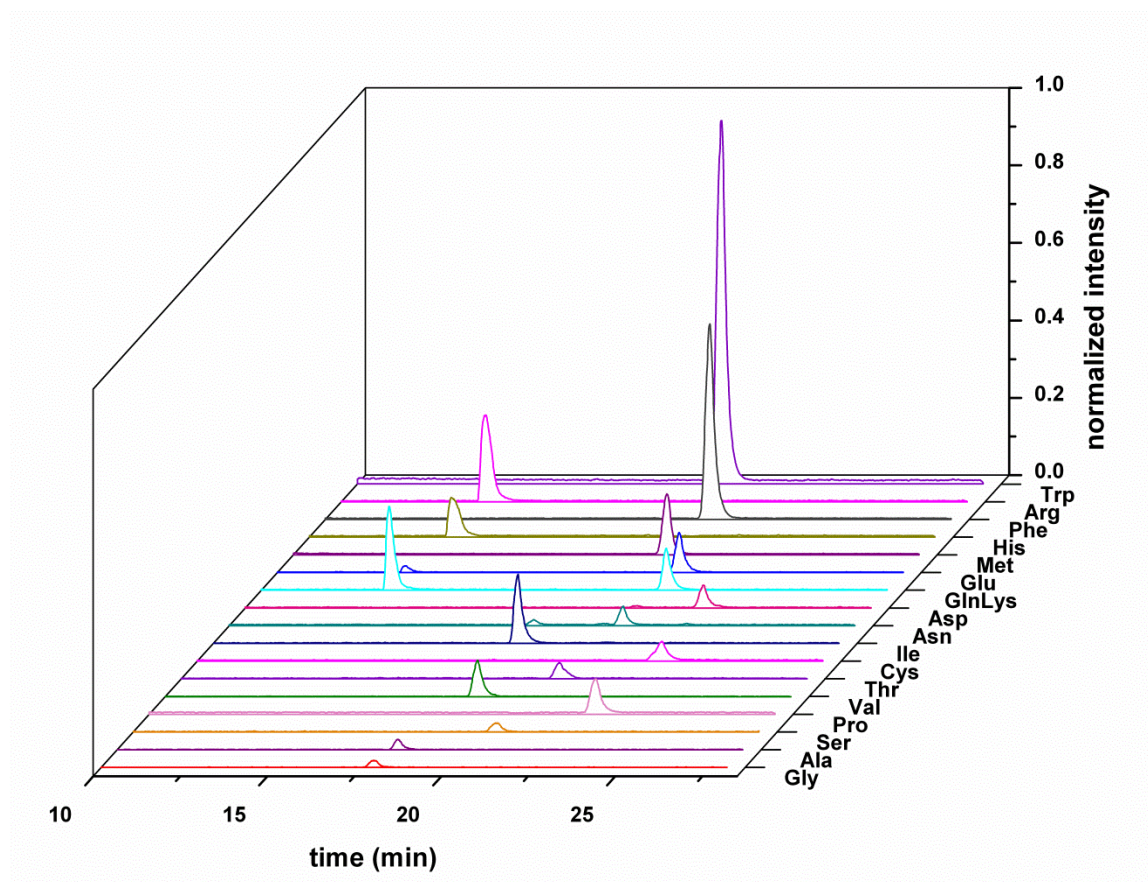


Figure 2.4: Extracted ion electropherograms for a mixture of 18 amino acids. CE capillary: 50 μm ID, 80 cm; BGE and modifier: 0.2% formic acid, 50% methanol; modifier flow rate, 0.2 $\mu\text{L}/\text{min}$; Sample: 100 μM amino acids in BGE injected at 1 psi for 20 s; CE inlet, 30 kV; ESI needle, 4.3 kV; MS inlet capillary, 230 $^{\circ}\text{C}$; ion trap injection time 90 mS; scan range: m/z 70-250.

The amino acid mixture standards calibration was used to compare the performance of the presented interface and the commercial sheath flow interface provided with the LCQ^{DUO}. For the separation of amino acids using the sheath flow interface, the components of BGE and sheath liquid were the same as those used for our home-made

interface. The ESI needle of the commercial sheath flow interface was 22-gauge (0.0285" OD, 0.016" ID) and the separation capillary extruded approximately 1 mm from the ESI probe. The optimal sheath flow rate was found to be 1.0 $\mu\text{L}/\text{min}$ without using sheath gas or nebulizer gas. The sheath flow rate used here is ~ 4 fold larger than that used for our home-made interface, since the capillary column has to extrude out of the ESI probe, which requires a larger ESI tip OD and thus Taylor cone volume. It is also worthwhile to notice that, although the sheath gas and nebulizer gas help evaporation of the solvents, they create negative pressure around the ESI emitter and the pressure induced flow can accelerate the separation process and decrease the peak resolution⁸⁶. Due to the high sheath flow rate for the sheath-flow interface, use of sheath gas was often necessary for efficient desolvation.

The signal-to-noise ratio (SNR) of 100 μM of individual amino acids and the limit of detection (LOD) estimated by peak height over the concentration range 10 to 200 μM using two CE-ESI-MS interfaces are shown in Table 2.1. The home-made interface showed significantly improved detection limits (average 5-fold improvement) compared to the commercial sheath-flow interface. This improvement is enabled by the junction-at-the-tip arrangement and the bevelled tip geometry, which requires smaller modifier flow rate and causes less dilution and increased ionization efficiency of the analytes.

Amino acid	Decoupling interface		Sheath-flow interface		Fold improvement over sheath-flow interface	
	R ²	LOD ^a	R ²	LOD ^a	LOD ^a	SNR ^b
Ala	0.9980	0.7	0.9981	3.8	5	11
Arg	0.9993	0.1	0.9702	0.4	3	3
Asn	0.9954	1.7	0.9783	7.4	4	5
Asp	0.9995	0.6	0.9963	2.3	4	3
Cys-Cys	0.9995	1.0	0.9813	10.9	11	6
Gly	0.9998	1.1	0.9677	6.3	6	4
Glu	0.9979	0.3	0.9950	1.3	4	4
Gln	0.9995	0.2	0.9939	1.1	4	6
His	0.9940	0.4	0.9992	2.4	6	6
Ile	0.9998	0.1	0.9800	0.4	4	6
Lys	0.9964	0.2	0.9731	0.4	2	2
Met	0.9966	1.2	0.9956	2.3	2	2
Phe	0.9985	0.1	0.9946	2.4	17	13
Pro	0.9996	0.9	0.9816	2.4	3	6
Ser	0.9989	3.4	0.9967	5.3	2	4
Thr	0.9995	1.7	0.9846	2.6	2	5
Trp	0.9998	0.1	0.9888	0.2	3	4
Val	0.9992	0.3	0.9904	1.3	5	6

Table 2.1: Amino acids calibration with sheath flow interface and the built-in-house interface.

CE conditions: 75 μ m ID \times ~ 75 cm bare fused silica capillary for CE separation; 75 μ m ID \times ~ 90 cm capillary for modifier delivery; voltage at CE inlet vial 24 kV, ES voltage 4.3 kV; Sample concentration 200,150, 100, 50, 25,10 μ M of each amino acid (except that the glycine concentrations were doubled), 50 μ M was spiked into each sample as internal standard; 0.5 psi 20 s pressure injection; background electrolyte and modifier/sheath flow, methanol/water/formic acid (v/v/v) 50:49.8:0.2; 0.4 psi was applied the CE inlet vial to accelerate the separation.

MS conditions: LCQ^{Duo} ion trap MS scan range m/z 70 ~ 250, heated capillary temperature 230 °C, ion trap injection time 100 mS. Modifier flow rate for the decoupling interface 0.2 μ L /min, sheath flow rate for the commercial interface 1 μ L /min. **a** LOD was calculated by $3\sigma_{\text{blank}}/m$, where σ_{blank} is the standard deviation of the signal of blank, m is the slope of calibration curve. **b** SNR was measured at 100 μ M of each amino acid.

2.3.4 CE-MS separation without EOF or with reversed EOF

Another feature of the 'junction-at-the-tip' interface that the sheathless interface does not possess is that it allows the bulk flow from CE column to be zero or even towards the capillary inlet. As the negatively charged, hydrophilic bare fused silica capillary wall can interact with some analytes, neutral coated capillaries that eliminate charge and hydrophobic interaction, as well as electroosmotic flow, are widely used for the separation of proteins, peptides and carbohydrates. In the absence of bulk flow from the CE column, the sheathless interface emitter cannot spray without assisting pressure applied at the capillary inlet; however, for the 'junction-at-the-tip' arrangement, the modifier flow can flush the analyte out of the microvial and support a stable spray. Figure 2.5 demonstrates this situation by using a neutral coated capillary to separate three basic proteins, cytochrome C, lysozyme and ribonuclease A. In the acidic BGE, 100mM pH 3.1 $\text{NH}_4\text{Ac}/\text{MeOH}$ (v/v) 9:1, the positively charged protein molecules migrate towards the cathode under electric field without EOF, and they are transported to the bevelled tip surface for electrospray ionization by the low modifier flow after arriving at the microvial at the outlet.

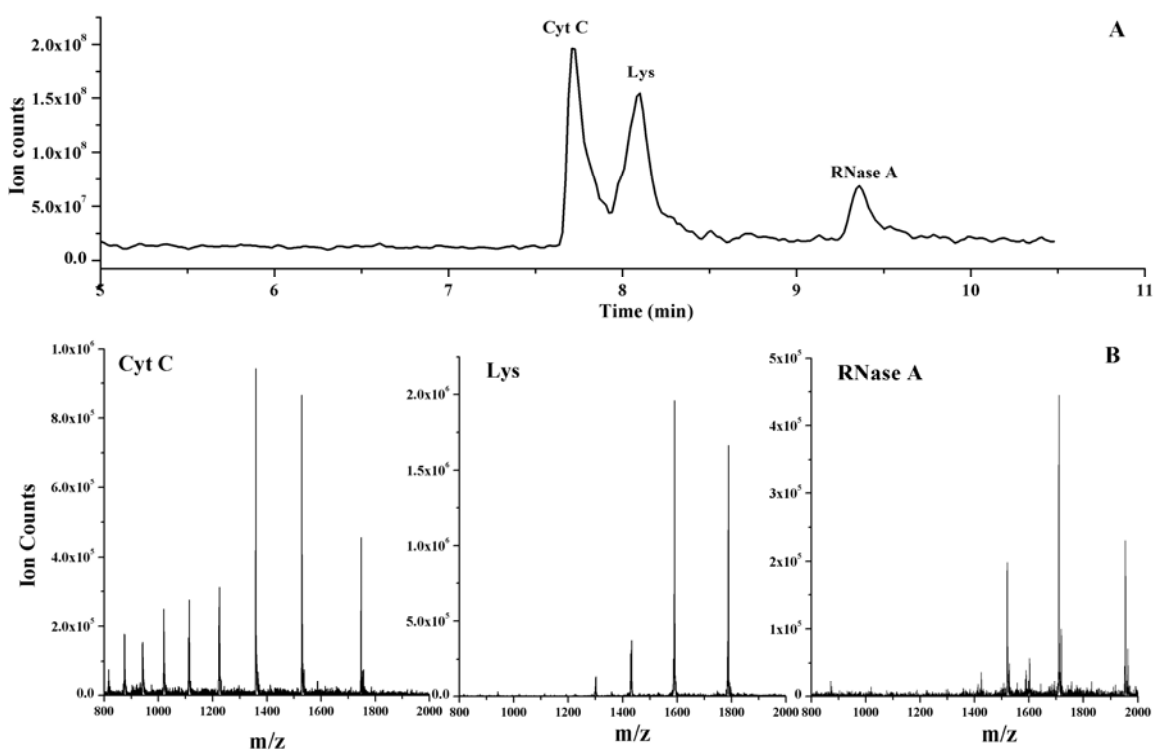


Figure 2.5: Total ion electropherogram (A) and mass spectra (B) of three basic proteins separated under positive polarity with a neutral-coated capillary. CE capillary, 50 μm ID, 67 cm long; BGE, 100 mM NH_4Ac , pH 3.1: MeOH (v/v) 9:1; modifier, methanol:water:formic acid (v/v/v) 90:9.8:0.2, 1.0 psi; sample, 100 mg/mL of protein mixture in BGE injected at 1.0 psi for 10 s; ion trap MS scan range, m/z 800~2000.

The modifier flow does not only maintain the circuit, transport the analytes to the site of electrospray, supply the solution for electrospray, but can also supplement the BGE when the EOF goes towards the inlet. Experimental results of continuous electrophoretic pumping of two analytes, sodium dodecyl sulphate (SDS) and benzenetricarboxylic acid (BCA), shown in Figure 2.6AB, give an example of this type of application. Both analytes were dissolved in the basic BGE (methanol/20mM pH 7.3 NH_4Ac / H_2O (v/v/v) 75:15:10) and the capillary column was filled with the sample solution. The modifier components were the same as BGE to facilitate a negative electrospray. When positive 30 kV was applied at the CE inlet, the EOF towards the outlet brings the negatively charged

SDS ions to outlet electrode (Figure 2.6A); while when negative 30 kV was applied at the CE inlet, the direction of EOF was reversed, the electrophoretic mobility of the negatively charged BCA ions overcomes the electroosmotic mobility, making the net mobility towards the outlet (Figure 2.6B). When the EOF is toward the inlet, the modifier solution in the microvial can split into two directions - one way is to go into the capillary column to supplement the BGE, the other way is to transport the analyte molecules to the site of electrospray. In this case, the volume flow rate of the modifier solution needed to supply the BGE and the electrospray solution is larger than that of sustaining the electrospray alone.

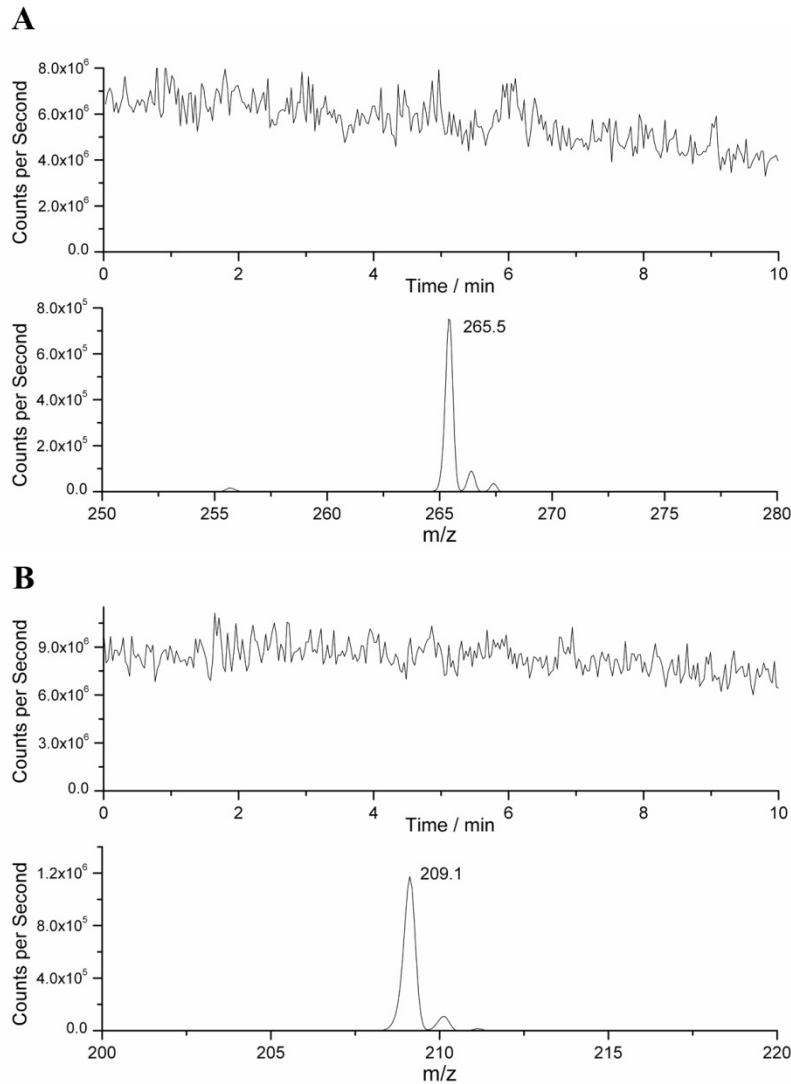


Figure 2.6: Total ion electropherogram and mass spectra of continuous CE infusion of (A) SDS and (B) 1, 2, 4-Benzenetricarboxylic acid.

75 μm ID \times 75 cm bare fused silica capillary for CE infusion, 75 μm ID \times 90cm capillary for modifier delivery. BGE and modifier: methanol/20mM pH 7.3 $\text{NH}_4\text{AC}/\text{H}_2\text{O}$ (v/v/v) 75:15:10.

(A) EOF flows toward the CE outlet. CE inlet voltage +30 kV, ES voltage -3.3 kV; 2.5 psi pressure was applied at the modifier vial. Sample concentration was 0.1 mM in BGE. MS scan range was m/z 250~280.

(B) EOF flows towards the CE inlet. All the CE conditions were the same as (A) except that the voltage applied at CE inlet was -30kV. 3.5 psi pressure was applied at the modifier vial. Sample concentration was 0.5 mM in BGE. MS scan range was m/z 200 ~ 220.

2.3.5 CE-UV-ESI-MS analysis of catecholamines and HPLC peptide calibration standards

Incorporation of online UV detection to CE-MS can provide complementary information on the analytes. Spectrometric information could be obtained from optical spectrometry and structure information can be obtained from mass spectrometry. Here, catecholamine and HPLC peptides were chosen to demonstrate this strategy because they absorb in the UV region and are amenable to ESI. Catecholamines are important neurotransmitters and neurohormones released by the adrenal glands in situations of stress such as psychological stress or low blood sugar levels⁸⁷. Since the chemical structure of the catecholamines (Figure 2.7) are close to that of the aromatic amino acids, the same conditions used for amino acids previously were applied to separate the catecholamines and their analog tyrosine. Figure 2.8 shows the UV trace and total ion electropherograms (TIE) of catecholamines and the tyrosine standard mixture. Comparing the UV trace and TIC, the dopamine peak always has a little tailing; however, the peaks of DOPA and tyrosine do not tail in either the UV trace or the TIE. This observation suggests that the tailing is mainly determined by the properties of the analyte and run buffer. It was also observed that these analytes show different order of sensitivity when detected by the two detection methods: epinephrine is the least sensitive at UV 200 nm but the most prominent by ESI-MS detection; the UV signal of norepinephrine is considerably higher but the ESI-MS signal is lower compared to other analytes. By applying two detection methods in one run, one can choose the method that has a stronger signal-to-noise ratio for a specific analyte to perform quantitative study. Table 2.2 shows

the limit of detection of catecholamines by CE-ESI-MS. The experimental conditions were the same as those used for calibration of amino acid standards.

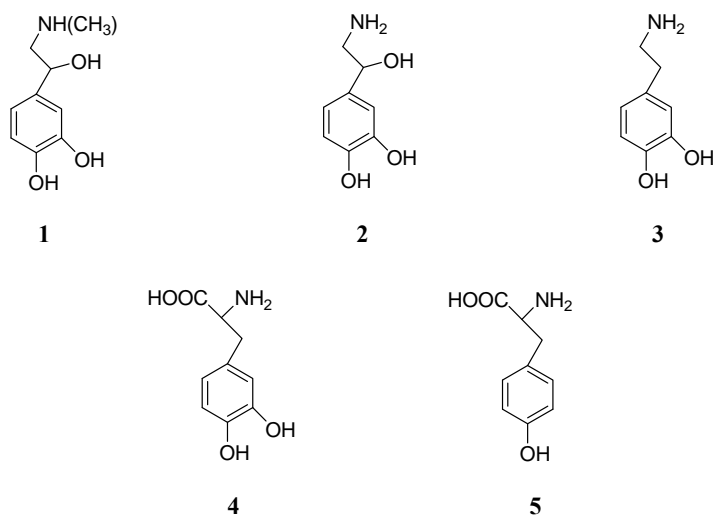


Figure 2.7: Chemical structures of the catecholamines and their analog tyrosine. 1. epinephrine; 2. norepinephrine; 3. dopamine; 4. DOPA; 5. tyrosine.

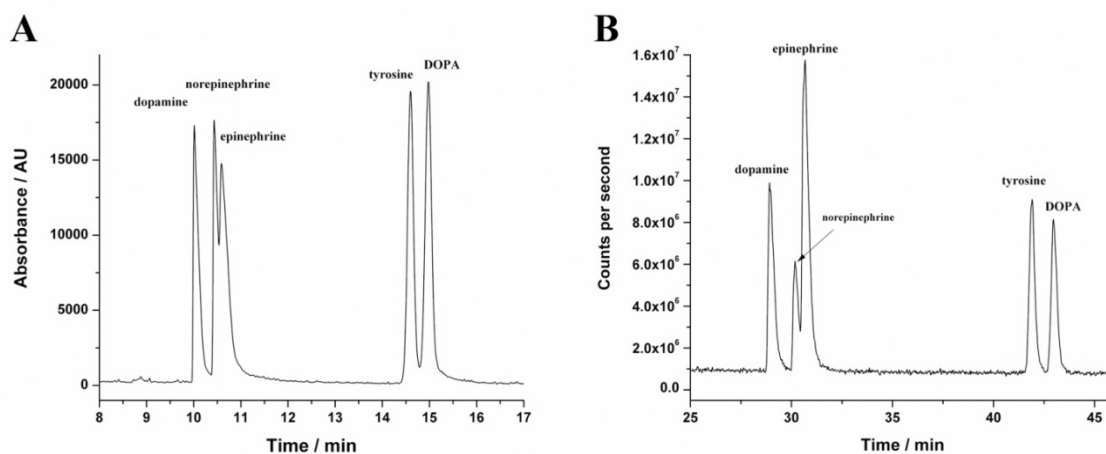


Figure 2.8: CE-UV-ESI-MS analysis of catecholamines and tyrosine standard mixture.

(A) UV trace of the catecholamines and tyrosine. (B) Total ion electropherogram for the catecholamines and tyrosine. Experimental conditions: sample concentration, 150 μ M each; CE capillary 75 μ m ID \times 122 cm, inlet to UV window 40cm; capillary for modifier delivery 75 μ m ID \times 70 cm; capillary inlet voltage, 30 kV; ES voltage, 4.3 kV; sample injection, 5s at 0.5psi; background electrolyte and modifier, methanol/water/formic acid (v/v/v) 50:50:0.2; UV detection wavelength, 200 nm; ion trap MS scan range, m/z 145 ~ 210; 1.2 psi pressure was applied at modifier reservoir.

Analytes	Detected m/z	Linearity correlation (r)	LOD / μ M
Tyrosine	182	0.9997	0.17
DOPA	198	0.9992	0.25
dopamine	154	0.9997	0.09
Epinephrine	184	0.9991	0.08
Norepinephrine	170	0.9964	0.45

Table 2.2: Calibration curve linearity and LOD of the catecholamines.

Experimental conditions: sample concentration, 100, 50, 25, 12.5 μ M; CZE capillary 75 μ m ID \times 98 cm; capillary for modifier delivery, 75 μ m ID \times 75 cm; CZE voltage, 30 kV; ES voltage, 4.3 kV; sample injection, 10 s at 0.5 psi; background electrolyte and modifier, methanol/water/formic acid (v/v/v) 50:49.8:0.2; 0.5 psi pressure were applied at both the CE buffer vial and the modifier vial. MS conditions: ion trap scan range, m/z 145~210, heated capillary temperature 200 $^{\circ}$ C, on trap injection time 100 mS.

To separate the HPLC peptide standards, 50% acetonitrile and 0.2% formic acid in deionized water was used as the BGE because the mixture of acetonitrile and water has a lower viscosity in which peptides could migrate faster. Figure 2.9 shows the UV trace and summed extracted ion electropherogram of the HPLC peptide standards. As angiotensin II contains one basic acidic amino acid residue, arginine, whose side chain could bear a positive charge, it migrates fastest in spite of its longer chain. Only the doubly charged ion of Angiotensin II at m/z 524 was used in the extracted ion electropherogram because its intensity is much stronger than the singly charged ion. Since the total length of the separation capillary was three times the distance from the inlet to UV window, the migration times in the MS electropherogram were also three times of that in the UV trace. In the UV trace, only four peaks could be detected and they were not fully resolved; while in the summed extracted ion electropherogram, all the five peaks were detected and the first three peaks were fully resolved due to longer migration time. Again, the signal intensities of the analytes change order in different detection

methods. Although Leu enkephalin and Met enkephalin, which only differ by one amino acid residue, coelute last, they were resolved in the second dimension of separation in gas phase (Figure 2.9C). At the concentration of 1 $\mu\text{g}/\text{mL}$ for each component, the detected MS signal-to-noise ratios were 6, 14, 25, 24, 21 for Gly-Tyr, Val-Tyr-Val, Leu enkephalin, Met enkephalin and angiotensin II respectively.

The two experiments only provide simple examples to prove the possibility of CE-UV-ESI-MS. Due to the limitation of using commercial CE instrument, the UV detection window is located too far away from the MS inlet so that the resolution of the UV peaks could be much smaller than that of the MS peaks. If this problem could be resolved, the UV detection can provide more information on the analytes.

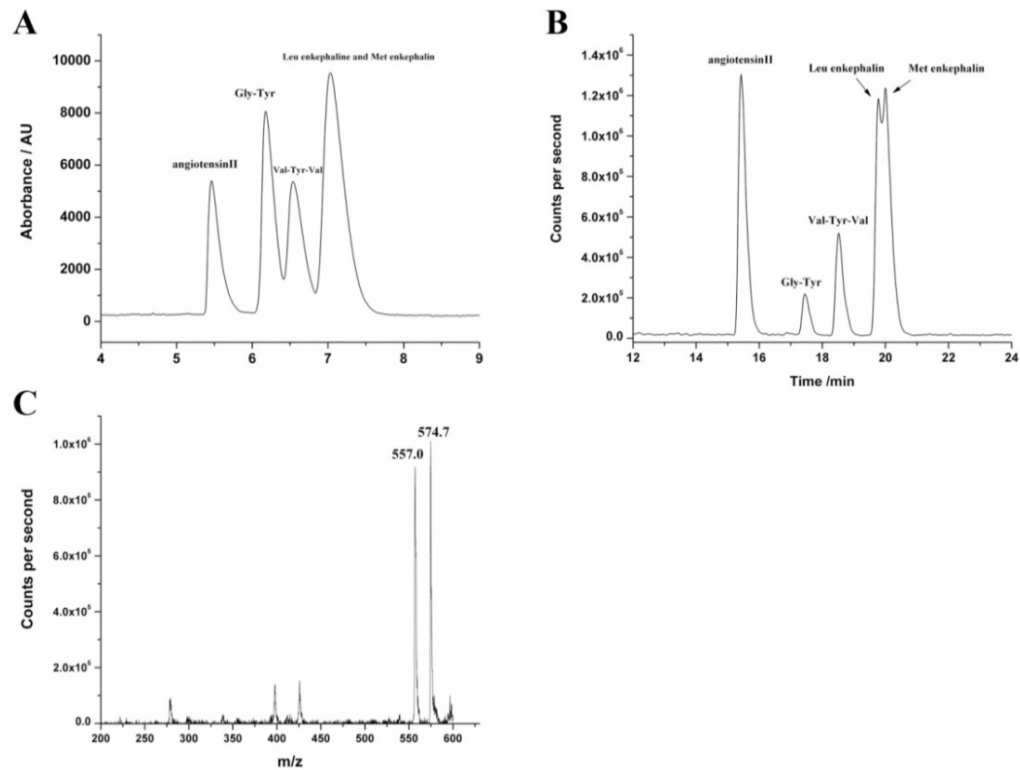


Figure 2.9: CE-UV-ESI-MS of HPLC peptide standard mixture.

(A) UV trace of the HPLC peptide standard mixture. (B) Summed extracted ion electropherogram of the HPLC peptide standard mixture. Angiotensin II $[M+2H^+]^{2+}$ m/z 524, Gly-Tyr $[M+H^+]^+$ m/z 239, Val-Tyr-Val $[M+H^+]^+$ m/z 381, Leu enkephalin $[M+H^+]^+$

m/z 557, and Met enkephalin $[M+H]^+$ m/z 575. (C) Spectrum at 19.88min when Leu enkephalin and Met enkephalin coeluted.

Experimental conditions: sample concentration, 40 $\mu\text{g/mL}$ for each component; CZE capillary 75 $\mu\text{m ID} \times 122 \text{ cm}$, inlet to UV window 40 cm; capillary for modifier delivery 75 $\mu\text{m ID} \times 70 \text{ cm}$; voltage at the capillary inlet, 30 kV; ES voltage, 4.3 kV; sample injection, 3 s at 0.5 psi; background electrolyte and modifier, acetonitrile/water/formic acid (v/v/v) 50:50:0.2; UV detection wavelength, 200 nm; ion trap MS scan range, m/z 200 ~ 600; 1.2 psi pressure was applied at modifier reservoir.

2.3.6 Automated CE-ESI-MS system

The presented CE-ESI-MS interface is easily incorporated into commercial CE and MS instruments. With the MDQ or PA800 plus capillary electrophoresis system (Beckman Coulter Inc, CA) programmed CE-MS sequence runs can be performed automatically. Figure 2.10 shows the total ion electropherograms of 15 successive separations of Angiotensin I&II peptides using PEI coated capillary. The polarity of CE was set negative since the positively charged capillary wall generates EOF towards the s. s. sprayer needle, which serves as the anode for both CE and electrospray. Although the electrophoretic mobility of the peptides in acidic BGE is toward the inlet, the strong forward EOF overrides the electrophoretic mobility and carries all the analytes to the outlet. With the automated controls of sample injection, voltage ramping, modifier flow supply provided by commercial instruments, good reproducibility of the separation can be achieved. The variations of migration time and the peak height of the traces shown in Figure 2.10 are very small from run to run.

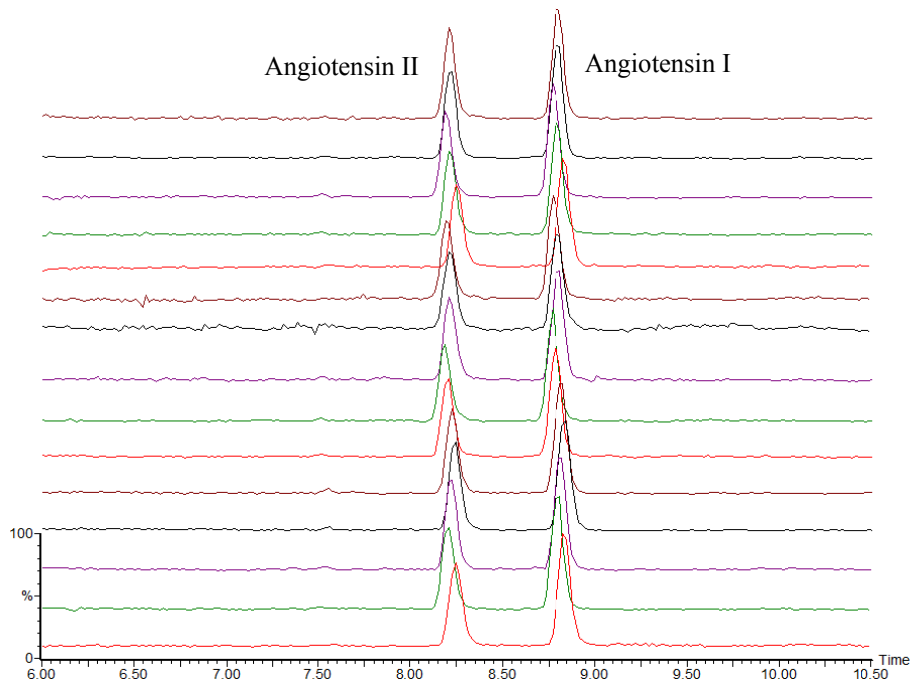


Figure 2.10: Total ion electropherograms of 15 successive programmed sequence runs of Angiotensin I&II.

Capillary: 80 cm \times 50 μ m ID, polyethyleneimine coated; BGE: 1% formic acid, 25% methanol; Modifier, 0.1% formic acid, 75% isopropanol, 1 psi; Sample: 20 μ M Angiotensin I and II in water : BGE (v/v) 9:1 injected at 5 psi for 5 s; CE inlet, -30 kV; needle, +4.3 kV; Q-TOF MS scan range m/z 410~550; sample cone voltage, 30 V; sample cone temperature 150°C.

2.4 CONCLUSIONS

The CE-ESI-MS interface using a flow-through microvial described in this chapter, featuring robustness, longevity, sensitivity, ease of fabrication and adaption to a commercial instrument, provides a competitive alternative to the current CE-MS coupling techniques. The bevelled tip geometry design guarantees the small modifier flow rate and minimizes the dilution effect. The low modifier flow in the microvial formed by the interior of the sprayer needle provides stable electric contact and improves the electrospray ionization efficiency. This interface can accommodate any type of capillaries, with or without EOF, or even EOF towards the inlet. Good sensitivity and reproducibility

were achieved by incorporating the interface into an automated, controlled CE and MS instruments.

Chapter 3: Mass transport in the flow-through microvial of a capillary electrophoresis-mass spectrometry interface

3.1 INTRODUCTION

A new CE-ESI-MS interface with a flow-through microvial, which decouples the electrical and solution flow rate requirements of the separation and ionization processes, has recently been designed and applied in different kinds of sample analysis by our group⁸². It uses a 360 μm outer diameter CE capillary inserted as far as possible into a stainless steel emitter needle with a bevelled tip, so that the space enclosed by the end of CE column and inner surface of stainless steel tip forms an open flow-through microvial. Figure 3.1A shows a schematic of the approximate arrangement of the CE outlet microvial. A chemical modifier solution supplied by an additional grounded reservoir is added at a low flow rate to the microvial to support the effluent flow rate and sustain stable electrospray. This low flow rate chemical modifier pushes the effluent from CE to the outside of the tip, and stabilizes the electric contact by constantly providing fresh electrolyte into the space in the microvial with minimal dilution to the sample. This setup has been used for many types of compounds⁸² and has the advantages of using more durable larger outer diameter capillaries, good sensitivity, and compatibility with a larger range of usable flow rate⁸⁵.

However, there are concerns about possible postcolumn band broadening introduced by the micro flow through vial at the sprayer tip. This concern is also relevant for other “junction-at-the-tip” CE-ESI-MS interfaces⁷⁵⁻⁸⁰, where the separation capillary is usually surrounded by a tapered outer tube but does not extrude out of it, and the CE effluent mixes with a makeup flow inside the ESI emitter. Although the band broadening of CE in free solution has been extensively studied^{5,6,88}, these studies mainly focus on on-column peak broadening factors such as injection length, longitudinal diffusion, wall adsorption

and Joule heating, and little attention has been paid to the postcolumn band broadening issues. In this chapter, investigation focuses on the flow profiles of the CE effluent and the chemical modifier inside the flow-through microvial and the effects of these flows on the peak shapes through both numerical simulation and CE-MS experiments. It is demonstrated that the MS detected peak is not distorted significantly with the presence of a low flow chemical modifier inside the nanoliter postcolumn volume microvial. The approach established in this work is also applicable for studying similar postcolumn band broadening issues in liquid chromatography and chip-based separation techniques⁸⁹ with different types of postcolumn detectors.

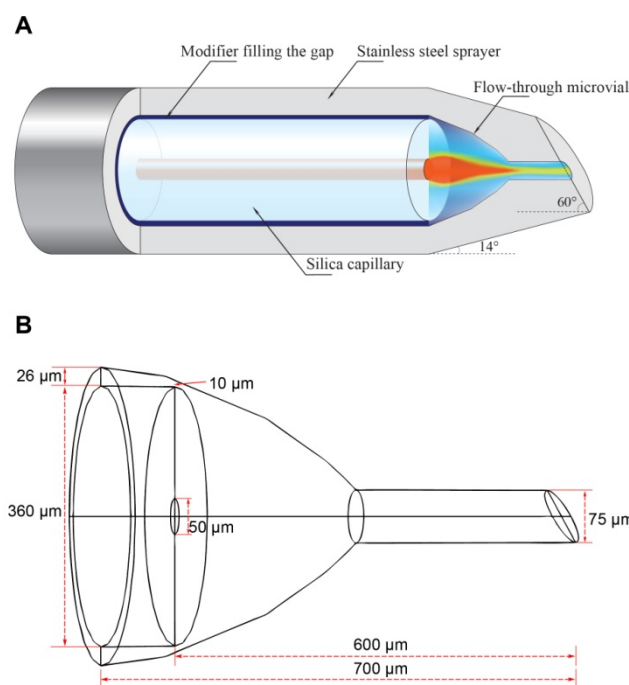


Figure 3.1: (A) Schematic of the flow-through microvial of a junction-at-the-tip capillary electrophoresis mass spectrometry interface. (B) Geometry of the flow-through microvial established in COMSOL where the electro osmotic flow mixes with the modifier solution.

A 360 μm outer diameter CE column is inserted into the stainless steel emitter and the space enclosed by the end of CE column and inner surface of stainless steel tip forms an open flow-through microvial for CE outlet. The CE effluent mixes with the modifier solution inside the microvial. The microvial was composed of two parts, a parabolic-shaped micro chamber and a 75 μm ID straight microchannel which ends with a 60 degree beveled angle. Both parts may contribute to band broadening. The length of the tapered part of the stainless steel tip was 700 μm . The distance from the silica capillary end to the outlet of the stainless steel tip was 600 μm . The gap between the outer surface of the silica capillary and the inner surface of the stainless steel tip began from 26 μm and shrank to 10 μm gradually. The OD of the silica capillary was 360 μm and ID was 50 μm .

3.2 THEORY

The mass balance equation (3-1) governs the mass transport process in the flow-through microvial, depicted in Figure 3.1A, and in turn determines the band broadening of a chemical species coming through the CE-MS interface⁸⁵.

$$\frac{\partial c}{\partial t} = -\vec{v} \cdot \nabla c - \nabla \cdot (D \nabla c) + R \quad (3-1)$$

The right side of eq (3-1) includes three terms: the convective flux term $-\vec{v} \cdot \nabla c$, the diffusion flux term, $-\nabla \cdot (D \nabla c)$, and the chemical reaction term, R . For the notations used in eq (3-1), c is the concentration of a species, t is the time, \vec{v} is the net velocity of this chemical species, D is the diffusion constant of the chemical species in the medium and R is the chemical reaction rate. In fact, the origins of all the contributors to the peak width can be found in the mass balance equation. For example, in capillary zone electrophoresis, injection length determines the initial condition of the mass balance equation; longitudinal diffusion is attributed to the diffusion flux term; analyte-analyte interaction and analyte-wall interaction are related to the kinetics of chemical reaction term R ; and pressure induced laminar flow, Joule heating, temperature gradients, electromigration dispersion, nonuniform electric field are all sources of nonuniform net velocity, \vec{v} . Accordingly, the band broadening caused by the post-column volume can also be analyzed by the mass balance equation. Because the geometry of the microvial at the tip is irregular and the flow inside is driven by pressure, the nonuniform flow pattern is the major source of post-column band broadening.

3.3 MODELING

Because of the complexity of microvial geometry and the differential equations used to describe the flow patterns, we have to recourse to the finite element method to solve the flow field and mass transport process in the microvial. Three dimensional models simulating the flow-through microvial were constructed using the commercial software package COMSOL Multiphysics 3.5 (COMSOL Inc., Los Angeles CA). Concentration

profiles under different conditions after peaks pass through the microvial were generated by solving the momentum balance and mass balance equations sequentially, and then they were compared to the observed peak profiles in UV detection and MS detection experiments.

3.3.1 Geometry

The length of the tapered part of the stainless steel tip was measured to be 700 μm after bevelling. As shown in Figure 3.1B, the geometry of the open flow-through microvial was established in a three-dimensional Cartesian coordinates system. The microvial was enclosed by the end of the fused silica capillary column and the inner surface of the tapered stainless steel tube. The gap between outer surface of the silica capillary and the inner wall of the straight part of the stainless tube was 26 μm and gradually shrinks to 10 μm at the end of the silica capillary. The microvial was composed of two parts, a parabolic shaped micro chamber followed by a 75 μm ID straight micro channel which ends with a 60 degree bevelled angle. The distance from the end of silica capillary to the outlet of the microvial is 600 μm . The volume of the parabolic part of the microvial was estimated to be 15.5 nL by domain integration with COMSOL, and the volume of the straight channel part was 1.4 nL. The combined contribution to band broadening from both parts is estimated in this paper. Meshing parameters were set as follows: maximum element size scaling factor 0.35, element growth rate 1.35, mesh curvature factor 0.3, mesh curvature cutoff 0.005, resolution of narrow regions 0.85, and maximum element size on the boundaries for modifier entrance 20 μm . Total number of mesh elements was 35698.

3.3.2 Physical conditions

Figure 3.2 depicts the general process of the physical modeling. First, the hydrodynamic flow inside the microvial was solved by the Navier – Stokes equation (3-2) coupled with continuity equation for incompressible continuum (3-3), where \vec{v} is the velocity vector, p is the static pressure, ρ is fluid density, η is dynamic viscosity, and I is the identity matrix.

$$\rho(\vec{v} \cdot \nabla \vec{v}) = \nabla \cdot [-pI + \eta(\nabla \vec{v} + (\nabla \vec{v})^T)] \quad (3-2)$$

$$\nabla \cdot \vec{v} = 0 \quad (3-3)$$

Eq (3-2) states a balance between inertia force and the sum of pressure gradient and viscous friction of the fluid. It is assumed that the density and viscosity of the fluid are constant, and the velocity field does not vary with time once it reaches the steady state. For simplicity, the physical parameters of water at 25°C were used for the fluid mixture inside the microvial.

The steady state solution of the velocity field was obtained with the boundary conditions listed below:

$$\vec{v} = 0 \quad (3-4)$$

$$\vec{v} = v_0 \vec{n} \quad (3-5)$$

$$p = 0 \quad (3-6)$$

Equation (3-4) is the boundary condition for the inner surface of the microvial, which implies that the fluid at the wall is stationary. Equation (3-5) is set as the boundary conditions for the entrances of CE bulk flow and modifier flow, v_0 corresponds to the linear velocity of electroosmotic flow or modifier flow respectively, and \vec{n} indicates the

flow direction is normal to the boundary. Equation (3-6) gives the boundary condition for the outlet of the microvial.

Numerical solutions of the incompressible Navier-Stokes equations $\vec{v}(x,y,z)$ were stored in the model and passed onto the next step for solving the mass balance equation (3-7) along with these initial condition and boundary conditions (3-8 ~ 3-12):

$$\frac{\partial c}{\partial t} = -\vec{v} \cdot \nabla c - \nabla \cdot (D\nabla c) \quad (3-7)$$

$$c = 0 \quad \text{at } t = 0 \quad (3-8)$$

$$c = f(t) \quad (3-9)$$

$$c = 0 \quad (3-10)$$

$$\vec{n} \cdot (-D\nabla c + c\vec{v}) = 0 \quad (3-11)$$

$$\vec{n} \cdot (-D\nabla c) = 0 \quad (3-12)$$

Electromigration in the microvial region was not considered here since the surface of the metal needle has a uniform voltage and so the potential gradient inside the microvial is negligible. The diffusion coefficient was estimated as $5 \times 10^{-10} \text{ m}^2/\text{s}$ for small molecules, as we found that the longitudinal diffusion is not significant in such a short time scale (several seconds) for the peaks passing through the microvial. Equation (3-8) is the initial condition of the overall domain which defines that no analyte fills the microvial at the beginning. In Eq (3-9), $f(t)$ is a function of time that describes the concentration of analyte at the entrance for CE bulk flow, which could be a constant, a well-defined Gaussian function, or fitted curve of UV traces in the following simulation. Equation (3-10) is the boundary condition for the modifier entrance. Equation (3-11) defines that there is no normal flux across the inner wall of the microvial. Equation (3-12) confines the

material flux at the outlet boundary to be convective only. Time-dependent solver was chosen for the mass balance equation (3-7). The initial time step was set as 0.005 s, and the maximum time step was set as 0.02 s. Solutions $c(x, y, z, t)$ were saved every 0.02 or 0.04 s. All the calculations were done by a PC with an AMD Athlon 64×2 dual core processor and 4G RAM.

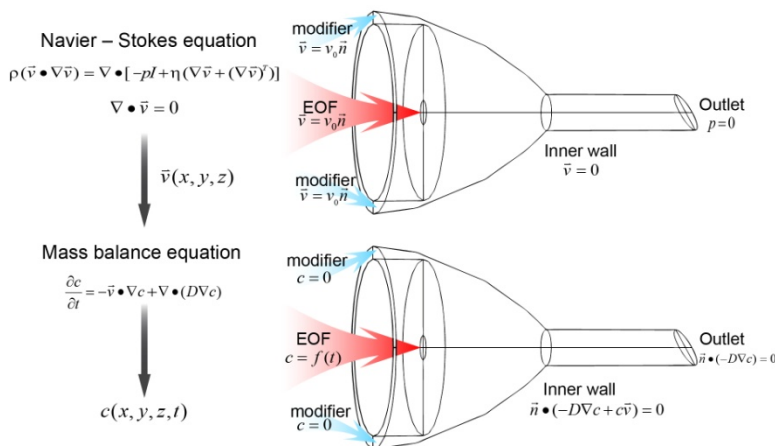


Figure 3.2: Illustration of the physical modeling process and boundary conditions. Numerical solutions of the Navier-Stokes equation were passed on to the mass balance equation to solve concentration distribution of analyte in the microvial.

3.4 MATERIALS AND METHODS

3.4.1 Chemicals and materials

Tryptophan, DOPA (D, L-3,4-dihydroxyphenylalanine) and epinephrine were purchased from Sigma-Aldrich (St. Louis, MO, USA). Ammonium acetate buffer (0.1 M pH 3.1) was from Beckman Coulter; isopropanol (HPLC grade) and formic acid (88%), dimethyl sulfoxide (DMSO) were from Fisher Scientific (Nepean, Ont., Canada). Fused silica capillary (75 and 50 μm ID, 360 μm OD) was purchased from Polymicro Technologies (Phoenix, AZ). A polyethylenimine (PEI) capillary coating solution was

obtained from Gelest, Inc. (Morrisville, PA). All analytes were dissolved in the ammonium acetate buffer, stored at -4 °C and diluted to 50 µM before use.

3.4.2 Instrumentation

CE-UV experiments were performed on a P/ACE MDQ capillary electrophoresis system (Beckman Coulter Inc., Fullerton, CA). A 50 µm ID, 78 cm long (68 cm to detection window) PEI coated capillary was used for separation. Samples were injected by 0.5 psi pressure at the inlet for 14 s. Ammonium acetate buffer (0.1 M pH 3.1) was used as the background electrolyte (BGE). Before each run, the capillary was rinsed with the BGE for 3 min. During the separation, -16.2 kV was applied across the capillary to generate an electroosmotic flow toward the capillary outlet. The composition of the buffer in the outlet vial was the same as the chemical modifier that would be used in the CE-MS experiments. The UV detection wavelength was set at 200 nm. 10% DMSO spiked in the run buffer was used as the EOF marker. The cartridge temperature was set at 27 °C during the separation.

CE-ESI-MS experiments were performed by coupling a P/ACE MDQ electrophoresis system with a modified capillary cartridge (Beckman Coulter Inc., Fullerton CA) for external detectors, which could host both the capillary for separation and the capillary for chemical modifier delivery, and a Micromass Q-TOF 1E mass spectrometer (Waters, Milford MA) with the nanospray source replaced by our homemade interface. The setup for the CE-ESI-MS interface was as described in Chapter 2. The major parameters for MS operation were set as follows: source temperature 120 °C, cone voltage 16 V, scan range 160 to 220 amu, scan time 0.5 s, and inter scan delay 0.1 s. To match the experimental conditions used in UV detection as much as possible, a 50 µm ID, 68 cm long PEI coated

capillary was used for separation. The 0.1 M pH 3.1 ammonium acetate buffer was used as the BGE, and the isopropanol/water/formic acid (v/v/v) 75/24.8/0.2 mixture was used as the chemical modifier. Samples were injected by 0.5 psi pressure at the inlet for 12 s to load the same amount of sample as that of the CE-UV experiment. To obtain the same electric field strength applied as for UV detection, -10.1 kV was applied at the CE inlet, and 4 kV was applied at the electrospray needle. A 75 μm ID, 80 cm long bare fused silica capillary was used for chemical modifier delivery. The pressure applied at the modifier vial was 1~ 4 psi, to generate a flow rate of 60~240 nL/min. All of the CE-MS separations were operated under room temperature without coolant circulation.

3.5 RESULTS AND DISCUSSION

3.5.1 Simulation of steady-state flow patterns in the flow-through microvial

Compared to conventional on-column optical detection methods, such as an absorption spectrometry, the small volume at the end of the CE capillary in a junction-at-the-tip CE-MS interface is expected to contribute to some additional band broadening. Based on the model definition, it is expected that the flow rates of the EOF and modifier will play an important role in determining the extent of band broadening and changes in peak shapes. The aim of this study is to find the conditions under which this type of band broadening is negligible compared to the total band broadening during a CE-MS run. Three models representing three typical situations were constructed. In the first model, situation (i), both the EOF rate and modifier infusion rate were set at 100 nL/min. In the second model, situation (ii), the EOF rate was set at 200 nL/min, and the modifier flow rate was set at zero. In the third model, situation (iii), the EOF flow rate was set at zero and the modifier flow rate was 200 nL/min. In this case the analytes exit the capillary based only on

electrophoretic migration. Figure 3.3 A-C compare the flow fields simulated under these different boundary conditions. Figure 3.3 D-F show the concentration distributions of the analyte in the microvial, corresponding to the three situations described above, respectively, when the analyte is continuously infused by electrokinetic pumping. The steady state solution of the mass balance equation was acquired by letting $f(t) = \text{constant} = 1 \text{ mM}$ and using the stationary solver to solve the following equation:

$$\frac{\partial c}{\partial t} = 0 = -\vec{v} \cdot \nabla c - \nabla \cdot (D \nabla c) \quad (3-13)$$

Under common conditions when both EOF and modifier flow rate are moderate, as described in the first situation, the flow pattern inside the microvial has ordered laminar flow characteristics, and the modifier helps to push the analyte out of the microvial. The analytes do not travel through the microvial at a constant velocity. At the entrance of the microvial, the CE bulk flow rate suddenly drops as it enters a much larger space and then increases to a higher level later on, as soon as all the fluid is pushed into the narrower straight micro channel exit. Guided by the flow profile and chamber geometry, the analyte concentration near the center of the microvial entrance is less diluted by the chemical modifier and the fluid along the central line moves the fastest. Despite the fact that the analyte molecules diffuse toward the peripheral region where the modifier has a very low concentration of analyte, the modifier flushes them toward the exit. At the outlet of the microvial, the analyte concentration is diluted by approximately two times as the total flow volume is increased by one fold.

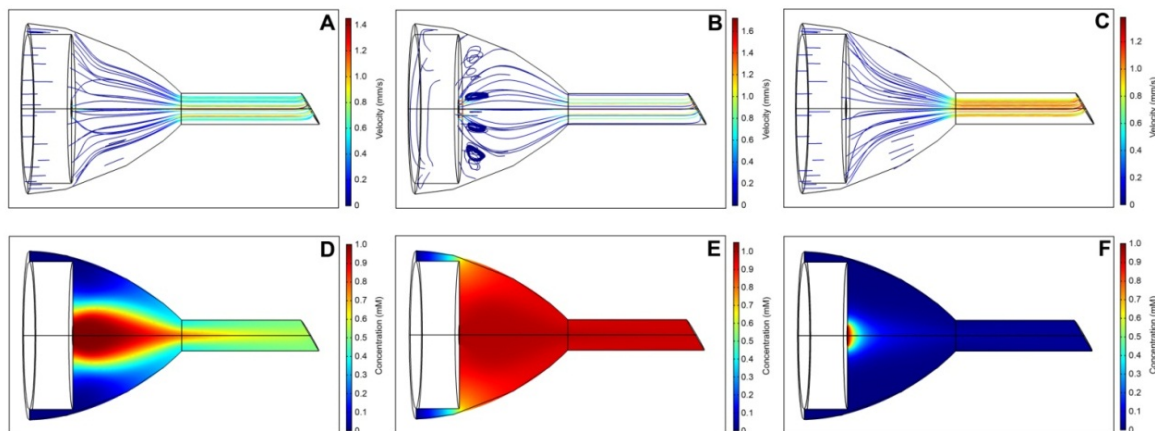


Figure 3.3: (A-C) Simulated velocity field and (D-F) concentration distribution when analyte is constantly infused into the microvial under different conditions. (i) both EOF rate and modifier flow rate are set at 100 nL/min (A, D); (ii) EOF is set at 200 nL/min and modifier flow rate is set at zero (B, E); (iii) EOF is set at zero and modifier flow rate is set at 200 nL/min (C, F).

In the second scenario, when the modifier flow is absent, the eddy flows emerge at the corners of the chamber so that a dead volume forms. Lacking the flow contribution from the modifier, the flow streams from the silica capillary are more divergent when they enter the parabolic micro chamber. The analyte diffuses more rapidly toward the dead volume region, and they quickly fill the chamber.

The third situation has been demonstrated experimentally in Chapter 2. When the EOF is suppressed by the neutral capillary coating or in low pH BGE, the modifier itself could sustain a stable electrospray and flush out the analytes. As seen in Figure 3.3C, the flow streams that originate from the chemical modifier entrance converge into the center of micro chamber and eventually go into the exit channel.

3.5.2 Simulation of band broadening for a transient analyte peak

To get a clear view of the processes occurring as a peak passes through the microvial, we simulated the situation where a Gaussian peak with amplitude of 1 mM, standard deviation of 4 s exits the CE capillary. To make such simulation possible, we first defined

$$f(t) = e^{-\frac{1}{2} \times \left(\frac{t-12}{4}\right)^2} \quad (3-14)$$

and the transient solutions of the mass balance equation were then calculated. The averaged concentrations on the outlet boundary at each time step for the above three types of situations were sent to a spreadsheet and plotted versus time in Figure 3.4. From these data, it can be concluded that it only takes at most 4 s for the peak center to travel through the microvial under the circumstance that EOF is absent; and the peak widths in the time domain are increased by no more than 3 s compared to the original peak.

Figure 3.5 illustrates the time progress as a Gaussian peak travels through the microvial in Situation (i). The analyte concentration exiting the CE capillary reaches a maximum at 12 s, while the outlet of the microvial experiences maximum concentration at 15 s. During the first half of the Gaussian peak, the concentration distribution shows a profile that is similar to the steady state solution in Figure 3.3D. The analyte zone expands when it comes out of the 50 μm ID fused silica capillary, and this zone gradually shrinks in the radial direction as the parabolic chamber shrinks to a 75 μm ID channel. The radius of the sample stream could be approximated as the sum of the radius of hydrodynamic flow streams that originate from the 50 μm ID capillary and the diffusion induced radius⁹⁰. As the second half of the Gaussian peak enters the microvial, the concentration of analyte exiting the capillary decreases and the rear part of the analyte

concentration distribution also reveals a parabolic profile. Throughout the 20 s process, the analyte zone is always kept in the central part of the chamber.

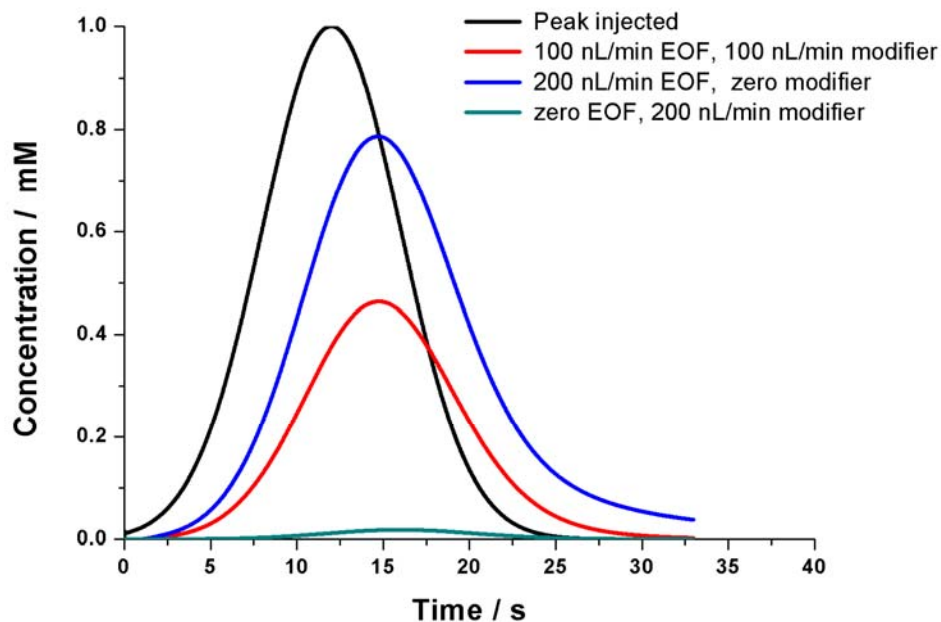


Figure 3.4: Simulation of peaks eluted from the microvial if a transient Gaussian profile peak (peak height 1 mM, peak centre 12 s, standard deviation 4 s) is injected into the microvial.

A three parameter Gaussian function $f(t) = A \exp(-1/2(t-t_0)/\sigma)^2$ was used to fit the eluted curves under different situations: (i) both EOF rate and modifier flow rate are set at 100 nL/min, $A = 0.461$ mM, $t_0 = 14.90$ s, $\sigma = 4.381$ s ; (ii) EOF is set at 200 nL/min and modifier flow rate is set at zero, $A = 0.772$ mM, $t_0 = 15.04$ s, $\sigma = 4.693$ s ; (iii) EOF is set at zero and modifier flow rate is set at 200 nL/min, $A = 0.118$ mM, $t_0 = 16.11$ s, $\sigma = 4.336$ s.

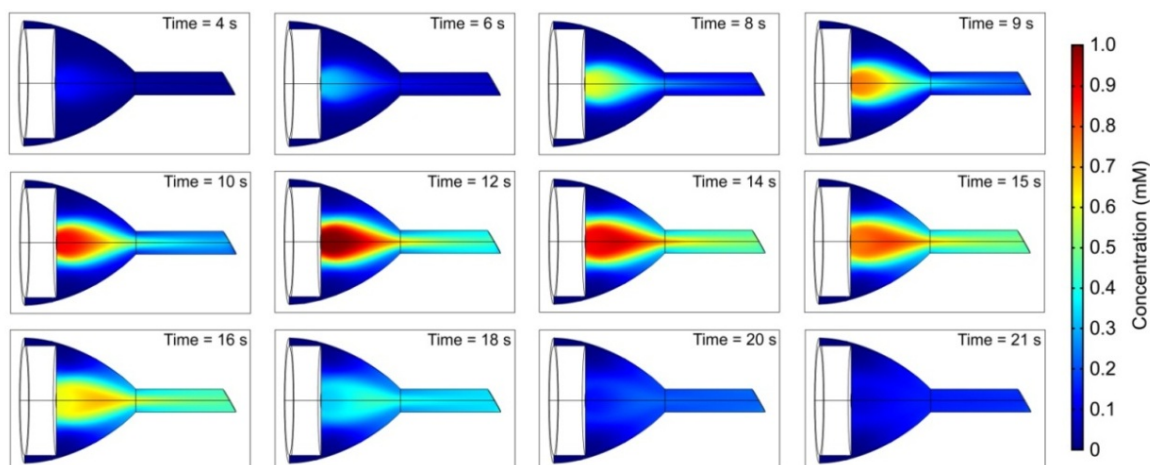


Figure 3.5: Simulated time progress of analyte concentration distribution in the microvial.

A Gaussian peak (peak height 1 mM, center 12 s, standard deviation 4 s) is injected with the EOF rate of 100 nL/min and the modifier flow rate of 100 nL/min.

3.5.3 Experimental verification of modeling results

For the purpose of investigating peak broadening in the postcolumn region experimentally, CE-UV and CE-ESI-MS runs were conducted separately. Tryptophan, DOPA, and epinephrine were chosen as analytes because they all possess UV-absorbent functional groups and basic amine groups that are easily ionized by positive ion ESI. The effective capillary length, sample injection time, field strength, and background electrolytes were arranged to be consistent in the UV and MS runs, in order to eliminate band broadening caused by other factors when comparing the peak widths. As coolant circulation was not available in our CE-MS experiments, the cartridge temperature for the UV runs was set at room temperature (27°C), to offset heating from the UV lamp. In the UV experiment, the outlet vial contained the chemical modifier solution used for CE-MS experiment instead of background electrolyte in order to simulate the situation that the end of the silica capillary was surrounded by the modifier flow during the CE-MS runs.

The linear velocity of EOF was measured to be 2.043×10^{-3} m/s (~ 240 nL/min), and the modifier flow rate as 3.28×10^{-5} m/s (~ 60 nL/min) for 1 psi pressure applied at the modifier vial. Variation of the detected MS signal intensity under different modifier flow rates was insignificant and this suggests that the MS detector responds to the mass flux of analytes under these conditions. Therefore, the dilution effect is not a concern.

According to the above parameters determined experimentally, the EOF and modifier linear velocities were used as boundary conditions in the numerical simulation to generate the flow field in the microvial for different modifier delivery rates. UV data were exported as ASCII files using 32 Karat software (BeckmanCoulter, LA) and then imported to Origin 7.0 to perform baseline subtraction and normalization. The peak data were then imported into COMSOL Multiphysics to define the function $f(t)$ in Eq (3-9). These data were interpolated by piecewise cubic functions and the user defined function served as the boundary conditions for the EOF entrance in the mass balance equation. The convective flux on the outlet boundary was integrated for each time step, normalized to the maximum point, and then plotted versus time to simulate the real peak detected by MS.

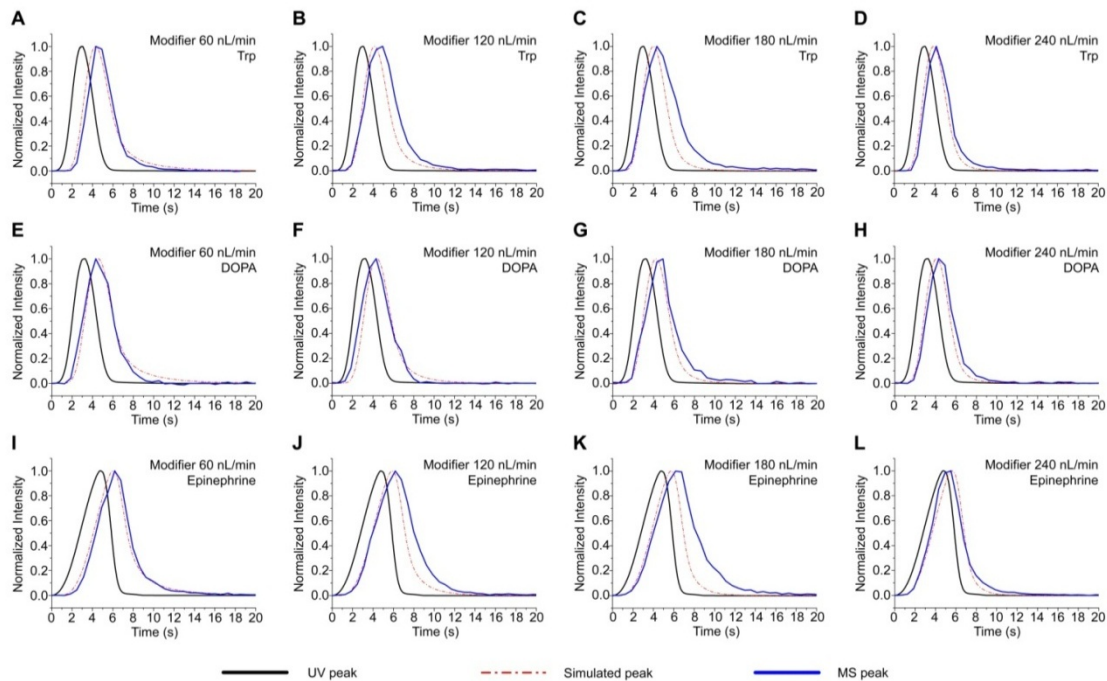


Figure 3.6: Comparison of UV detected peaks, COMSOL simulated peaks, and MS detected peaks of tryptophan, DOPA, and epinephrine under different modifier flow rate.

(A),(B),(C), and (D), tryptophan, modifier flow rate 60, 120, 180, and 240 nL/min, respectively; (E),(F), (G), and (H), DOPA, modifier flow rate 60, 120, 180, and 240 nL/min, respectively;(I), (J), (K), and (L) Epinephrine, modifier flow rate 60, 120, 180, and 240 nL/min, respectively. EOF rate is 240 nL/min.

Figure 3.6 shows the comparisons of UV peaks, simulated MS peaks, and MS detected peaks for three analytes under different modifier flow rates. The time scale in this figure does not reflect the analyte migration time in the whole separation process; it starts from the moment that the front of the analyte peak enters the microvial. The UV traces of tryptophan and DOPA have symmetric Gaussian profiles, while the epinephrine peak is fronting due to electromigration dispersion⁹¹. Table 3.1 summarizes the peak width (4 times of standard deviation) of all the UV, simulated and MS peaks.

	UV peak widths (s)	COMSOL simulated MS peak widths (s)				MS detected peak widths (s)			
		Modifier flow rate (nL/min)				Modifier flow rate (nL/min)			
		60	120	180	240	60	120	180	240
Tryptophan	3.75	4.93	4.60	4.37	4.21	4.54	5.68	6.08	4.35
DOPA	3.96	5.12	4.79	4.56	4.39	5.30	5.30	5.25	4.65
Epinephrine	5.11	6.21	5.86	5.63	5.48	6.09	7.29	7.70	5.57

Table 3.1: Comparison of peak widths (in seconds) of UV detected peaks, COMSOL simulated peaks and MS detected peaks of tryptophan, DOPA and epinephrine.

The fact that several MS peaks show longer tailing than the simulated ones suggests that there is some error in the model or some variation in the experiments. Possible sources of error in the modeling include: (i) the manufacturer’s tolerances limit the geometric precision of the inner surface of the microvial; (ii) uncertainty in the gap between the end of the CE column and microvial, which cannot be measured directly; (iii) the density and viscosity of the fluid in the microvial could vary with the volumetric flow rate ratio of the EOF and the chemical modifier; (iv) numerical errors accumulated from solving the two differential equations. There are also several possible sources of experimental error: (i) the lack of temperature control in the CE-MS operation gives rise to extra band broadening caused by temperature gradient and Joule heating; (ii) the liquid volume of the Taylor cone that resides on the beveled sprayer tip surface increases as the total flow rate goes up, which might also become a source of dead volume when the modifier flow is relatively high; (iii) the data acquisition rate of MS detector was 0.6 s per scan, which is much slower compared to the time step set in the modeling; (iv) bubbles due to electrolysis inside the microvial might disturb the transportation process.

Despite the possible systematic errors discussed above, the results shown in Figure 6 and Table 1 provide us some insight on the extra band broadening that arises from the postcolumn dispersion. Since the variance of a peak is additive for independent contributors of band broadening⁷, provided that the environmental differences when running the UV and MS experiments are negligible, we can assume that the total variance of the MS peak is the sum of variance of the UV peak and the variance attributed to postcolumn band broadening, and thus it could be written as

$$\sigma^2_{MS} = \sigma^2_{injection} + \sigma^2_{diffusion} + \sigma^2_{other} + \sigma^2_{postcolumn} = \sigma^2_{UV} + \sigma^2_{postcolumn} \quad (3-15)$$

From Figure 3.4, when the injected peak width is 16 s, postcolumn variance is 15-27% of the total variance of the simulated MS peak, depending on the EOF and modifier flow rate. From data in Table 3.1, when the EOF flow rate is very fast and UV peaks are extremely narrow (peak width 3.7-5.1 s), the simulation results suggest that 13-42% of the total variance is contributed by postcolumn dispersion as the modifier flow rate varies. Compared to the UV peaks, the variance of the detected MS peaks increased from 15% to 62%, which might also include band broadening induced by other factors such as temperature gradient and Taylor cone dead volume. It is also clear that postcolumn band broadening varies with different operational conditions. Because of the additivity of variance⁷, the percentage contribution from the postcolumn band broadening to the total peak variance of a wider on-column peak will be smaller compared to a sharper on-column peak. Under certain conditions of modifier flow rate, the postcolumn variance is minimal and most of the UV peak features, like the fronting peak of epinephrine, are preserved in the MS peak shape (Figure 3.6 I-L). Thus, with careful optimization of flow rates, the peak shape may not be significantly affected by the postcolumn volume in the

micro flow through vial in the junction-at-the-tip configuration.

3.6 CONCLUSIONS

The flow dynamics and mass transport processes inside the flow-through microvial or other types of “junction-at-the-tip” CE-MS interfaces can be simulated using finite element method by constructing three-dimensional models in COMSOL Multiphysics. The simulation results demonstrate that the flow profile inside the microvial is laminar when a low flow rate of modifier solution is used. The chemical modifier helps to flush the analyte molecules out of the micro chamber and keeps them from stagnating in the microvial, and thus the peak shape is not distorted with the presence of the chemical modifier. The numerical predictions were verified by experimental results. Comparison of peaks observed by UV detection and MS detection reveals that the main features of the UV peak have been retained in the MS peak, although the peak width may increase to some extent depending on the width of the peak entering the microvial, the electrosmotic flow rate and the modifier flow rate. Nevertheless, the postcolumn band broadening can be minimized by optimizing the composition and flow rate of the chemical modifier. This study also provides an easy-to-use numerical approach to study general postcolumn band broadening issues in other separation techniques. The simulations can approach the experiment results closer by having finer meshing of the geometries if the computation power allows, and better temperature control with liquid cooling of the whole capillary in real experiments.

**Chapter 4: Basic compounds of drugs of abuse analyzed by capillary
zone electrophoresis – electrospray – mass spectrometry**

4.1 INTRODUCTION

Drug testing and analysis is an important research field for pharmacology, metabolism studies, forensic toxicology, and anti-doping drug screening in sports competitions. Although the LC-MS has a established reputation in this area⁹², CE-MS still has several advantages making the application of this technology valuable. Firstly, as the amount of sample specimen, which could come from blood, tissue, oral fluid, sweat, hair, urine, is usually very limited, the nano-litre range injection volume required by CE is ideal for real sample analysis. Secondly, for regular laboratory analysis of batches of samples, CE is more environmental friendly since the consumption of organic solvent is much less than that of LC. The volume of CE buffer vial is only approximately 2 mL, and typical modifier flow rate for our CE-MS interface is smaller than 1 $\mu\text{L}/\text{min}$; while LC runs at tens to hundreds of microlitre per minute. In addition, the fast separation and high efficiency of CE is suitable for clinical analysis of large amount of samples.

CE-ESI-MS have been applied in several categories of drug analysis in recent years^{59,93,94}. For basic compounds of drugs of abuse with amine-containing side chains, N-containing saturated or aromatic rings, electrospray ionization generally gives $[\text{M}+\text{H}]^+$ signals. Coupling CE to MS or MS^n , a second or even third dimension of separation in the gas phase increases the confidence of confirming the existence of a certain compound. Selected multiple reaction monitoring (MRM) is the most popular mode to analyze drug compounds qualitatively and quantitatively. In this way, interfering species that have an identical precursor mass-to-charge ratio, but a different fragmentation pattern, can be excluded. Among different types of mass analyzers, both ion trap and triple quadrupole can perform MRM analysis. However, triple quadrupole is usually a better choice for

interfacing with a continuous ion source, because of the higher sensitivity due to the higher duty cycle and faster scan rate. For a triple quadrupole mass spectrometer operating in MRM mode, the first quadrupole setting at specific DC and RF voltages selects the parent ions that possess a specific mass-to-charge ratio; then the selected parent ions collide with the inert gas molecule in the collision cell, which is usually another quadrupole operated in RF only mode; the collision induced fragmented daughter ions enter the third quadrupole, which is set at specific DC and RF voltages that only let ions with specific mass-to-charge ratio to go through. If there are multiple pairs of parent /daughter ions to be monitored, the DC and RF voltages applied on the three quadrupoles can be switched simultaneously among the parameters for these pairs of parent/daughter ions, allowing the detector to record the ion counts of each compound for a short period of time.

In this chapter, the analyses of two groups of basic drug standards using CE-ESI-MS with the flow-through microvial interface are demonstrated. The low flow rate requirement and low dilution effect of this CE-MS interface improves the detection sensitivity. The absence of nebulizer gas further improves the separation efficiency⁹⁵. Combined with MRM detection mode, the linear detection range of 0.5~250 parts per billion (ppb) can be achieved. Although only separation of standards were optimized, the method could be adapted to real sample analysis by using pre-treatment methods such as liquid – liquid extraction, or solid phase extraction^{95,96}.

4.2 MATERIALS AND METHODS

4.2.1 Chemicals and materials

Bare fused silica capillaries were purchased from Polymicro Technologies (Phoenix AZ). 88% formic acid, methanol (HPLC grade), sodium hydroxide (A.C.S. reagent) and ammonium hydroxide (A.C.S. reagent), were purchased from Fisher Scientific (Nepean ON). Stock solutions of basic drug mixture I (Figure 4.1) and II (Figure 4.2) in 10 mM pH 2.38 phosphate buffer were kindly provided by our collaborator at Beckman Coulter. Each component was present at 5 µg /mL with the exception of methoxamine, which was at 10 µg /mL. The stock sample solutions were diluted by 10 mM pH 2.38 phosphate buffer to double of the desired concentration, and then mixed with an equal volume of methanol prior to use. 20 mM ammonium acetate solutions were titrated by 0.1 M hydrochloric acid (A.C.S. reagent) to pH 2.5, 5 and 6.1, and by ammonium hydroxide (A.C.S. reagent) to pH 7.3 and 9, and then filtered through 0.22 micron filters (Millipore, Billerica, MA). The ammonium acetate buffer solutions were mixed with HPLC grade methanol 1:1 (v/v) before use as background electrolyte. The modifier solution was made by mixing HPLC grade MeOH/water/formic acid (v/v/v) 90:9.8:0.2.

4.2.2 Instrument and method

Bare fused silica capillaries for CE separation were flushed by methanol, 1 M NaOH, water, and BGE for 20 minutes each before use. Prior to each run, the capillary was rinsed by 2% (v/v) ammonium hydroxide for 3 minutes at 50 psi, water for 3 minutes at 50 psi, BGE for 5 minutes at 50 psi. For optimizing the BGE for separation of drug mixture I and II, 80 cm ×75 µm ID capillary was used for separation, samples were injected at 0.5 psi for 10 seconds, and 25 kV was applied at the inlet vial during

separation. For drug mixture I calibration, 80 cm×50 ID μm capillary was used for separation, samples were injected at 10 kV for 16 s, and 30 kV was applied at the inlet vial during separation. 0.5 μg/mL doxapram was spiked into the drug mixture I calibration standard solution as internal standard. To prepare calibration standards, 100 μL aliquots of doxapram, dissolved in methanol at 5μg/mL, were dispensed in clean glass tubes and left in the fume hood overnight for methanol evaporation. After that, 1 mL solutions of drug mixture I in 10 mM pH 2.38 phosphate buffer at different concentrations were added into each tube, and each tube was vortexed about 10 seconds. These standard solutions were mixed with methanol 1:1 (v/v) before analysis. The final concentrations of each component in the calibration standard mixture were 250, 125, 62.5, 31.2, 15.6, 7.81, 3.91, 1.95, 0.98, 0.49 ng/mL. To check sample carry over from the previous run, blank solutions with internal standard only were injected as sample after every 5 runs of the standard.

Interfacing of the capillary electrophoresis system with mass spectrometry was realized by using the flow-through microvial interface described in Chapter 2. Mass analysis was carried out using Finnigan LCQ*Duo ion trap (Thermo Scientific, Waltham MA) for the BGE optimization. Electrospray voltage was set at 4.4 kV, and the heated capillary temperature was set at 230°C. The scan range was m/z 170~270. The ion trap injection time was set at 150 mS. The MS scanning parameters were optimized on peak m/z 212 by continuous infusion of a 10 μM methoxamine solution using the ‘Autotune’ function.

A Xevo TQ mass spectrometer (Waters, Milford, MA) was operated in multiple ion monitor (MRM) mode for drug mixture I calibration. The cone temperature was set at

150°C. The cone voltage, collision energy, parent and daughter ion masses for each compound were optimized while continuously infusing the drug mixture I solution by electrokinetic pumping. The optimized parameters are listed in Table 4.1. The dwell time for each ion channel was set at 0.035 s. Scan time was set at 1 second.

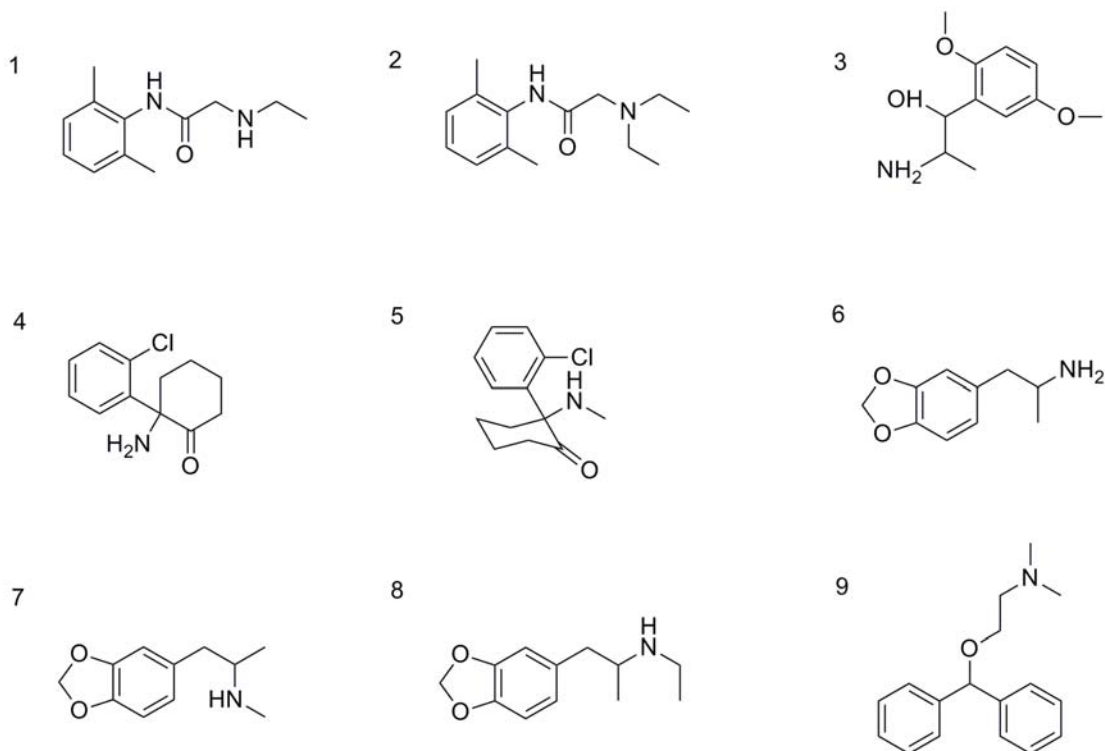


Figure 4.1: Chemical structures of drug mixture I.

1. Monoethylglycinexylidide (MEGX); 2. Lidocaine; 3. Methoxamine; 4. Norketamine; 5. Ketamine; 6. 3,4-Methylenedioxyamphetamine (MDA, 3, 4-); 7. 3,4-Methylenedioxymethamphetamine (MDMA, 3, 4-); 8. 3,4-Methylenedioxy-*N*-ethylamphetamine (MDEA, 3, 4-) 9. Diphenhydramine.

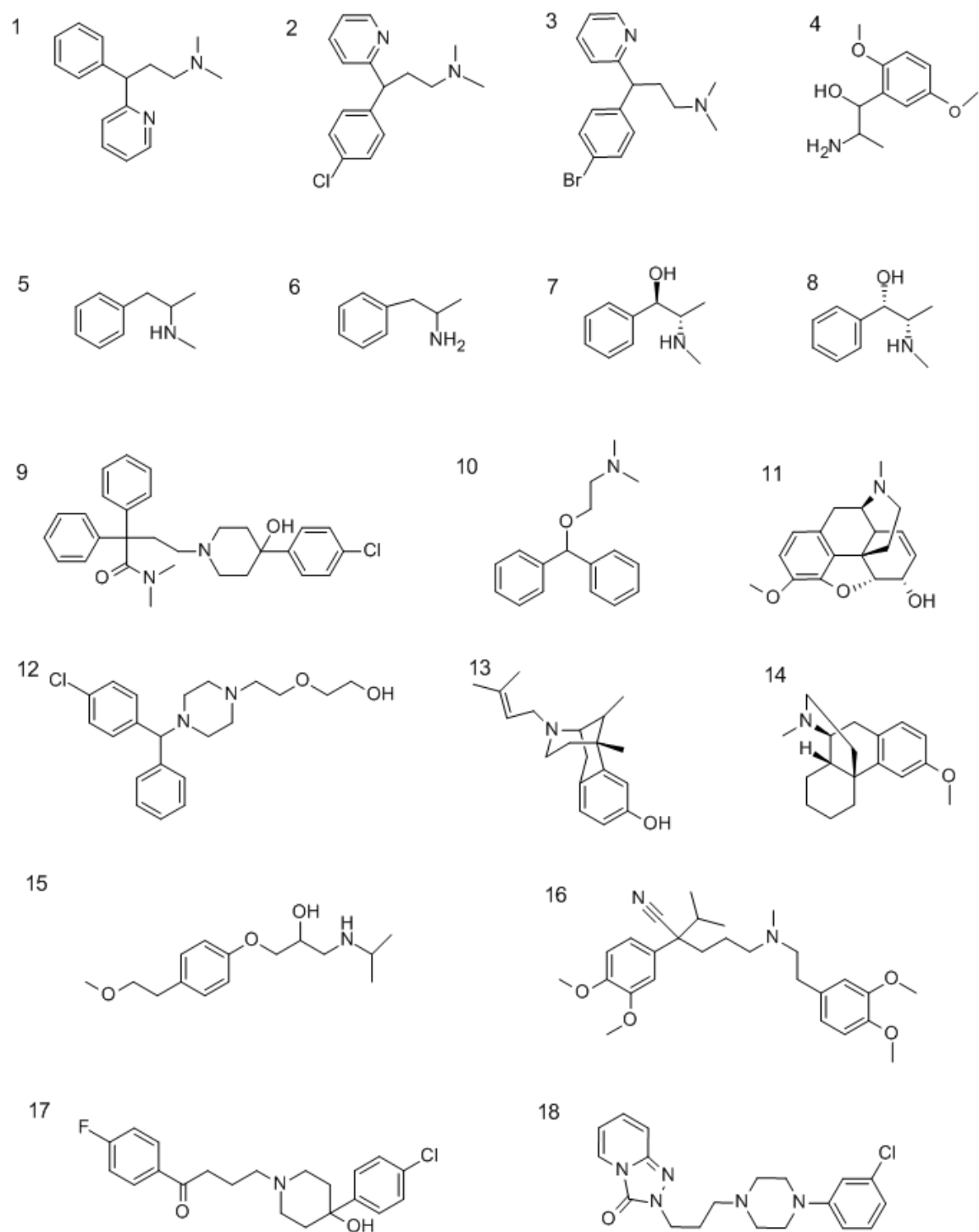


Figure 4.2: Chemical structures of drug mixture II.

1. Pheniramine; 2. Chlorpheniramine; 3. Brompheniramine; 4. Methoxamine;
 5. Methamphetamine; 6. Amphetamine; 7. Ephedrine, (-)-; 8. Pseudoephedrine, (+)-;
 9. Loperamide; 10. Diphenhydramine; 11. Codeine; 12. Hydroxyzine; 13. Pentazocine;
 14. Dextromethorphan; 15. Metoprolol; 16. Verapamil; 17. Haloperidol; 18. Trazodone.

4.3 RESULTS AND DISCUSSION

The drug mixtures were provided in pH 2.38 phosphate buffer as they had been well characterized previously in this buffer system using capillary electrophoresis with photodiode array (PDA) detection by our collaborator at Beckman Coulter⁹⁷. Figure 4.1 and 4.2 show the chemical structures of these basic drugs, which suggest the suitability of electrospray ionization detection. The aromatic rings make these compounds have greater surface activity and amine groups make them easily charged by protons under acidic conditions. Although the analytes are all basic drugs, the pK_a of the amine groups can be quite different, depending on whether they are primary, secondary, tertiary, or aromatic amines, and the induction effect caused by adjacent functional groups. Intramolecular and intermolecular hydrogen bonding also affect the basicity of the amine groups in water solution. Based on this consideration, pH of the background electrolyte is a critical factor for optimizing the CE separation of these compounds. Ammonium acetate was chosen as the electrolyte for its volatility, and 50% methanol was added into the background electrolyte to suppress the current and improve the electrospray stability. In order to prevent peak distortion, 50% methanol was also added into the sample solution to decrease the conductivity of the sample plug. Acidic background electrolytes (pH 2.5) were first tested for the separation. However, due to the low electroosmotic flow and the conductivity difference between the sample zone and buffer zone, tailings of the peaks were quite significant. In addition, as most of the amine groups are fully charged under very acidic condition, the resolutions of the extracted ion peaks in the acidic buffers (Figure 4.3A, 4.5A) are not optimal. Increasing the pH of BGE resulted in better peak resolution and separation (Figure 4.3, 4.5) because of the larger net charge difference on

these compounds. When the BGE is basic, formic acid in modifier solution provides protons to charge the analyte molecules in the microvial before electrospray ionization. Based on these comparisons, 20 mM pH 7.3 NH₄Ac/MeOH (v/v) 1:1 was the optimal BGE for drug mixture I CE-MS separation, and 20 mM pH 9 NH₄Ac/MeOH v/v 1:1 was the optimal for separation of drug mixture II. Figure 4.4 and 4.6 show the extracted ion electropherograms under the optimal separation conditions for drug mixtures I and II respectively. Ephedrine and pseudoephedrine are diastereomers which possess similar size-to-charge ratio in the aqueous phase and same mass-to-charge ratio in the gas phase. They were only partially resolved by CZE under this condition (Figure 4.6). Strategy for further improvement of the separation efficiency might include adding chiral additives, such as cyclodextrins, in the background electrolyte to modify the net mobility of this pair of diastereomers.

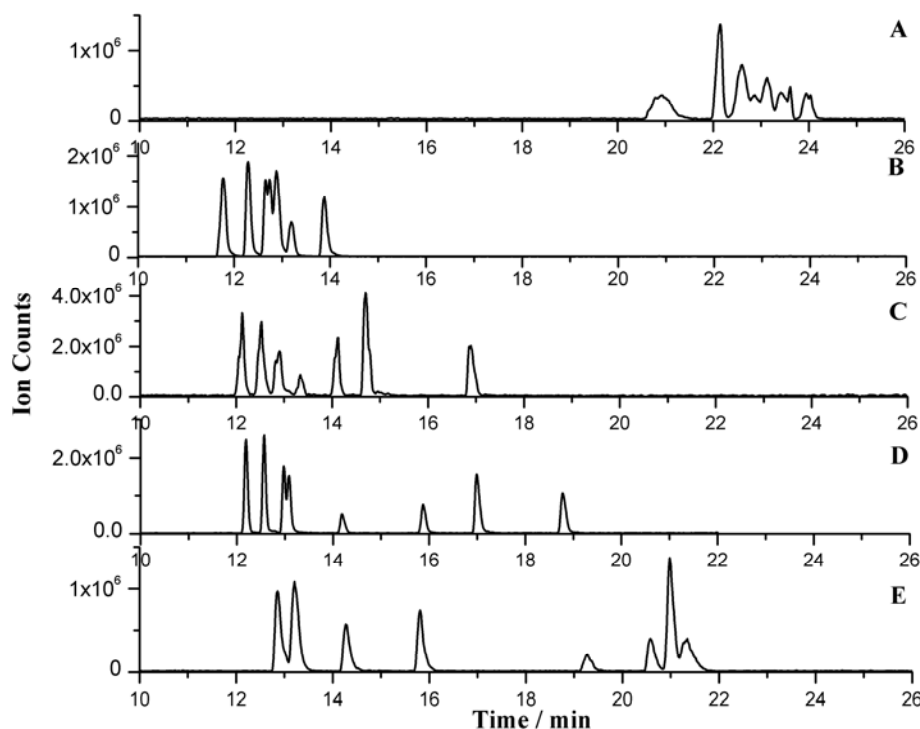


Figure 4.3: Summed extracted ion electropherograms of separation of drug mixture I under different conditions.

Background electrolyte: (A) 20 mM pH 2.5 NH₄Ac/MeOH v/v 1:1; (B) 20 mM pH 5 NH₄Ac/MeOH v/v 1:1; (C) 20 mM pH 6.1 NH₄Ac/MeOH v/v 1:1; (D) 20 mM pH 7.3 NH₄Ac/MeOH v/v 1:1; (E) 20 mM pH 9 NH₄Ac/MeOH v/v 1:1. Modifier solution: 90% MeOH and 0.2% formic acid. Samples were in 5 mM phosphate buffer and 50 % methanol at concentration of 2.5 µg/mL, except that methoxamine was at 5 µg/mL, and were injected by applying 0.5 psi for 10 seconds at the inlet vial. MS detection was performed by Finnigan LCQ*Duo ion trap in full scan mode.

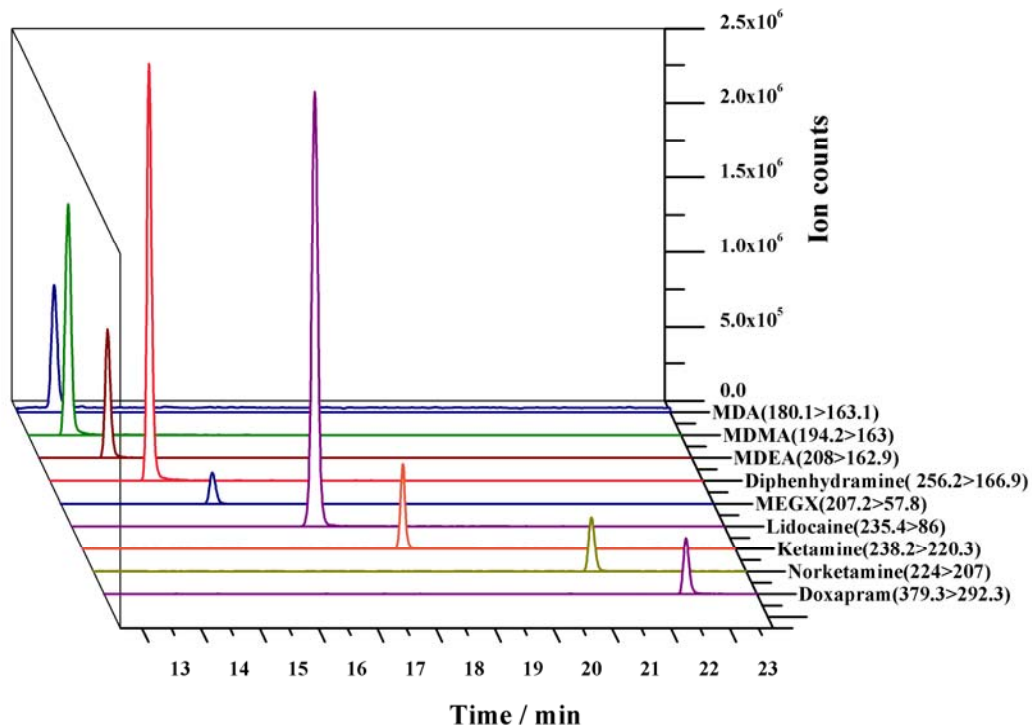


Figure 4.4: Extracted ion electropherograms of separation of drug mixture I. Mass analysis was performed by Xevo TQ mass spectrometer in MRM mode. Concentration of each component was 250 ng/mL. Background electrolyte: 20 mM pH 2.5 NH₄Ac/MeOH v/v 1:1; Modifier solution: 90% MeOH and 0.2% formic acid. Samples were injected by applying 10 kV at the anode electrode for 16 s.

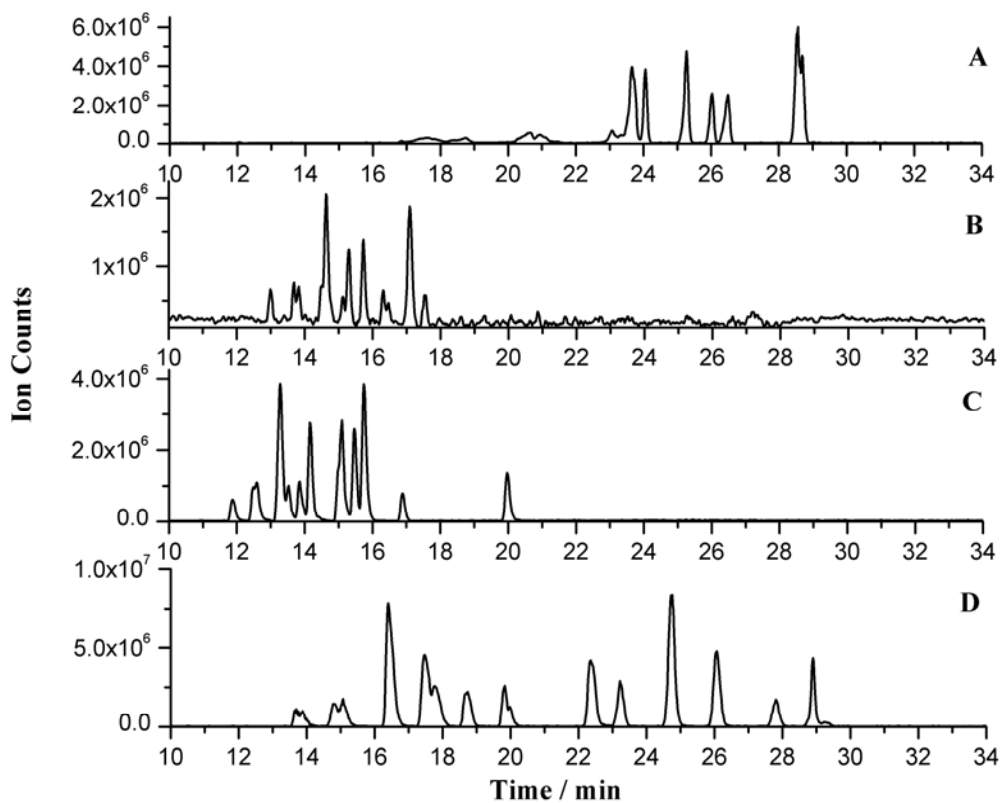


Figure 4.5: Summed extracted ion electropherograms of separation of drug mixture II under different conditions.

(A) 20 mM pH 2.5 $\text{NH}_4\text{Ac}/\text{MeOH}$ v/v 1:1; (B) 20 mM pH 5 $\text{NH}_4\text{Ac}/\text{MeOH}$ v/v 1:1; (C) 20 mM pH 7.3 $\text{NH}_4\text{Ac}/\text{MeOH}$ v/v 1:1; (D) 20 mM pH 9 $\text{NH}_4\text{Ac}/\text{MeOH}$ v/v 1:1.

Modifier solution: 90% MeOH and 0.2% formic acid. Samples were in 5 mM phosphate buffer and 50 % methanol at concentration of 2.5 $\mu\text{g}/\text{mL}$, except that methoxamine was at 5 $\mu\text{g}/\text{mL}$, and were injected by applying 0.5 psi for 10 seconds at the inlet vial. MS detection was performed by Finnigan LCQ Duo ion trap in full scan mode.

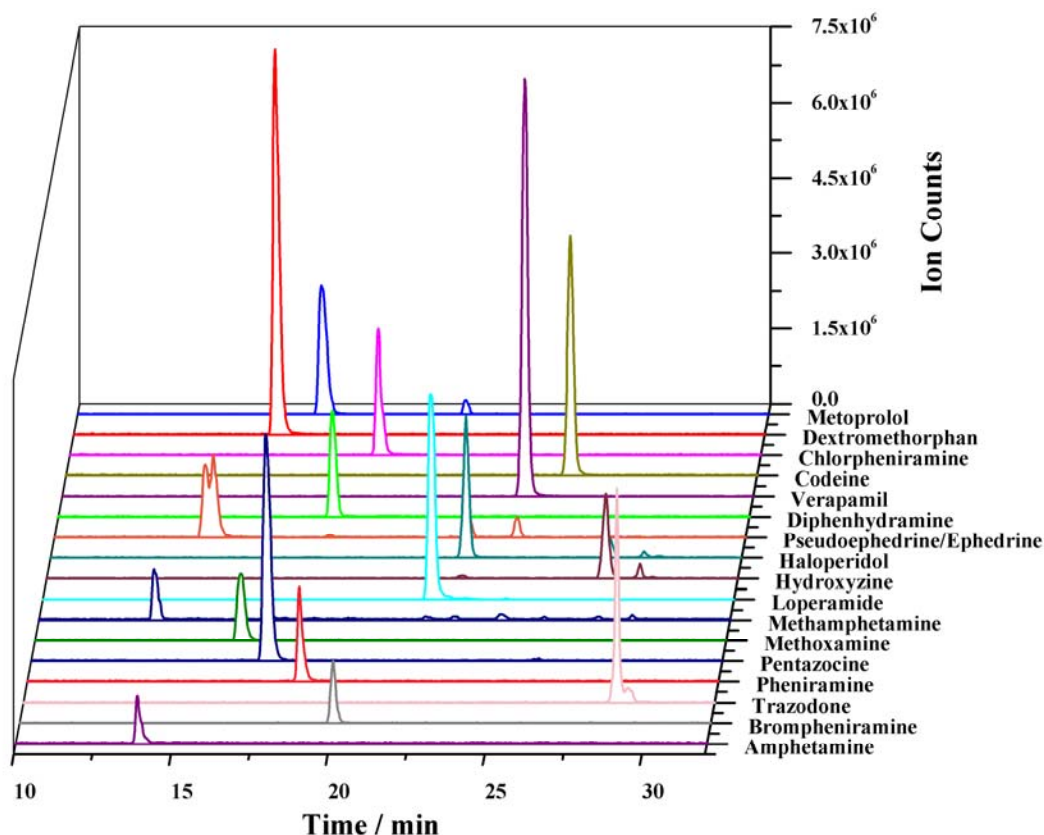


Figure 4.6: Extracted ion electropherograms of separation of drug mixture II. Mass analysis was performed by Finnigan LCQ Duo ion trap in full scan mode. Background electrolyte: 20 mM pH 9 NH₄Ac/MeOH v/v 1:1; Modifier solution: 90% MeOH and 0.2% formic acid.

Calibration of drug mixture I was performed on a triple quadrupole mass spectrometer using MRM mode. To limit the current and achieve better resolution, 50 μ m ID capillary was used instead of 75 μ m ID capillary. Before running the standards, electrokinetic injection was compared with pressure injection. It was found that the peak intensities and widths resulting from 10 kV 16s injection were similar to those from 1 psi 20 s injection. As electrokinetic injection has better reproducibility², it was employed for all the calibration runs. The MRM detection parameters for each ion channel, and the linear quantitation range and correlation coefficient of each component of drug mixture I are

summarized in Table 4.1. With the high sensitivity and specificity of the MRM detection, the LOD of these basic drugs can be as low as in the 0.5~8 ppb range.

	Parent ion / m/z	Daughter ion/ m/z	Cone voltage/V	Collision energy /V	Linear range / [ng/ mL]	Correlation coefficient
MDA	180.1	163.1	15	10	7.81-250	0.9911
MDMA	194.2	163	20	15	0.49-250	0.9985
MDEA	208	162.9	20	15	0.49-250	0.9999
Diphenhydramine	256.2	166.9	15	10	0.49-250	0.9826
MEGX	207.2	57.8	20	15	0.49-250	0.9941
Lidocaine	235.4	86	25	20	0.49-250	0.9976
Ketamine	238.2	220.3	25	15	1.95-250	0.9903
Norketamine	224	207	20	13	0.98-250	0.9990
Doxapram (IS)	379.3	292.3	25	25	-	-

Table 4.1: MRM detection conditions, linear quantitation range and correlation coefficient of drug mixture I.

4.4 CONCLUDING REMARKS

A robust CZE-ESI-MS method has been developed for the separation and detection of basic compounds of drugs of abuse. Good peak resolution and detection limit down to 0.5~8 ppb range were achieved by using basic ammonium acetate buffer as background electrolyte and acidic modifier. With proper sample pre-treatment, this method can be applied for quantitative determination of basic drugs from biological fluid, such as plasma or urine, or even other biological specimens such as hair or tissue in the future.

**Chapter 5: Flow-through microvial facilitates interface of capillary
isoelectric focusing with electrospray ionization mass spectrometry**

5.1 INTRODUCTION

Capillary isoelectric focusing (cIEF) is a promising method for the separation of amphoteric compounds with different isoelectric points and can be used for analyzing peptides, proteins, and protein complexes in biological samples¹⁰. When a second dimension of separation based on mass-to-charge ratio is added, the combination of cIEF and mass spectrometry (MS) can be even more powerful for biomolecule characterization and can provide pI and molecular weight information analogous to traditional two-dimensional gel electrophoresis (2DE). For protein characterization and proteomics studies, cIEF-MS offers not only high resolution but also the additional benefits of full automation, as well the large amount of quantitative and qualitative information obtainable from MS or tandem mass spectrometry.

The first demonstration of coupling cIEF and MS by electrospray ionization (ESI) was introduced by Tang et al. in 1995⁹⁸. Other researchers have shown the feasibility of probing protein refolding⁹⁹, phosphorylation¹⁰⁰, glycosylation¹⁰¹, high affinity ligands screening¹⁰², intact noncovalent protein complex¹⁰³, and *E.coli* proteomics¹⁰⁴⁻¹⁰⁹ based on improved strategies for cIEF-ESI-MS. However, in spite of its potential advantages and applications for protein analysis, some concerns need to be addressed before this technology can be widely adopted. To begin, many of the traditional cIEF reagents are not ESI compatible. For example, the strong inorganic acids and bases, which are usually used as the anolyte and catholyte, must be replaced by volatile organic acids and bases for ESI-MS detection. The high concentrations of carrier ampholytes that coelute with the analyte also present a challenge for ESI-MS, as they can suppress analyte ionization and create spectral interferences⁹⁸. Interfaces incorporating micro dialysis junctions¹¹⁰⁻¹¹² or

free-flow electrophoresis devices¹¹³ for online removal of the carrier ampholytes have been demonstrated; however, these features create a dead volume that leads to reduced separation efficiency. In order to improve the resolution and mitigate diffusion, cIEF is usually done in an anticonvective medium such as aqueous solutions of ethylene glycol and poly(ethylene oxide)¹¹⁴, which are not compatible with an ESI source. While most researchers had to perform cIEF-ESI-MS without adding any anticonvective agent into the ampholytes/sample mixture, the Varenne group found that a solution of 30% glycerol can be used to replace the aqueous polymer gel for retaining the high resolution of cIEF¹¹⁵ and later applied it in MS detection^{116,117}. On the other hand, the presence of glycerol in the electrospray solution during hydrodynamic mobilization increases the viscosity and decreases the overall volatility of the solution, leading to decreased ionization efficiency.

The conventional cIEF process involves two steps: focusing of the sample and carrier ampholyte mixture within an established pH gradient and mobilization of the focused analyte zones toward the detector. Another problem that needs to be addressed when interfacing with ESI-MS is the lack of a catholyte reservoir at the terminus of the cIEF capillary during the focusing stage. Early cIEF-ESI-MS interfacing attempts employed a semi online approach, in such a way that the capillary terminus was placed in a vial of catholyte during the focusing stage and then installed into the sheath-flow ESI source prior to mobilization^{98-100,104-107,118-121} or retracting the capillary into the sheath liquid tubing during the focusing step, so that the sheath liquid could act as the catholyte-solution and provide electrical contact during the focusing stage^{36,122,123}. Another strategy used a sheath liquid interface without the auxiliary gas, so that the capillary tip could be

positioned outside the metal tubing for both focusing and ESI¹²⁴. However, in normal polarity cIEF, the sheath liquid solution delivered by a syringe pump needs to be manually switched from a basic catholyte, which facilitates focusing, to an acidic modifier solution that provides a stable electrospray. To avoid this step, Yang et al.¹¹⁰ and Zhang et al.¹⁰⁸ used reversed polarity for cIEF focusing, so that the acidic sheath liquid that served as the analyte during the focusing stage also worked as an electrospray solution. Mokaddem and co-workers developed a method in which a plug of catholyte was left to fill the terminal end of the cIEF capillary, while the anodic end is filled with the protein-ampholyte mixture^{116,117}. In this case, the plug of catholyte, rather than the sheath liquid, replaces the catholyte vial by providing the required chemistry for focusing and no switching of the sheath liquid is required.

Following focusing, the mobilization of the focused sample zones toward the MS detector can be driven by hydrodynamic flow, electroosmotic pumping, or electrophoretic migration. Hydrodynamic flow is the simplest to achieve, by applying a pressure at the inlet vial or raising the inlet vial higher than the outlet. However, the resulting parabolic flow profile reduces the resolution achieved during focusing. Electroosmotic flow mobilization occurs spontaneously in bare fused silica capillaries, both during and after the focusing stage. However, EOF can be difficult to control due to the changes in average pH and the field strength in the capillary as the pH gradient moves through the capillary. As a result, capillary coatings that suppress EOF are often used in cIEF and pure EOF mobilization is often undesirable. Electrophoretic mobilization, also called chemical mobilization, is achieved by introducing anions or cations, other than hydroxide ions or protons, into the focused sample zone to replace the local hydroxide ions or

protons, respectively, charging the amphoteric analytes so that they can migrate toward the cathode or anode under electric field¹²⁵. This approach provides selective mobilization of amphoteric species and should not create any additional band-broadening of the focused protein zones, although the correlation between migration time and isoelectric point might not be as linear as with hydrodynamic mobilization.

All three approaches for mobilization, or combinations thereof, have been demonstrated in cIEF-ESI-MS. Lee et al.^{99-101,104,105,119,120,126} and Smith et al.^{103-104,106,107,118,121,127} used a protocol that combines gravity induced hydrodynamic flow with electrophoretic mobilization. As the sheath flow liquid for positive ion mode ESI usually contains organic acid and the electrospray electrode works as cathode for cIEF in normal polarity mode, the conjugate base of this acid can migrate back into the capillary and cause electrophoretic mobilization. Sheath liquid induced electrophoretic mobilization also works for ESI-MS detection without assisted pressure at the inlet^{98,122-124}. Zhang et al. demonstrated combined hydrodynamic and electroosmotic flow mobilization for reversed polarity cIEF-MS using bare fused silica capillary¹⁰⁸. However, the applied pressure has to be carefully programmed to optimize the peak resolution due to the bidirectional electroosmotic flow of the catholyte and ampholyte zones and variations in the lengths of the zones during the mobilization process.

The previously described CE-MS interface with a flow-through microvial at the end of the separation capillary provides special advantages that facilitate online cIEF-MS. The chemical modifier solution introduced at a low flow rate carries the analyte from the capillary terminus to the site of ESI even when there is no bulk flow in the separation capillary, while minimizing dilution of the analyte^{82,85,128}. In this chapter, the use of this

interface for combining cIEF with ESI-MS is demonstrated by using glycerol as an anti-convective agent. Two different strategies, using either a part of the capillary or the flow-through microvial of the CE-MS interface as the catholyte reservoir for bare fused silica capillaries or neutral coated capillaries, respectively, were developed for automated cIEF-electrospray ionization (ESI)-MS.

5.2 MATERIALS AND METHODS

5.2.1 Chemicals and materials

Glacial acetic acid (A.C.S. reagent), 88% formic acid, methanol (HPLC grade), and ammonium hydroxide (A.C.S. reagent), were purchased from Fisher Scientific (Nepean ON). Glycerol (for electrophoresis $\geq 99\%$), urea (for electrophoresis), sodium hydroxide (95%~100%), and myoglobin (from horse heart), lysozyme (from chicken egg white) were purchased from Sigma Aldrich. IEF protein standards (ribonuclease A, pI 9.45; carbonic anhydrase II, pI 5.9; β -lactoglobulin, pI 5.1), a peptide standard (CCK flanking peptide, pI 3.6) and carrier ampholyte mixtures for pH range of 3 to 10 (Fluka® and Pharmalyte® brands), were obtained from Beckman Coulter Inc. (Brea, CA). Bare fused silica capillaries were purchased from Polymicro Technologies (Phoenix AZ). A polyvinyl alcohol (PVA) coated capillary was purchased from Agilent Technologies (Santa Clara, CA). A neutral, hydrophilic “N-CHO” type capillary was obtained from Beckman Coulter, Inc. (Brea CA).

The carrier ampholytes solutions were diluted in glycerol/water (v/v) 30:70 to a concentration double that desired for analysis and stored at 4°C. Mixtures of the protein standards were also prepared in glycerol/water and stored as aliquots at -20°C. Sample

solutions were prepared daily by mixing equal volumes of the protein standards and an ampholyte solution prepared in 30:70 (v/v) glycerol/water. The final concentrations of proteins in the ampholytes/glycerol mixture were ribonuclease A 300 $\mu\text{g/mL}$, carbonic anhydrase II 50 $\mu\text{g/mL}$, β -lactoglobulin 50 $\mu\text{g/mL}$, CCK flanking peptide 25 $\mu\text{g/mL}$, and myoglobin 125 $\mu\text{g/mL}$.

5.2.2 Capillary isoelectric focusing

cIEF was performed on a MDQ or PA800+ Capillary Electrophoresis System (Beckman Coulter, Brea CA) using a modified capillary cartridge that can accommodate both the separation capillary and the modifier delivering capillary for external detection. The bare fused silica capillaries used for separation were 67 or 85 cm long with 50 μm ID and were preconditioned by rinsing with 1 M NaOH, 0.1 M NaOH, and water for 30 min each. To create a stable and reproducible surface condition, the separation capillary was rinsed with 6 M urea, 2% formic acid, water, and catholyte for 3 min each using a pressure of 40 psi prior to each run. The modifier delivering capillary was prefilled by the modifier solution before each run.

Because the length of capillary required to reach the mass spectrometer inlet was longer than that required for resolution of the focused protein bands, the capillary was only partially filled with sample solution. A “sandwich” injection method was used to fill the bare fused silica capillary. The capillary was first fully filled with catholyte, and then, a long plug of sample was injected, followed by a plug of anolyte. The resulting configuration is shown in Figure 5.1A. The injection parameters were determined empirically by observing the time required to push a plug of analyte through a capillary filled with the 30% glycerol/water solution using a pressure of 2 psi. Injection times and

pressures were then calculated on the basis of the proportion of the capillary to be filled with the sample solution. Isoelectric focusing with the uncoated capillary was carried out with the capillary inlet placed in a vial containing the anolyte solution, composed of 50 mM or 125 mM formic acid in 30% glycerol/water, and the capillary terminus installed in the interface. The catholyte, which was contained in the capillary, was a solution of 100 mM ammonium hydroxide in 30% glycerol/water. A potential of 30 kV was applied at the capillary inlet, while the interface was grounded during focusing. The modifier solution, composed of methanol/water/acetic acid (v/v/v) 50:48:2 or methanol/water/formic acid (v/v/v) 50:48:2, was delivered to the microvial at the separation capillary terminus at a flow rate of 0.3 $\mu\text{L}/\text{min}$ after 22 min of focusing, unless otherwise specified, by applying pressure to the modifier vial via the CE instrument.

When the neutral N-CHO capillary was used, to protect the surface from being exposed to highly basic solutions, an alternative procedure was used. Prior to each run, the coated capillaries were rinsed with 6 M urea, water, 2% formic acid, and 30% glycerol for 3 min each using a pressure of 40 psi. The capillary was then fully filled by the sample/ampholyte mixture, followed by a plug of the anolyte solution (50 mM formic acid in 30% glycerol) which occupied 50% of the capillary length, resulting in a 1:1 ratio. Just before the onset of focusing, the modifier delivering capillary was filled with the catholyte solution (0.1 M ammonium hydroxide) and then placed in a vial containing the modifier solution (water/methanol/formic acid (v/v/v) 50:48:2), as shown in Figure 5.1B(i). Upon application of the high voltage, the modifier solution vial was pressurized (~ 1 psi) to deliver catholyte to the microvial, while the modifier solution gradually filled the modifier capillary, replacing the catholyte solution. The duration of the focusing step

is therefore determined by the flow rate in the modifier capillary and the combined volume of the capillary and needle interior. Electrophoretic mobilization was initiated when the acidic modifier solution displaced the catholyte in the microvial, as shown in Figure 5.1B (ii).

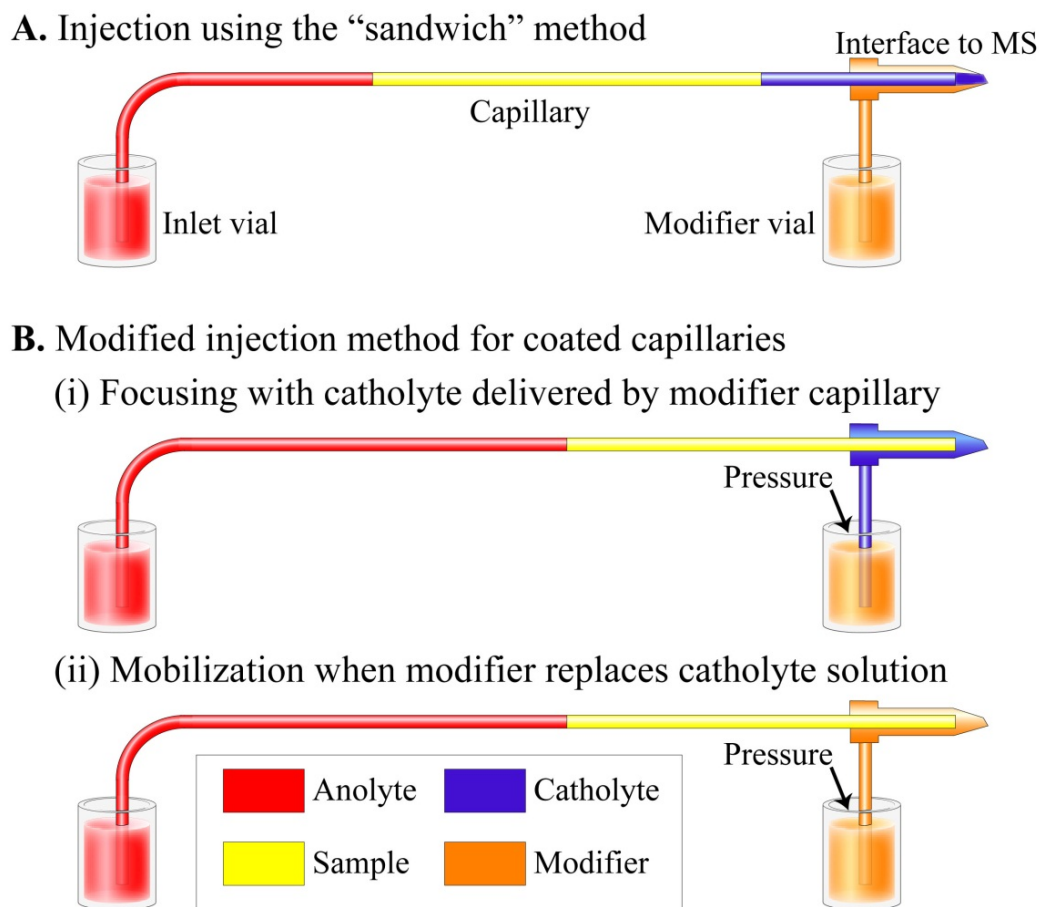


Figure 5.1: Injection techniques for automated cIEF-MS.

(A) “Sandwich” injection method for bare fused silica capillaries. The modifier vial starts to be pressurized to deliver acidic modifier solution when the focused sample zone gets close to the capillary outlet.

(B) Modified method for covalently neutral coated capillaries. (i) Before separation starts, the modifier delivery capillary is prefilled by catholyte solution with one end connected to the modifier vial. (ii) The pressurized modifier vial delivers basic catholyte solution to the microvial during the focusing stage and acidic modifier solution to the microvial during the mobilization stage. The duration of the focusing step is determined by the flow rate in the modifier capillary and the combined volume of the capillary and

needle interior. The lengths of the CE separation capillary and modifier delivery capillary are not drawn to proportion.

5.2.3 Electrospray ionization-mass spectrometry

Interfacing with mass spectrometry was carried out using the previously described flow-through microvial interface developed in our laboratory^{82,128}. Mass analysis was carried out using either a Finnigan LCQ^{Duo} ion trap (Thermo Scientific, Waltham MA) or Micromass Q-TOF 1E mass spectrometer (Waters, Milford MA) with the standard ESI source removed. Detection parameters were optimized by direct infusion of 0.1 mg/mL lysozyme in the modifier solution. For the ion trap, the heated capillary MS inlet temperature was set at 250-300 °C, and the ion trap injection time was 200 mS. The inlet cone of the Q-TOF MS was maintained at 150 °C and a potential of 60 V. Both instruments were operated with an electrospray potential of 4 kV and detector scan range of m/z 1000-2000. The electrospray voltage and data acquisition on the mass spectrometer were started after 25 min of focusing, unless stated otherwise. All time scales shown in the electropherograms start from the beginning of focusing.

5.3 RESULTS AND DISCUSSION

5.3.1 Suitability of the interface for cIEF-MS interfacing

There has been a great deal of progress over the past 15 years in increasing the compatibility of cIEF with MS detection. The focus of our own work on this subject has been to develop an interfacing strategy that retains previous advances while also requiring no specialized instrumentation and being fully amenable to automation. The

enabling piece in providing this performance is the flow-through microvial CE-ESI-MS interface developed in our laboratory, which consists of a custom fabricated stainless steel needle, internally tapered and externally beveled at the tip, into which the terminal end of the capillary is inserted^{82,128}. The small volume contained between the end of the capillary and the interior of the needle tip constitutes a flow-through microvial, while the beveled outer surface of the needle tip is the site for electrospray ionization. Modifier solution is introduced through a separate capillary, which is connected via the orthogonal port of a tee union, so that the solution flows around the edges of the cIEF capillary and into the microvial.

This design provides several features that make it well suited for the challenge of interfacing cIEF with ESI-MS^{82,85,128}. The flow-through microvial at the cIEF capillary terminus ensures stable electrical contact during the focusing and mobilization steps. The modifier solution can provide a flow of catholyte during the focusing step or an acidic solution to accomplish electrophoretic mobilization of the focused analyte zones, and switching between the two can be accomplished automatically using a standard CE instrument. Our interface can accommodate bare fused silica capillaries for cIEF, where both EOF and electrophoretic mobility play roles for mobilization, as well as the coated capillaries that are commonly used to eliminate electroosmotic flow and minimize wall interactions. In the case of electrophoretic mobilization in a neutral coated capillary, the modifier solution can transport the analyte in the microvial to the outer surface of the beveled sprayer tip and support a stable electrospray even when there is no bulk flow inside the separation capillary. The small volume of the microvial also minimizes the

dilution effect and postcolumn band broadening¹²⁸; in this way, better sensitivity and resolution can be achieved.

5.3.2 cIEF in bare fused silica capillaries using a partial filling technique

The Varenne group has previously demonstrated a strategy of the use of a plug of the catholyte at the terminal end of the capillary, rather than using a catholyte vial, or the sheath liquid, to provide the hydroxide ions needed to establish and maintain the pH gradient throughout the focusing process^{116,117}. Considering that the practical separation capillary length (at least 67 cm for the MDQ system and 85 cm for the PA800 plus system) is much longer than that required for effective resolution of the focused analyte bands, we therefore adopted a “sandwich” injection method, where the sample zone is flanked by zones of anolyte and catholyte at the anodic and cathodic ends of the capillary, respectively. To accomplish this, a plug of anolyte was injected into the capillary after the sample and catholyte plugs to push the analyte zone closer to the cathodic end and thus shorten the analysis time, as illustrated in Figure 5.1A and Figure 5.2A.

It should be noted that the electric field strength in the sample/ampholytes zone, sandwiched between the anolyte and catholyte zones, is much greater than in the case where the entire capillary is filled by the sample/ampholytes mixture, because the conductivity in that zone is much lower than in the anolyte and catholyte zones. This can be explained by considering the three discontinuous electrolyte zones as three resistors in series. Based on Ohm’s law, the electric field strength in sample/ampholytes zone E_s can be expressed as

$$\begin{aligned}
E_s &= \frac{R_s}{R_s + R_c + R_a} \times \frac{V_{total}}{L_s} \\
&= \frac{1}{f_s \times \left(1 + \frac{f_c}{f_s} \times \frac{\kappa_s}{\kappa_c} + \frac{f_a}{f_s} \times \frac{\kappa_s}{\kappa_a}\right)} \times \frac{V_{total}}{L_{total}}
\end{aligned} \tag{5-1}$$

where R_s , R_c , and R_a are the resistances of the sample/ampholytes zone, catholyte zone, anolyte zone respectively, V_{total} is the voltage applied across the capillary, L_{total} is the total length of the capillary, L_s is the length of the sample/ampholytes zone, f_s , f_c and f_a are the percentages of the capillary lengths occupied by sample/ampholytes, catholyte, and anolyte respectively, κ_s , κ_c , and κ_a are the conductivities of the sample/ampholytes, catholyte, anolyte solution respectively. Given the condition that $\kappa_s \ll \kappa_c, \kappa_a$ ¹²⁹⁻¹³¹, especially after focusing, and $f_s \geq f_a, f_c$ in the application, the field strength across the sample/ampholytes zone could be approximated as

$$E_s \approx \frac{1}{f_s} \times \frac{V_{total}}{L_{total}} = \frac{V_{total}}{L_s} \tag{5-2}$$

Upon applying 30 kV across the capillary, focusing of the ampholytes establishes the pH gradient in the sample zone, accompanied by the displacement of the whole zone toward the cathode due to the electroosmotic pumping. Meanwhile, the decreasing conductivity in the sample/ampholytes zone leads to increased electric field strength in this zone, which also keeps the sample and ampholytes focused during mobilization (Figure 5.2B).

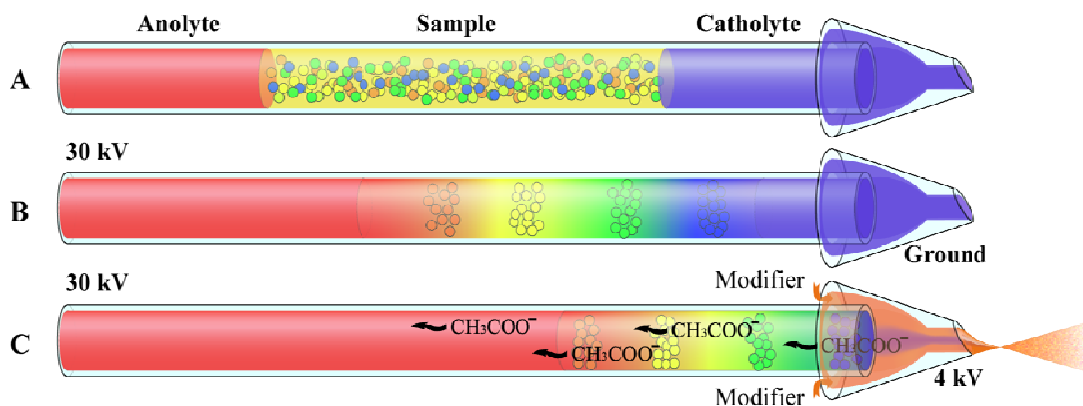


Figure 5.2: Schematic illustration of cIEF-MS process with the bare fused silica capillary.

(A) A catholyte plug, sample/ampholytes mixture plug, anolyte plug are injected into the capillary sequentially. (B) A 30 kV voltage is applied across the capillary; the pH gradient starts to form in the sample/ampholytes zone with concurrent electroosmotic mobilization; the effluent brought out by EOF from the capillary fills the microvial. (C) The high pH boundary of the focused sample/ampholytes mixture zone arrives at the microvial, and pressure is applied in the modifier vial to deliver modifier solution to the ESI interface; the acetate ions in the modifier solution migrate back into the capillary and initiate electrophoretic mobilization; 4kV is applied on the sprayer needle for ESI detection.

5.3.3 cIEF with electroosmotic and electrophoretic mobilization

When performing cIEF in bare fused silica capillaries, it is inevitable that there will also be some electroosmotic mobilization throughout the focusing and mobilization stages, due to the average pH > 3 in the capillary. The overall electroosmotic velocity,

$v_{eof,net}$, is

$$v_{eof,net} = f_a \mu_a E_a + f_s \mu_s E_s + f_c \mu_c E_c \quad (5-3)$$

where f_a , f_s , and f_c are the percentages of capillary length occupied by the anolyte, sample/ampholytes, and catholyte; μ_a , μ_s , and μ_c are the electroosmotic mobilities of the anolyte, sample/ampholytes, and catholyte, respectively; E_a , E_s , and E_c represent the electric field strength of each zone. Although the fraction of capillary length occupied by each zone varies during mobilization, the field strengths in the anolyte and catholyte

zones are very small due to their high conductivity compared to the sample/ampholytes zone, so the major contribution to the net electroosmotic flow velocity comes from the sample/ampholytes region. This has been demonstrated by Thormann et al.¹³⁰⁻¹³² using computer simulations of the cIEF process with electroosmotic mobilization. Their computer modeling also predicted that, with initial plugs of catholyte and ampholytes inside the bare fused silica capillary, i) the pattern of the focused ampholyte zone will not be disrupted during electroosmotic mobilization, although the local electroosmotic flow velocity varies along the capillary; ii) the magnitude of the net EOF experiences three stages, a fast dropping stage during focusing, followed by an almost constant, slightly declining stage as the length of catholyte zone gets smaller, and then a linear decreasing stage as the ampholyte zone gradually migrates out of the capillary terminus¹³⁰⁻¹³².

It is also important to realize that, although the magnitude of the electroosmotic velocity varies along the length of the capillary, at any moment, the bulk solution at any cross section moves at the same net velocity determined by Eq (5-3), due to the continuity of the incompressible fluid. This net cathodic electroosmotic flow fills the microvial with catholyte¹²⁸ and ensures the electrical continuity during the first 10 to 20 min of separation, before the modifier vial is pressurized to deliver electrolyte to the microvial. Using the injection method shown in Figure 5.1A, the concurrent focusing and electroosmotic mobilization stage starts at the onset of the electric field. As a result, the plug of catholyte at the terminal end plays the additional role of ensuring that the EOF does not push the high pH boundary of the ampholytes zone to the capillary terminus before focusing is complete.

During the concurrent focusing and electroosmotic mobilization stage, before the high pH boundary of the ampholyte zone reaches the capillary terminus (Figure 5.2B), the net cathodic EOF and the small field strength in the catholyte zone prevent the acetate or formate ions in the modifier solution from penetrating the catholyte zone and electroosmotic pumping is the only driving force for the transportation of the sample/ampholyte zone toward the detector. To prove this, the same “sandwich” injection method was also applied with a PVA coated capillary (85 cm×50 μm), where the EOF was eliminated. In this case, the mobilization of the ampholyte zone was not observed within 60 min after the current dropped to minimum, even when the catholyte occupied only 1/8 of the capillary (Data not shown). Further evidence is that the time to start the modifier infusion before the sample/ampholyte zone reaches the microvial does not affect the retention times of the analyte and the current characteristics. As the length and the electric field strength of the focused ampholytes zone are almost constant before it reaches the capillary terminus, the velocity of this zone could be considered nearly constant during this mobilization stage.

When the high pH boundary of the ampholytes zone reaches the microvial of the CE-MS interface, acetate or formate ions from the modifier solution penetrate the ampholytes zone, due to the large field strength in this zone and the decreased net EOF and, thus, initiate electrophoretic mobilization by replacing the hydroxide ions and lowering the local pH (Figure 5.2C). Meanwhile, the decreasing net EOF also contributes to the transportation of the zones toward the detector until most of the ampholytes migrate out of the capillary.

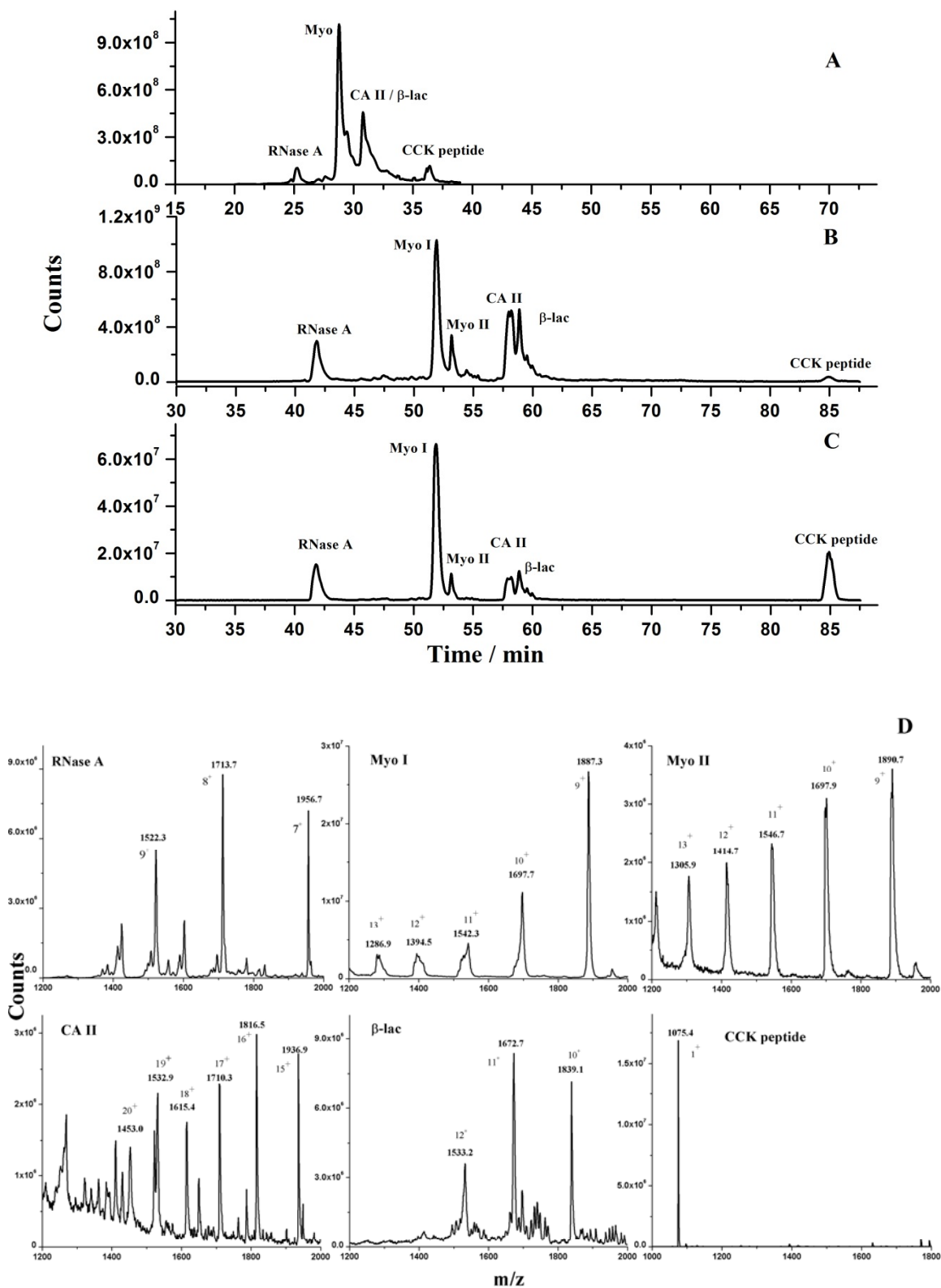


Figure 5.3: Separation of protein mixtures in bare fused silica capillary with pressure (A), and without pressure (B-D) applied at the capillary inlet.

Conditions: Proteins were mixed with 1% (v/v) Fluka® pH 3-10; anolyte 50 mM formic acid in 30% glycerol; catholyte 100 mM ammonium hydroxide in 30% glycerol; modifier solution methanol/water/acetic acid (v/v/v) 50:48:2. No cooling for capillary was used. (A) Total ion electropherogram of cIEF-MS with 1psi pressure applied at CE inlet after 20 minutes of separation. Other conditions: 67 cm×50 μm ID capillary; ratio of catholyte/sample/anolyte injection length 1:2:1; modifier was infused at 0.6 μL/min; Heated capillary temperature of the LCQ MS inlet was set at 300°C. (B) Total ion electropherogram with no pressure applied at the CE inlet after IEF. (C) Summed extracted ion electropherogram (RNase A [M+8H]⁸⁺ ion at m/z 1714, Myo [M+9H]⁹⁺ ion at m/z 1887, CA II [M+16H]¹⁶⁺ ion at m/z 1817 and [M+15H]¹⁵⁺ ion at m/z 1937, β-lac [M+10H]¹⁰⁺ ion at m/z 1839, CCK peptide [M+H]⁺ ion at m/z 1075), and (D) mass spectra for the proteins separated by cIEF-MS in B with combined electroosmotic and electrophoretic mobilization. Conditions: 85 cm×50 μm ID capillary, ratio of catholyte/sample/anolyte injection length approximately 2:5:3; modifier solution was infused at 0.3 μL/min. Heated capillary temperature of LCQ MS inlet was set at 250°C.

Figure 5.3B shows the total ion electropherogram for the separation of protein standards using cIEF with combined electroosmotic and electrophoretic mobilization, using glycerol as a stabilizing medium. The presence of glycerol in the focusing medium prevents protein aggregation or precipitation, improves the resolution of cIEF separations, and reduces the magnitude of the electroosmotic flow¹¹⁶. However, when glycerol is introduced into the electrospray ionization source by hydrodynamic mobilization, its high viscosity and low volatility lead to reduced electrospray stability and ionization efficiency. This has previously been managed using high temperature gas desolvation (100 °C nebulizer gas and 350 °C drying gas)^{116,117}, but this strategy leads to temperature gradients along the capillary and a nebulizer gas induced suction effect. With the flow-through microvial CE-MS interface, pressure applied at the inlet vial can be avoided during mobilization, resulting in little glycerol introduced into the ESI source. The electroosmotic/electrophoretic mobilization approach provides increased electrospray stability and reduced background signals from the ampholytes, as well as improved peak resolution compared to hydrodynamic mobilization (Figure 5.3A). The

two myoglobin isoforms were fully resolved in the total ion electropherogram (TIE, Figure 5.3B), and carbonic anhydrase II (pI 5.9) and β -lactoglobulin (pI 5.1) were almost fully resolved in the summed extracted ion electropherogram (Figure 5.3C). The averaged mass spectra under each peak are shown in Figure 5.3D.

5.3.4 Optimization of experimental conditions and reproducibility

Different injection lengths of the catholyte, anolyte, and sample plugs were tested to determine the impact of the length of the various zones on cIEF resolution and relative sensitivity. Figure 5.4A and 5.4B show the effect of varying the length of the catholyte plug while keeping the sample/ampholyte plug length consistent at one-quarter of the total capillary length. The elution time of the peaks in Figure 5.4A was about 5 min faster than those in Figure 5.4B, as the distance that the sample zone needed to travel was approximately 10 cm shorter. However, the resolution was not improved significantly by having more catholyte inside the capillary, with the exception of the minor myoglobin isoform, which appears as a small shoulder of the major myoglobin peak (Figure 5.4B). The impact of sample zone injection length was also investigated while keeping the catholyte plug length constant. In Figure 5.4C, by increasing the length of the sample/ampholyte plug to half of the total capillary length, the two isoforms of myoglobin, carbonic anhydrase II and β -lactoglobulin, were better resolved, and the relative detection sensitivity was improved. The peak capacity also increased due to the longer effective capillary length available for the protein separation. For these reasons, a 1:2:1 ratio for the injection length of catholyte/sample/anolyte was used for all subsequent experiments in bare fused silica capillaries.

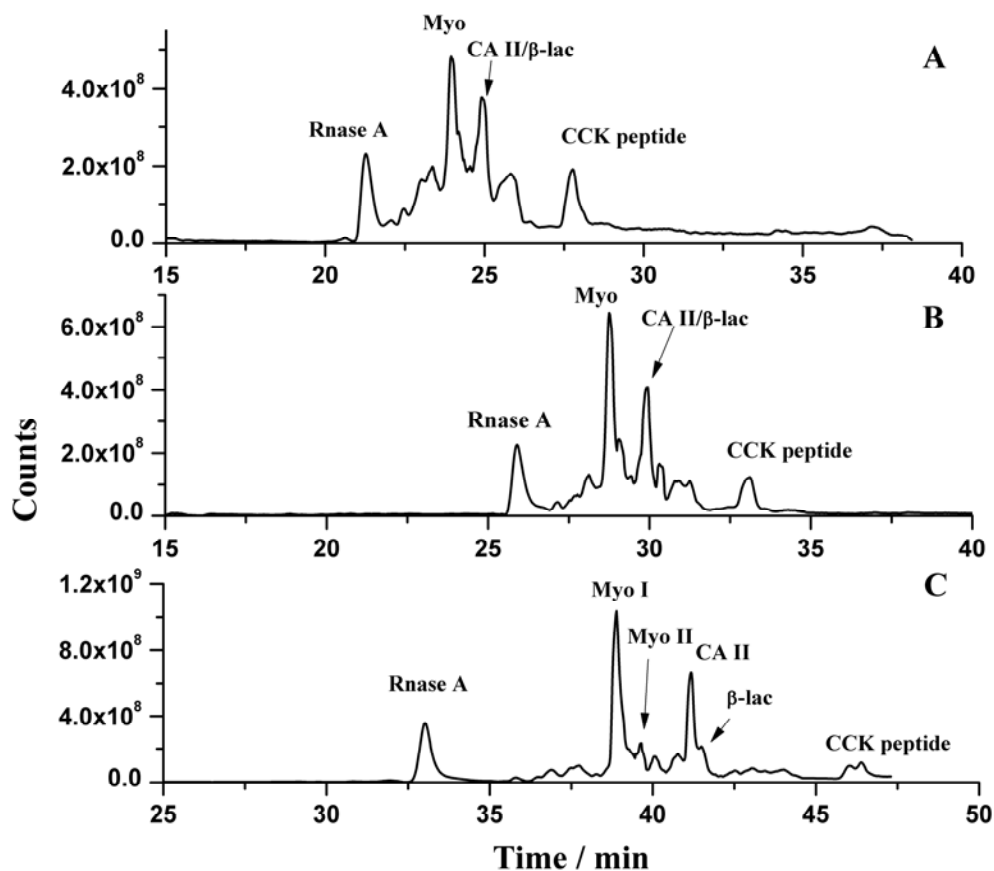


Figure 5.4: Total ion electropherogram of separation of protein mixture in bare fused silica capillary with different ratio of catholyte/sample/anolyte injection length.

(A) 5:2:1; (B) 2:1:1; (C) 1:2:1. Modifier solution methanol/water/acetic acid (v/v/v) 50:48:2 was infused at 0.3 $\mu\text{L}/\text{min}$ after 12 minutes of focusing. ESI voltage and MS data acquisition started after 15 minutes of focusing. Coolant temperature was 25 $^{\circ}\text{C}$. Other conditions were the same as Figure 5.3B.

The reproducibility of cIEF is a major concern and difficult to achieve in practice due to the adsorption of proteins on the capillary wall. Using 6 M Urea to rinse the capillary before each run could wash away most of the adsorbed proteins and improve the reproducibility of protein detection time and current characteristics¹¹⁴. Consecutive runs with programmed focusing and mobilization sequences and temperature control of the capillary were performed to evaluate the effects of ampholyte concentration, anolyte

concentration, and modifier composition on the cIEF performance, because the flow-through microvial interface facilitates the full automation of cIEF-ESI-MS. Table 5.1 lists the average (and standard deviation) of the migration times for the most basic pI marker, RNase A (pI 9.4), and the most acidic pI marker, CCK peptide (pI 3.6), using various compositions of the ampholyte, anolyte, or mobilizer solution.

	Anolyte formic acid concentration	Modifier solution acid content	Ampholyte concentration (v/v)	time, minutes average (standard deviation)		
				RNase A	CCK peptide	Difference (CCK peptide - RNase A)
A	50 mM	2% acetic acid	1.0%	34.2 (1.9)	51.0 (1.8)	34.2 (1.9)
B	50 mM	2% acetic acid	1.5%	33.3 (1.9)	49.5 (2.0)	34.2 (1.9)
C	50 mM	2% acetic acid	2.0%	30.7 (0.3)	46.0 (0.3)	15.3 (0.2)
D	125 mM	2% acetic acid	1.5%	35.2 (0.8)	52.8 (1.5)	17.6 (0.7)
E	125 mM	2% formic acid	1.5%	34.3 (3.0)	48.5 (3.2)	14.2 (0.3)

Table 5.1: Migration times of RNase A (pI 9.4) and CCK peptide (pI 3.6) of repeated cIEF-MS runs under different conditions.

Catholyte/sample/anolyte injection length ratio was 1:2:1. Catholyte was 100 mM ammonium hydroxide in 30% glycerol. Anolyte was 50~125 mM formic acid in 30% glycerol. Modifier solution containing 50% methanol and 2% acetic or formic acid was infused at 0.3 μ L/min. Coolant temperature was 20 °C. The average and standard deviation of migration times were calculated based on 4~5 consecutive runs. Electropherograms are not shown.

Additional insight into the reproducibility of the cIEF process can be obtained by examining the current profiles for each run (Figure 5.5). Similar trends were observed under the five conditions listed in Table 5.1. The current first decreases during the concurrent focusing and electroosmotic mobilization process and then reaches a minimum and stabilizes for a short period of time as the conductivity of the focused zone does not change dramatically after focusing but before arriving at the microvial of the CE-MS interface. As the ampholytes/sample zone starts to migrate out of the capillary,

the fraction of capillary occupied by the highly conductive anolyte increases, and the acetate or formate ions in the modifier solution migrating through the ampholytes/sample zone initiate the electrophoretic movement of the amphoteric compounds. With the ampholyte zone exiting the capillary and the acetate/formate ions migrating toward the anode, the current quickly increases, eventually reaching a plateau when all the ampholytes have exited the capillary. The small discrepancies of the current from run to run during the second mobilization stage can be observed due to minor variations of the bare fused silica capillary surface and the high volatility of the modifier solution.

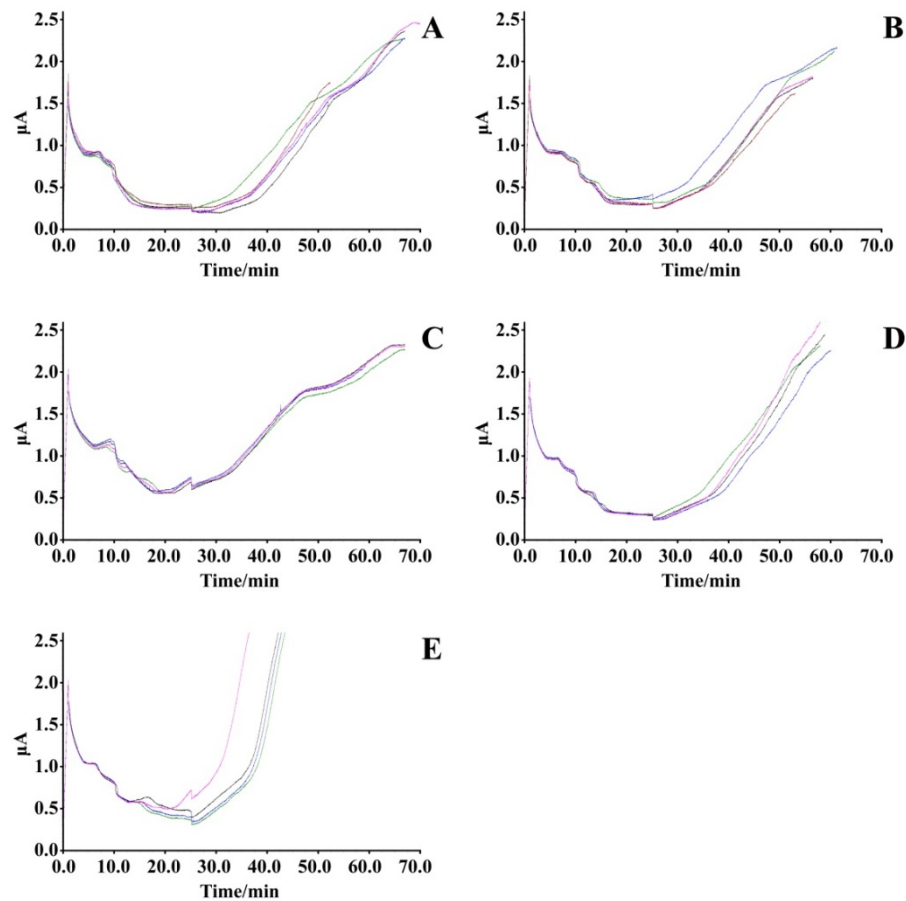


Figure 5.5: Current profile of replicates of cIEF-MS runs with bare fused silica capillary under different conditions.

Experimental conditions as listed in Table 5.1. Catholyte/sample/anolyte injection length ratio was 1:2:1. Catholyte was 100 mM ammonium hydroxide in 30% glycerol. Modifier solution was infused at 0.3 $\mu\text{L}/\text{min}$. Coolant temperature was 20 $^{\circ}\text{C}$. A-C. Anolyte 50 mM formic acid in 30% glycerol, modifier methanol/water/acetic acid (v/v/v) 50:48:2, Fluka® pH 3-10 ampholytes concentrations 1%, 1.5%, 2% respectively. D-E. Anolyte 125 mM formic acid in 30% glycerol, Fluka® pH 3-10 ampholytes concentrations 1.5%, modifier solution methanol/water/acetic acid (v/v/v) 50:48:2 or methanol/water/formic acid (v/v/v) 50:48:2, respectively.

The ampholyte type and concentration are perhaps the most important conditions for obtaining good cIEF reproducibility. Initially, both Fluka and Pharmalyte brand ampholytes (pH 3-10) were tested; however, it was observed that the Pharmalyte ampholytes resulted in unusually long analysis times and required a significant pressure applied at the capillary inlet vial in order to observe any protein peaks, and the detected peaks were very broad. It has been previously reported that Pharmalyte pH 3-10 ampholytes can form dynamic coating on the fused silica capillary surface and reverse the direction of the EOF toward the anode¹⁰⁸. This appears to be the case, even with 30% glycerol as an EOF suppressing agent. As a result, only Fluka pH 3-10 ampholytes were used for further optimization. Regarding the ampholyte concentration, Table 5.1 and the current traces (Figure 5.5) show that the migration time and current reproducibility were improved using a higher concentration of ampholytes because of the improved buffering capacity. These observations are consistent with previous investigations, which have shown that higher ampholyte concentrations give better resolution but decreased signal because of the ion suppression effect⁹⁸. A slight improvement in the reproducibility of the migration times of pI markers was observed by increasing the formic acid concentration in the anolyte from 50 mM to 125 mM. Considering the impact on peak resolution, reproducibility, and MS sensitivity, an ampholyte concentration of 1.5% (v/v) and 125 mM formic acid anolyte were chosen

as the optimal conditions for focusing. Using 2% formic acid in the modifier solution instead of 2% acetic acid increased the current during mobilization (Figure 5.5E), as the mobility of the formate ions is faster than that of acetate ions. This also leads to faster electrophoretic mobilization of the protein zones and shorter migration times but no obvious improvement in peak resolution.

5.3.5 cIEF-MS in a neutral coated capillary with electrophoretic mobilization

When bare fused silica capillaries for cIEF are used, protein interactions with the negatively charged wall may interfere with the separation. Although the presence of glycerol in the sample solution should reduce these interactions, some residual interaction may remain. Capillaries with a neutral, hydrophilic coating eliminate electrostatic and hydrophobic interactions of proteins with the wall and eliminate EOF, regardless of the average capillary pH or the presence of different ampholyte species. As the covalent wall coating cannot be exposed to solutions with $\text{pH} > 10$, such as the catholyte, the alternative injection strategy depicted in Figure 5.1 B (i) was used. The sample zone was extended to the capillary terminus, while the modifier capillary delivered catholyte to the flow-through microvial for the duration of the focusing, followed automatically by the acidic modifier solution which initiated electrophoretic mobilization (Figure 5.1B(ii)).

Figure 5.6 shows a separation performed in this manner, with detection using the Q-TOF mass spectrometer. Compared to the LCQ Duo ion trap, the ion source of the Q-TOF instrument has limited desolvation capabilities as the sample inlet cone temperature could only be heated up to 150 °C and the cone gas is not used for the low flow rate ESI. Previous attempts to use this instrument with pressure mobilization yielded very low signals (not shown) due to the sample medium containing 30%

glycerol entering the MS inlet. However, it is possible to use it in conjunction with electrophoretic mobilization in neutral coated capillaries, since this mobilization method selectively mobilizes amphoteric species and almost does not introduce any glycerol into the ion source.

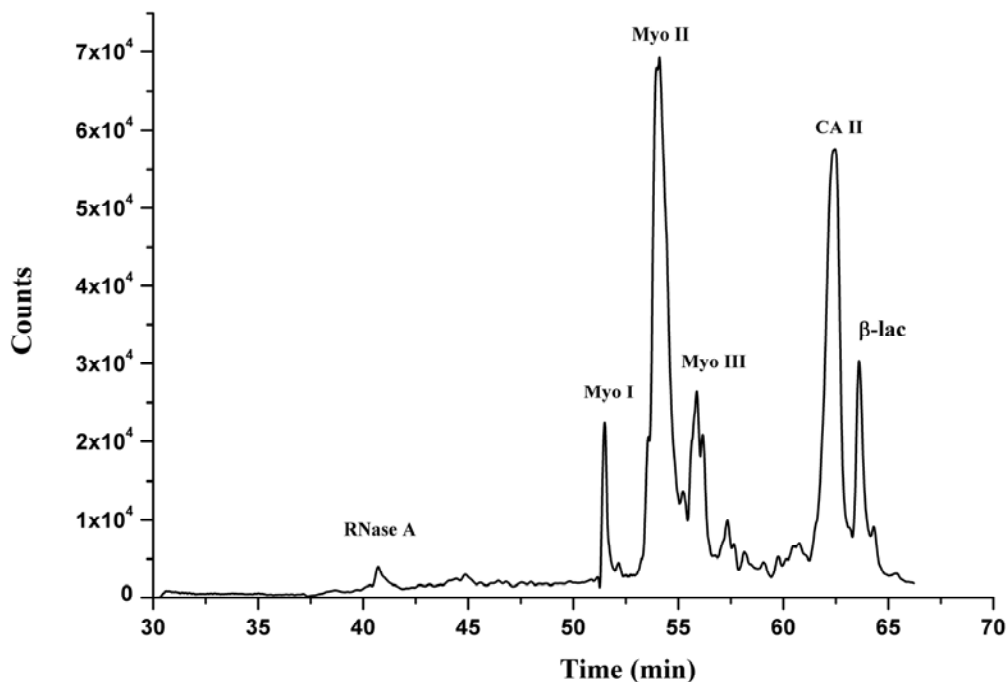


Figure 5.6: Total ion electropherogram for a protein mixture separated by cIEF with electrophoretic mobilization in a neutral coated capillary.

Conditions: N-CHO capillary, 67 cm \times 50 μ m ID; modifier delivery capillary, 90 cm \times 75 μ m ID; ratio of anolyte/sample injection length 1:1; anolyte 50 mM formic acid in 30% glycerol, catholyte 100 mM ammonium hydroxide, proteins mixed with 2% (v/v) Fluka® pH 3-10 ampholytes in 30% glycerol; modifier solution methanol/water/formic acid (v/v/v) 50:48:2 infused at approximately 150 nL/min. Electrospray voltage and data acquisition started after 30 minutes of separation. No cooling for capillary was used.

Due to changes in capillary type, ampholyte concentration (2% v/v), and mass spectrometer type, the relative peak intensities in Figure 5.6 differ from those observed on the ion trap mass spectrometer. However, the pattern is similar to that achieved in bare

fused silica capillaries, with the exception that carbonic anhydrase II (pI 5.9) and β -lactoglobulin (pI 5.1) are better resolved in the total ion electropherogram, due to the elimination of protein wall interactions and increased ampholyte concentration. An unexpected third isoform of myoglobin is also visible at 51.5 min, which may be due to improper storage of the sample solution leading to protein degradation. The final marker, CCK flanking peptide (pI 3.6), was not detected within reasonable migration time due to a gradual drift of the acidic portion of the pH gradient toward the capillary inlet which can be mediated by incorporating an ampholytic spacer species that has an isoelectric point that is just below the range of the pH gradient¹¹⁴.

5.4 CONCLUSIONS

A simple interfacing strategy for cIEF-MS has been demonstrated that combines the advantages of glycerol as an anti-convective medium and flexibility regarding the choice of capillary type and mobilization strategy. The flow-through microvial configuration ensures electrical continuity at the cathode end of the capillary, the supply of the catholyte and mobilizer solution during the focusing and mobilization process, and the transfer of analyte from cIEF capillary to ESI for mass spectrometry detection using automated CE systems. Reasonable separation efficiency was achieved with cIEF in bare fused silica and neutral coated capillaries. For cIEF in bare fused silica capillaries, electroosmotic flow can be a part of mobilization strategy if the process is well understood and well controlled. The combination of glycerol as an anti-convective agent with electroosmotic/electrophoretic mobilization provides increased resolution and relative ESI-MS sensitivity compared to pressure mobilization by reducing the amount of viscous glycerol entering the ESI source of the mass spectrometer and reducing dilution

of the analytes. The entire cIEF-ESI-MS process can be automated using commercial CE and MS instruments and should prove useful for separation and characterization of different types of biomolecules.

**Chapter 6: Field distribution in an electrospray ionization source
determined by finite element method**

6.1 INTRODUCTION

For mass spectrometers with atmospheric ion sources, the efficiency of transferring the ions from the high pressure region to the low pressure region is critical for detection sensitivity. In terms of an electrospray ionization source, the ion transferring process includes two stages – the first stage is from the sprayer tip to the sampling orifice, which is under atmospheric pressure, and the second stage is from the sampling orifice to the mass analyzer, which is backed up by a mechanical pump. For the second stage, RF-only multipole ion guides¹³ have been adopted by manufacturers to cool down and focus the ion beam before they enter into the mass analyzer region. However, less attention has been paid to the sampling efficiency of the ions into the orifice. Conventional ESI-MS suffers from low sampling efficiency due to the divergent electric field in the source. It has been estimated that in some cases fewer than 1 in 10^5 ions formed reach the mass spectrometer detector, and more than 99% are blocked from entry into the mass spectrometer^{133,134}.

The large electric field strength at the tip of the sprayer is responsible for the generation of charged droplets, and the electric field distribution in the ion source chamber governs the movement of charged species in the atmosphere. From this point, precisely controlling the electric field is of great importance for improving ion generation and transmission efficiency, and ultimately improving the detection sensitivity. This is especially true at lower flow rate when the ionization efficiency is sufficient while the transmission efficiency is very low.

Previous work by our group^{135,136} has demonstrated that an oblong-shaped atmospheric pressure ion lens improves the performance of ESI sources at flow rates

from 0.2 to 5 μ L/min. Thompson and coworkers¹³⁷ also reported that a hemispherically shaped electrostatic lens at atmospheric pressure was able to compress the charges generated by nano-ESI and increase the average current density in the plume by a factor of 3. Using both the experimental results and theoretical calculations, the work presented in this chapter demonstrates how the voltage applied on the ion lens affects the electric field distribution in an ESI source, thereby changing the analytical performance. The use of an ion lens in conjunction with ESI shows that each sprayer voltage has an optimum ion lens potential with which an optimum ionization condition is achieved. To calculate the electric field strength, we used a commercial software package COMSOL Multiphysics 3.4, which is based on finite element method (FEM). Interpretation of the simulation results gives more insight into the electric field distribution at the sprayer tip, and the results could lead to the more systematic design and operation of ESI sources, as well as an improvement in signal intensity. This ion lens can be incorporated into the CE-ESI-MS interface for better sensitivity in the future.

6.2 THEORY OF ELECTRIC FIELD CALCULATION

The differential equation that governs the potential of the electrostatic field in an ESI source is:

$$\nabla \cdot \epsilon \nabla V = -\rho_v \quad (6-1)$$

where V is the voltage, ϵ is the permittivity of the dielectric material, and ρ_v is the charge density. Omitting the space charge in the source chamber, Eq (6-1) becomes the Laplace equation¹³⁸:

$$\nabla^2 V = 0 \quad (6-2)$$

An analytical solution of the Laplace equation (6-2) can be derived only with simple and ideal boundary conditions. The field of point-to-plane electrodes was first solved in the study of cold emission by Eyring et al¹³⁹. It was assumed that the point was shaped in the form of hyperboloids of revolution, so that Eq (6-2) could be reduced to a second-order ordinary differential equation in a hyperbolic coordinates system and was easily solved. The electric field at the tip obtained by this method was:

$$E_c = \frac{AV_c}{r_c \ln(4d/r_c)} \quad (6-3)$$

where V_c is the potential difference between point and plate, r_c is the radius of curvature at the tip, d is the distance from point to plane, and A is a constant which is equal to 2. Smith¹⁴⁰ assumed that the field intensity at the tip was in the form of Eq (6-3) and determined the value of A to be 1.499 by measuring the onset electro spray voltage. Jones and Thong¹⁴¹ used the method of images to calculate the field between an infinite ground plate and a semi-finite line of charge, assuming that the charge per unit length was constant along the capillary. A similar result for E_c to that of Smith¹⁴⁰ was obtained and the only difference was that in this case A had a value of $\sqrt{2}$.

Although analytical solutions are always accurate when the boundary conditions are met, they become limited when boundary conditions are not well defined, such as in the cases when the sprayer needle is not perpendicular to the curtain plate, or when it is not aimed at the center of the plate, or when the plate is not a perfect flat plane. In these situations, we have to resort to numerical methods to solve this differential equation. Generally, there are three numerical methods used to solve for the electric field: boundary element methods (BEM), finite difference methods (FDM) and finite element methods (FEM). The first two methods are conceptually simpler than the third one.

The boundary element method is also called the charge density method. In principle, it replaces the electrodes by a system of charges distributed on the electrode surfaces¹⁴². Boundaries are divided into n pieces of area and it is assumed that the charge density is uniform in each small area. Since the potentials applied on the electrode should be the same as those produced by the system of charges, according to Coulomb's law, the following formula should be satisfied:

$$V_k = \oint_S \frac{\rho_s dS}{4\pi\epsilon r} \approx \frac{1}{4\pi\epsilon} \sum_{j=1}^n \frac{\rho_{sj} \Delta S_j}{r_{jk}} \quad (6-4)$$

where V_k is the potential of element k on the boundary, ρ_{sj} is the charge density of element j , and r_{jk} is the distance between elements j and k , ΔS_j is the area of element j . From this relationship, a set of simultaneous linear equations forms and the charge distribution on the electrode can be determined. Finally, the potential and electric field of any point in the solution region can be integrated in a similar way to Eq (6-4). The advantage of this method over others is that the absence of interior elements and nodes reduces the total number of nodes dramatically and thus yields great saving in computer memory and computation time. However, variation in material properties within the region sometimes creates problems and formulation is more difficult¹⁴³.

In FDM, the solution space is treated as a regular lattice of discrete points, and only the potentials on grid points are solved. The calculation proceeds in two steps:

- (1) approximating the differential equation and boundary conditions by a set of linear algebraic equations (difference equations) on grid points within the solution region, and
- (2) solving the set of algebraic equations. As derived from the differential equation, in a

two-dimensional problem, the potential of a central point is equal to the average potential of the nearest four grid points around it.

$$V_{i,j} = \frac{1}{4}(V_{i-1,j} + V_{i+1,j} + V_{i,j-1} + V_{i,j+1}) \quad (6-5)$$

Similarly, in three dimensions, cubes are used to mesh the solution region and the potential of a central point is estimated as the mean of the potentials at the six nearest neighbors. Based on this relationship, three algorithms are commonly used to solve a problem with given boundary conditions: the iteration method, band matrix method and relaxation method. The commercial software SIMION (Scientific Instrument Services Inc., Ringoes, NJ, USA) employs an over-relaxation method, which reduces the number of iterations by adding an extra factor to the estimated potential¹⁴⁴. An obvious drawback of FDM is that the geometry can only be meshed by equal-sized squares or cubes, which leads to poor approximation and larger error on curved edges and corners, so FDM in its basic form is restricted to handling rectangular shapes and simple alterations.

Compared with FDM, FEM is a more powerful tool for handling irregular geometries and boundaries. Instead of finding an approximation of the differential equation itself, FEM is an approximation to its solution. Mathematically, of all the continuous functions $V(x,y)$ which satisfy the boundary conditions, the one which is the solution of the Laplace equation is the one that minimizes:

$$W(V) = \iint_{\Omega} \frac{1}{2} \varepsilon \left[\left(\frac{\partial V}{\partial x} \right)^2 + \left(\frac{\partial V}{\partial y} \right)^2 \right] dx dy \quad (6-6)$$

where Ω is the continuous solution region¹⁴⁵. The physical meaning of $W(V)$ is the total electric energy stored in the field. The mathematical requirement obeys the

physical principle that the potential distribution should be such that the total electric energy in the solution region is minimized. Generally, there are four steps involved in FEM¹³⁸:(1) discretizing the solution region into a finite number of elements, usually by using triangles or tetrahedrons; (2) deriving governing equations for a typical element; (3) assembling all elements in the solution region according to the minimum total energy requirement; and (4) solving the systems of linear algebraic equations obtained from previous steps. Typically, in a two-dimensional problem, approximation of voltage within a triangular element is a polynomial approximation, which is:

$$V_e(x, y) = a + bx + cy \quad (6-7)$$

where a , b , and c are constants inside this element. This assumption is the same as assuming that the electric field is uniform within the element, because the gradient of voltage remains constant inside this element. Based on Eq (6-6) and (6-7), the energy in a certain triangular element can be expressed by the coordinates of three vertexes (also called nodes) and the potentials on them. Summing the energy of all the elements together, the total energy stored in the entire region is expressed as:

$$W = \sum_{e=1}^N W_e = \frac{1}{2} \epsilon [V][C][V]^T \quad (6-8)$$

where $[V] = [V_1 \ V_2 \ V_3 \ \cdots \ V_k \ \cdots \ V_n]$, N is the total number of elements, n is the total number of nodes, and $[C]$ is the $n \times n$ global coefficient matrix, the elements of which are only related to the coordinates of the nodes. The minimum total energy requirement would be satisfied and a set of linear algebraic equations would be obtained by setting the partial derivative of W with respect to each nodal value of the potential to zero.

$$\frac{\partial W}{\partial V_k} = 0 \quad (6-10)$$

Thus, Eq (6-10) leads to:

$$\sum_{i=1}^n V_i C_{ik} = 0 \quad (6-11)$$

By solving the set of equations using a band matrix method, the voltages on each node can be obtained. The calculation is usually an extended process, the complexity of which depends on the number of nodal points.

In addition to providing good precision even with simple approximating functions, another merit of FEM is its ability to give continuous potential values over the entire region, so that the electric field can be calculated with acceptable accuracy. The limitation of FEM is that the linear function assumption within an element may cause errors. In addition, although the potential is continuous in the whole domain, the continuity of the gradient of the potential across inter-elements does not generally exist, bringing up a discrepancy against the Laplace equation which is a second-order differential equation of the potential. However, since the potential on the nodal point is accurate, by increasing the number of nodal points, it is possible to obtain the accuracy needed.

6.3 MATERIALS AND METHODS

6.3.1 Chemicals

α - and β -cyclodextrin were purchased from Sigma (St. Louis, MO, USA), and γ -cyclodextrin was purchased from Aldrich (Milwaukee, WI, USA). The cyclodextrin solutions were prepared by dissolving the powder in 10 mM certified A.C.S. grade

ammonium acetate (BDH Chemicals, Toronto, ON, Canada) to a concentration of 1.8×10^{-4} M for both α - and β -cyclodextrin and to 1.7×10^{-4} M for γ -cyclodextrin.

6.3.2 Instrumentation

A previously described home-built ion spray source¹³⁵ was used. The sprayer tip was positioned 15 mm from the curtain plate, and the orientation of the sprayer capillary was 60° with respect to the curtain plate (Figure 6. 1A). The sprayer tip was located off-axis to the aperture to prevent the neutral solvent from entering the mass spectrometer and to reduce contamination of the interface region. The 60° angle allowed lower mass ions at the outside of the spray plume to enter the mass spectrometer. Sample was introduced into the sprayer through a fused-silica capillary (150 μm OD, 50 μm ID; Polymicro Technologies, Phoenix, AZ, USA). The sample solution flow was controlled by a model 22 syringe infusion pump (Harvard Apparatus, South Natick, MA, USA), and a flow rate of 1-2 $\mu\text{L}/\text{min}$ was most frequently used in this work. The capillary was inserted into two concentric stainless steel tubes (Small Parts Inc., Miami Lakes, FL, USA) with standard wall thicknesses of 19 and 27 gauge, respectively. The inner tube held the silica capillary, and the space between the inner and outer tubes was used for the flow of the sheath gas (nebulizer). A stainless steel tee (Valco Instruments, Houston, TX, USA) held the sprayer in place and connected the nebulizer gas. The nebulizer gas was flushed concentrically with the sample flow to assist the breakdown and desolvation of charged droplets sprayed out of the end of the capillary. In this work, the nebulizer gas used was medical grade compressed air (Praxair, Mississauga, ON, Canada). The relative positions of the capillary tip, the inner stainless steel tube, and the outer stainless steel tube are illustrated in Figure 6.1B. The electrospray potential was applied through the mounting bracket of

the stainless steel tee. The ion lens was made from an oblong-shaped stainless steel ring with 1mm thickness (Figure 6.1C). The oval shaped inside was 15 mm long and 11mm wide. An arm on the mounting bracket was used to adjust the position of the ion lens with respect to the sprayer. The lens was set just behind the tip of the sprayer at 80° from the axis of the stainless steel sprayer. A CZE 1000R power supply (Spellman, Hauppauge, NY, USA) was used to provide high voltage to the lens. The ion lens was insulated from all other parts of the ion source.

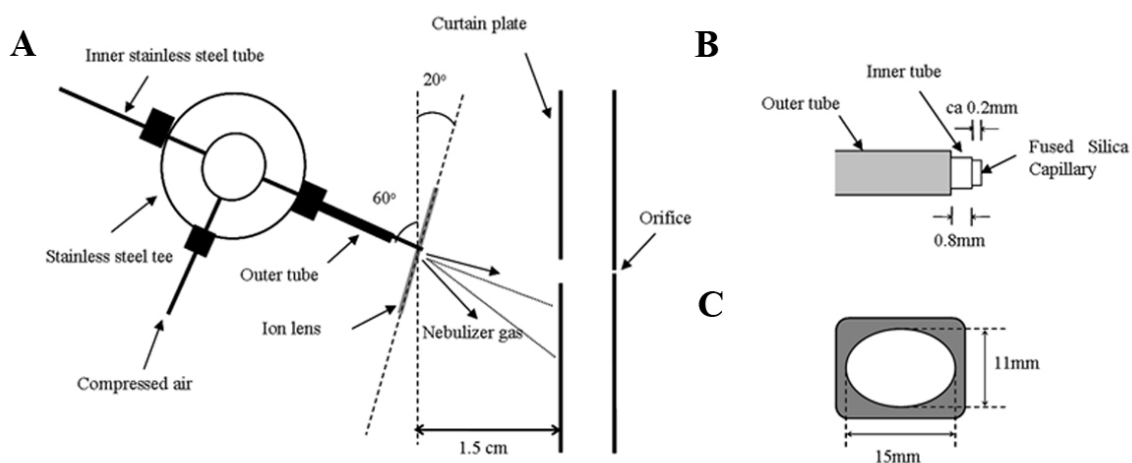


Figure 6.1: Schematic diagram of the ESI source with the atmospheric pressure ion lens.

(A) Ion lens and sprayer configuration. (B) Geometry of the capillary sprayer tip. The inner tube is positioned 0.8mm protruding out of the outer tube, and the tip of the silica capillary is protruding out of the inner tube by ca.0.2 mm. (C) Dimensions of the ion lens. The lens thickness is 1 mm.

The mass spectrometer used in this study was a prototype single quadrupole mass spectrometer from SCIEX (Toronto, ON, Canada), operated in positive ion mode. Ultra-high purity nitrogen from Praxair (manufacturer's stated purity 99.9995%) was used as the curtain gas.

6.4 MODELING

The use of COMSOL Multiphysics 3.4 includes creating geometries, setting physical properties and boundary conditions, generating and refining the mesh, and solving and post-processing the obtained data. The ion source chamber was represented by a cylinder of 15 cm height and 7 cm radius. The base of the cylinder represented the curtain plate, and the origin in the 3D Cartesian coordinate system was set at the center of this base. The symmetry axis of the cylinder was aligned with the z axis. The sprayer had a length of 3 cm and a radius of 0.2 mm, and was positioned 15 mm away from the curtain plate. The dimensions of the ion lens were the same as described in Figure 6.1C. Three 3D models of different configurations were built and the geometries are shown in Figure 6.2. Model A (Figure 6.2A) simulated the simplest situation wherein the sprayer was pointed to the center of the sampling aperture and was aligned with the symmetry axis of the cylinder. In model B (Figure 6.2B), we added an ion lens positioned 1mm back from the sprayer tip and orientated 90° with respect to the sprayer. Model C (Figure 6.2C) simulated the experimental setup as described in Figure 6.2A. Free mesh parameters were set as the following: maximum element size scaling factor 0.32, element growth rate 1.32, mesh curvature factor 0.22, mesh curvature cut-off 0.005, resolution of narrow regions 0.9. After meshing based on these parameters, the elements were refined once. The total tetrahedral elements of models A, B and C were 1834694, 1985905 and 1993375, respectively. The space charge was set to zero and the Laplace equation was solved in the cylindrical domain. The ion source chamber was at ground in all three models. The voltages on the sprayer and ion lens were set to different values in different

situations. Calculations were run on a PC with an AMD Athlon 64X2 dual core processor and 4G memory, and each run took no more than 3 hr.

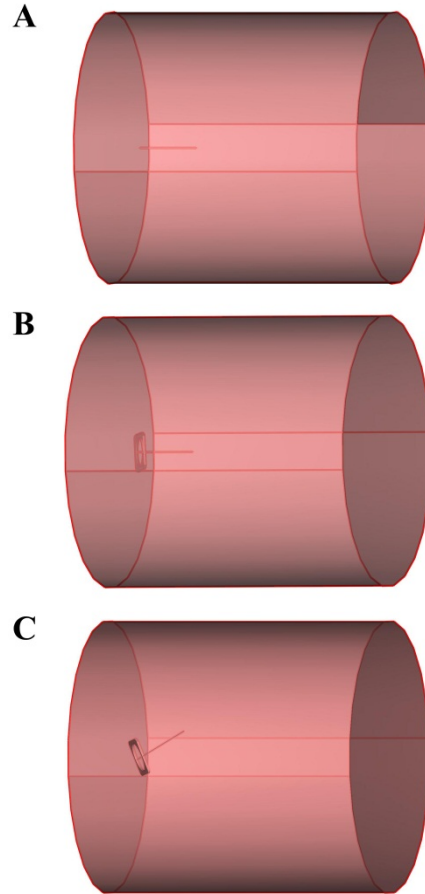


Figure 6.2: COMSOL Multiphysics configurations of the ESI source with ion lens. (A) Model A, the sprayer is perpendicular to the curtain plate and aligned with the z axis, no ion lens. (B) Model B, the sprayer is perpendicular to the curtain plate, and the ion lens is positioned 1mm back from the sprayer tip and orientated at 90° with respect to the sprayer. (C) Model C, the relative positions of the sprayer, curtain plate and ion lens are the same as illustrated in Figure 6.1A.

6.5 RESULTS AND DISCUSSION

To test the accuracy of the simulation results, a potential of 5000V was applied on the sprayer in model A. The calculated electric field intensity at the center of the sprayer tip surface is 8.446×10^6 V/m, which is quite close to the analytical solution, 8.766×10^6 V/m,

obtained by Eq (6-3) with A equal to 2. Integrating the z component of the electric field along the line from the center of the sprayer tip to the center of the curtain plate gives a value of 4999.354 V, which is almost equal to theoretically applied voltage of 5000 V. A third piece of evidence showing the consistency with the applied conditions is that the calculated total positive charge on the positive electrode is $1.899 \times 10^{-9} \text{C}$, which is very close to the total negative charge on the negative electrode of $1.926 \times 10^{-9} \text{C}$.

Model B investigates the effect of the ion lens on the electric field in the ESI source. The voltage on the sprayer is fixed at 5000V, while the voltage on the lens varies from 1000 to 4000 V. Figure 6.3 shows a comparison of the voltage and the norm of the electric field distributed along the line from the center of sprayer tip to the centre of the curtain plate. As the voltage on the ion lens increases, the potential drops more slowly near the sprayer tip (Figure 6.3A), suggesting that the electric field intensity at the tip gets smaller. This fact is shown more directly in Figure 6.3B. Within a 2 mm distance of the tip, the higher the voltage applied on the lens, the smaller the electric field intensity. The field intensity on the sprayer tip with a 4000 V ion lens is only half of that on a sprayer tip without the ion lens. From this point of view, the voltage on the ion lens should not be set too close to the voltage of the sprayer, otherwise, the potential gradient near the sprayer tip may not be able to generate an electric field strong enough to overcome the surface tension of the liquid, which would impede the whole ESI process.

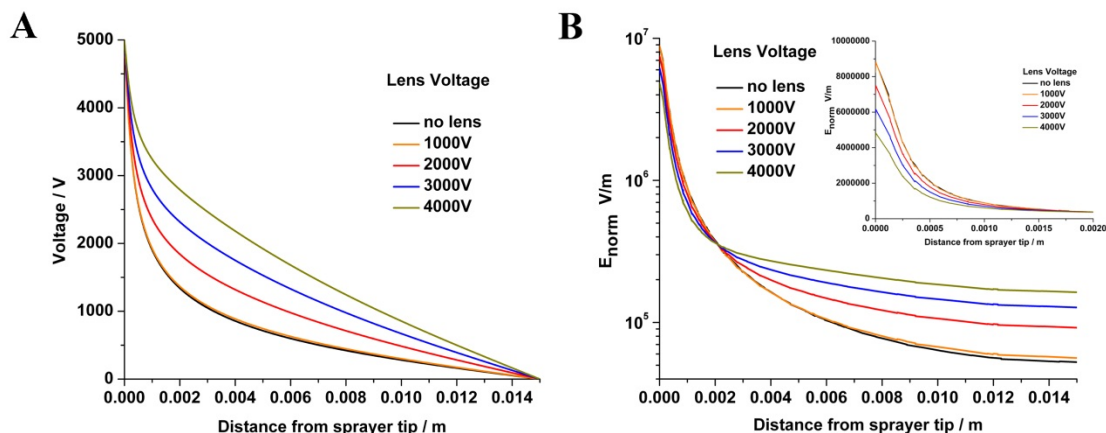


Figure 6.3: Voltage distribution (A) and magnitude of electric field strength (B) from the center of the sprayer tip to the center of curtain plate at different ion lens voltage.

The voltage on the sprayer is 5000 V. Inset: the magnitude of electric field close to the sprayer tip, from 0 to 2 mm, plotted in linear scales.

Although the addition of an ion lens on the sprayer may affect the efficiency of forming charged droplets, it provides the benefits of generating a more ‘homogenous’ electric field in the ion source. Despite the fact that the electric field intensity decreases all the way from the sprayer tip to the curtain plate, from Figure 6.3B, it is clear that applying higher voltage on the ion lens leads to a smaller drop in electric field in the whole space, and the electrostatic force applied on a charged species would be stronger later as it approaches the counter plate. This more ‘homogenous’ electric field would give a relatively more constant control on the flight of charged species during the flight time in the atmospheric region, rather than changing the direction of the ion motion abruptly at the beginning, which is the situation when there is no ion lens. As the electric field lines are always more divergent near the sharp tip of the sprayer (Figure 6.4B), and become more parallel near the flat curtain plate, it is obviously unfavorable to apply all the electrostatic force on the charged species at the beginning. From the

energy transformation point of view, since the voltage difference between the sprayer and curtain plate is finite, the total electric potential energy that a charged species possesses at the tip that would later be converted into kinetic energy is also finite. Without an ion lens, the voltage drops dramatically near the sprayer tip, and a large fraction of the total electric potential energy is immediately transformed into kinetic energy due to the work done by the large electric force. Adding an ion lens delays the conversion of electric potential energy into kinetic energy. Because the potential drops more gently near the sprayer tip and more linearly along the path to the sampling orifice under the influence of the ion lens, electric potential energy would be more evenly converted into kinetic energy along the path from the sprayer tip to the curtain plate. Thus, a larger portion of the charged species would be directed into the sampling aperture under the control of the more homogeneous electric field.

In addition to influencing the magnitude of the distribution of the field strength, the ion lens also modifies the direction of the electric field in the ion source. Figure 6.4A compares the equipotential surfaces of the electric field generated by a 5000 V sprayer, and a 5000 V sprayer with a 3000 V ion lens. Since in an electrostatic field the boundaries of conductors are equipotential surfaces themselves, the shape of the electrodes would have a great impact on the shape of equipotential surfaces near them. From Figure 6.4A, it can be seen that near the sharp tip of the sprayer, the curvature of the equipotential surfaces is quite large; while near the flat ion lens, the curvature of the equipotential surfaces is small. The flat shape of the ion lens has an effect of flattening the equipotential surfaces near it. When there is no ion lens, the curved equipotential surfaces near the sprayer tip imply that the potential drops dramatically in every direction,

so the field strengths in all the directions are large and comparable. When the ion lens is applied, the flatter potential surfaces near the sprayer tip make the potential drops mostly only in one direction – the direction that points directly to the curtain plate, so that the field strengths in other directions are much smaller. Thus the flatter equipotential surfaces produce a more convergent electric field than the curved ones. This is confirmed by the electric field line plot in Figure 6.4B.

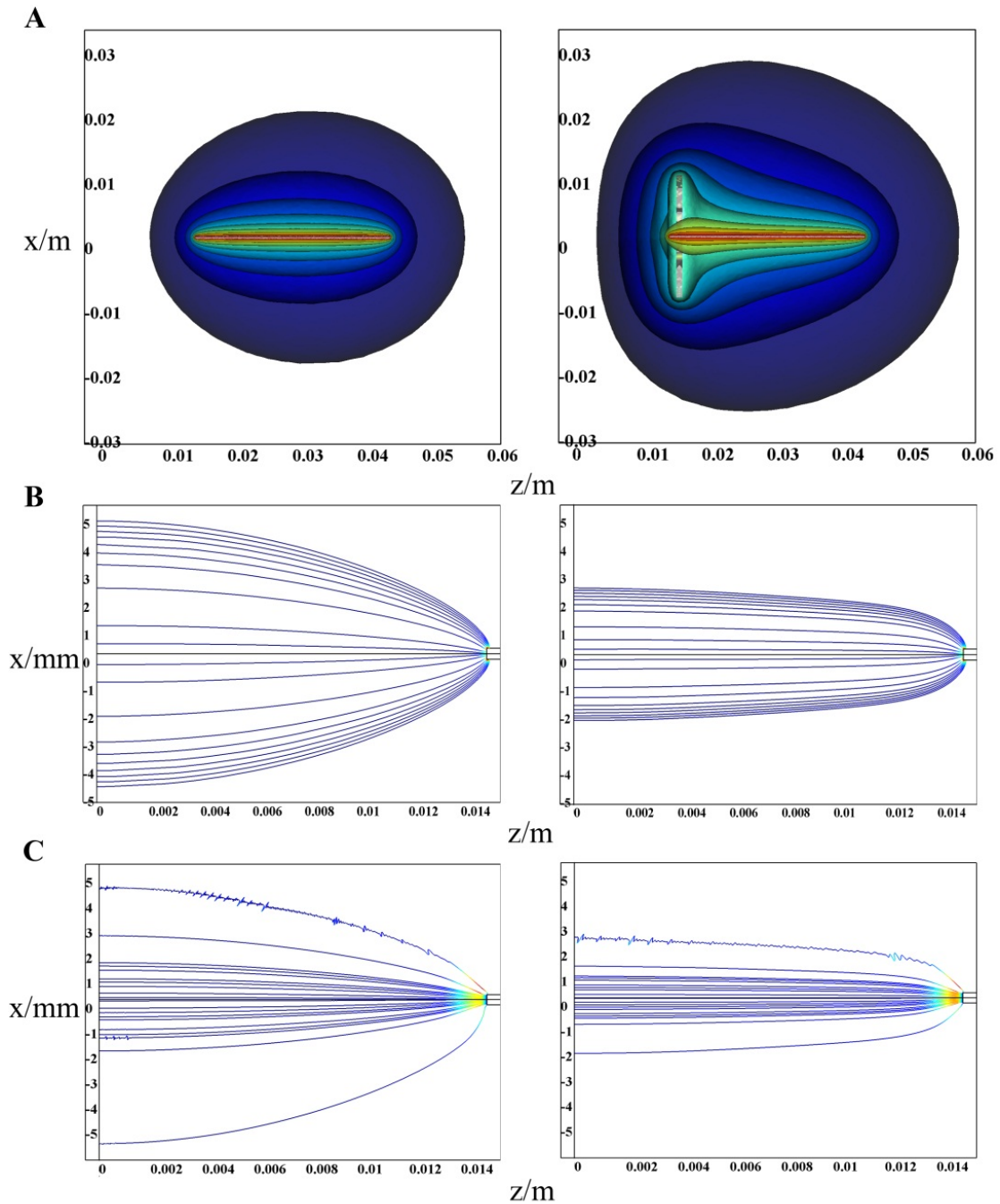


Figure 6.4: Simulation results of model A (left, sprayer 5000V, no ion lens) and model B (right, sprayer 5000 V, ion lens 3000 V).
 (A) Equipotential surfaces, the potential difference between two successive coloured layers is 500V. (B) Field lines between the curtain plate and the sprayer tip. (C) Trajectories of 1 micrometer radius droplets between the curtain plate and the sprayer tip.

To demonstrate the focusing effect of the ion lens, we also calculated the trajectories of water droplets with 1 micron radius and 50000 unit positive charges in the electric field according to the following equations.

$$m \frac{d^2 \vec{r}(t)}{dt^2} = q \vec{E} - \vec{F}_{drag} \quad (6-12)$$

$$\vec{F}_{drag} = \frac{1}{2} C_d \rho A \vec{v} \quad (6-13)$$

$$C_d = \frac{24}{Re} + \frac{6}{1 + \sqrt{Re}} + 0.4 \quad (6-14)$$

Here, m is the mass of the droplet, and q is the charges on the droplet. \vec{F}_{drag} is the drag force applied by the ambient atmosphere¹⁴⁶. C_d is the so-called drag coefficient, ρ is the density of air, A is the cross-sectional area of the droplet, and \vec{v} is the velocity of the droplet. Re is the Reynolds number, which is dimensionless and equals $\rho l v / \eta$, where l is the diameter of the droplet, and η is the viscosity of the air. Figure 6.4C shows ten trajectories of charged droplets that start from the surface of the sprayer tip. From the trajectories shown in these plots, the movements of droplets almost follow the track of field lines and they are confined in a much narrower region with the existence of an ion lens. Although the trajectory modeling is rather simple and unrealistic without considering the solvent evaporation and coulomb fission of the droplets, it reflects the focusing effect of the atmospheric ion lens. Another conclusion that we can draw, by comparing the equipotential plots and field lines plots at different ion lens voltage, is that the focusing effect of the ion lens becomes better when the voltage applied on it gets higher, because the field lines are more convergent to the central axis (Figures not shown). However, a higher ion lens voltage would cause lower local potential gradients

and thus lower the field intensity on the sprayer tip, which decreases the efficiency of forming charged droplets. To obtain the best performance, one has to choose a moderate voltage on the ion lens to balance between the focusing effect in the whole source region and the side effects brought about by reduction of the field intensity on the sprayer tip.

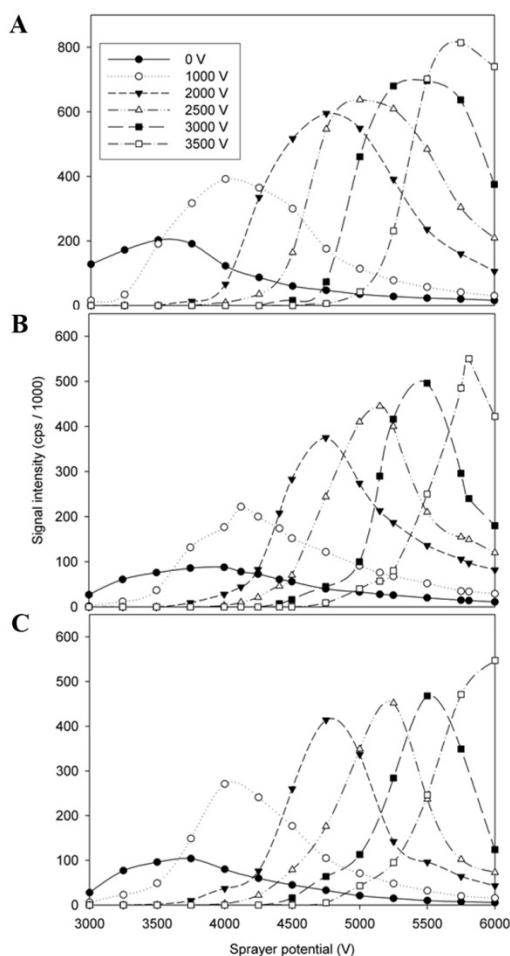


Figure 6.5: Signal intensity as a function of sprayer voltage at different ion lens voltages.

The ion lens voltages used are from 0 to 3500 V, (A) α -cyclodextrin, (B) β -cyclodextrin, and (C) γ -cyclodextrin.

Model C simulates the electric field in an ESI source according to experimentally measured parameters. Mass spectrometric signal intensities were recorded while varying the sprayer voltage at a series of ion lens voltage settings. For each cyclodextrin (CD) species (α , β , γ), the multiple ion scan mode of the mass spectrometer was used to

collect signal from a range of ± 5 m/z units around the m/z value of the protonated molecule. As shown in Figure 6.5, with increasing ion lens voltage, the onset and maximum signal shifted to higher sprayer voltage and this shift was very similar for each of the three analytes. In all cases, the voltage difference between the sprayer and the ion lens was in the range of 1250–1750V when onset signals could be detected, and in the range of 2500–3000V when maximum signal intensities were achieved. This observation implies that the electric field around the spray tip can be kept relatively constant by choosing an appropriate voltage difference between the sprayer and the ion lens. Only when the voltage difference between the sprayer and the ion lens is large enough can the electric field intensity be strong enough to spray the solution. Table 6.1 shows the calculated electric field intensity on the sprayer tip under the onset conditions. The similarity of these data can be explained by Eq (6-15). The onset electric field on the sprayer tip is the field required to overcome the surface tension of the liquid and cause instability of the static Taylor cone, leading to the formation of the charged jet,

$$E_{on} \approx \sqrt{\frac{2\gamma \cos\theta}{\epsilon_0 r_c}} \quad (6-15)$$

where γ is the surface tension of the solvent, ϵ_0 is the permittivity of vacuum, r_c is the radius of capillary, and θ is the half angle of Taylor cone, 49.3° ¹⁴⁰. Substituting the surface tension of water as 0.073 N/m, the radius of the capillary as 0.2 mm, the theoretical onset voltage to electrospray water is calculated to be 7.35×10^6 V/m. Table 6.2 shows the calculated electric field strengths on the sprayer tip under the maximum signal conditions. These data are also very similar to each other. The optimum field strengths are about 2×10^6 V/m stronger than those under the onset conditions.

Sprayer Voltage/V	3250	3750	4250	4500	5000
Ion Lens Voltage/V	1000	2000	2500	3000	3500
Field Strength 10^6 V/m	5.106	4.829	5.180	5.042	5.393

Table 6.1: Field strength at the sprayer tip for onset of signal under various conditions.

Sprayer Voltage/V	4000	4750	5250	5500
Ion Lens Voltage/V	1000	2000	2500	3000
Field Strength 10^6 V/m	6.574	6.787	7.138	7.000

Table 6.2: Field strength at the sprayer tip for optimum signal under various conditions.

As shown by the equipotential surfaces and field lines in Figure 6.6 and 6.7, the optimum electric fields to produce maximum signal are achieved by a combination of moderate electric field strength at the sprayer tip and flattened equipotential surfaces generated by the ion lens. Noticing that in Figure 6.5 the maximum signal intensity increases with increasing ion lens voltage and sprayer voltage, we can conclude that an increased voltage difference between the sprayer and curtain plate would provide higher kinetic energy to the charged species. This would then shorten the traveling time of the ion in the ion source region and restrict the dispersion induced by coulombic repulsion, and also increase the ionization efficiency due to higher collisional energy. More ions would then be directed into the sampling aperture and the signal intensity would be enhanced.

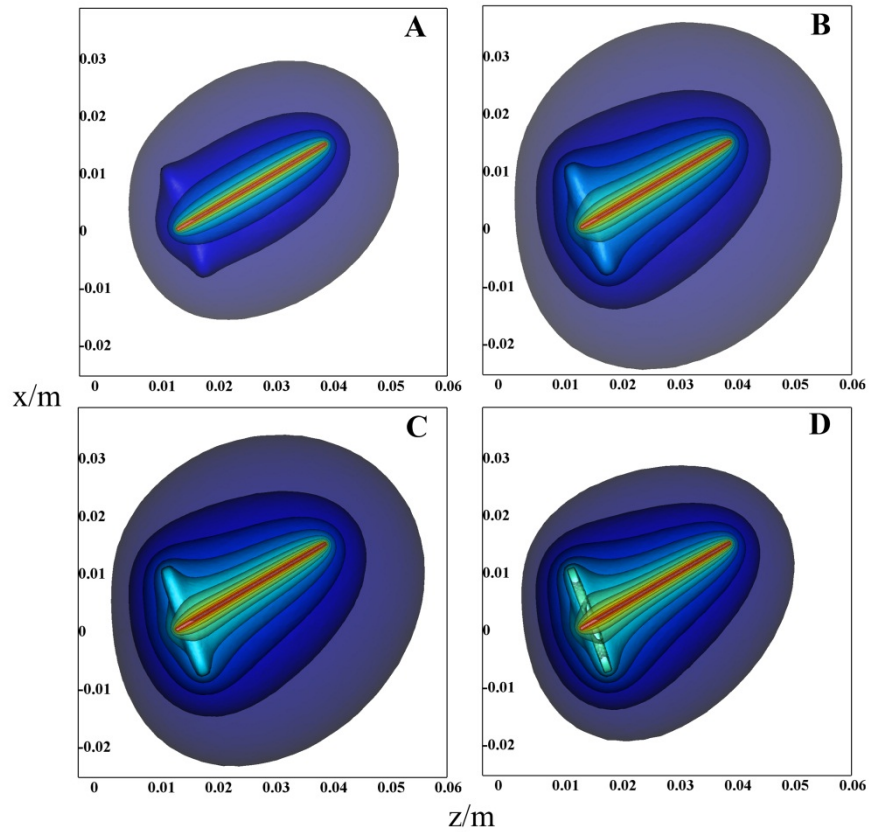


Figure 6.6: Equipotential surfaces for various voltage combinations of the sprayer and ion lens that result in maximum signal intensity.

The potential difference between two coloured layers is 400V: (A) sprayer 4000V, ion lens 1000 V; (B) sprayer 4750 V, ion lens 2000 V; (C) sprayer 5250V, ion lens 2500V; and (D) sprayer 5500V, 3000 V.

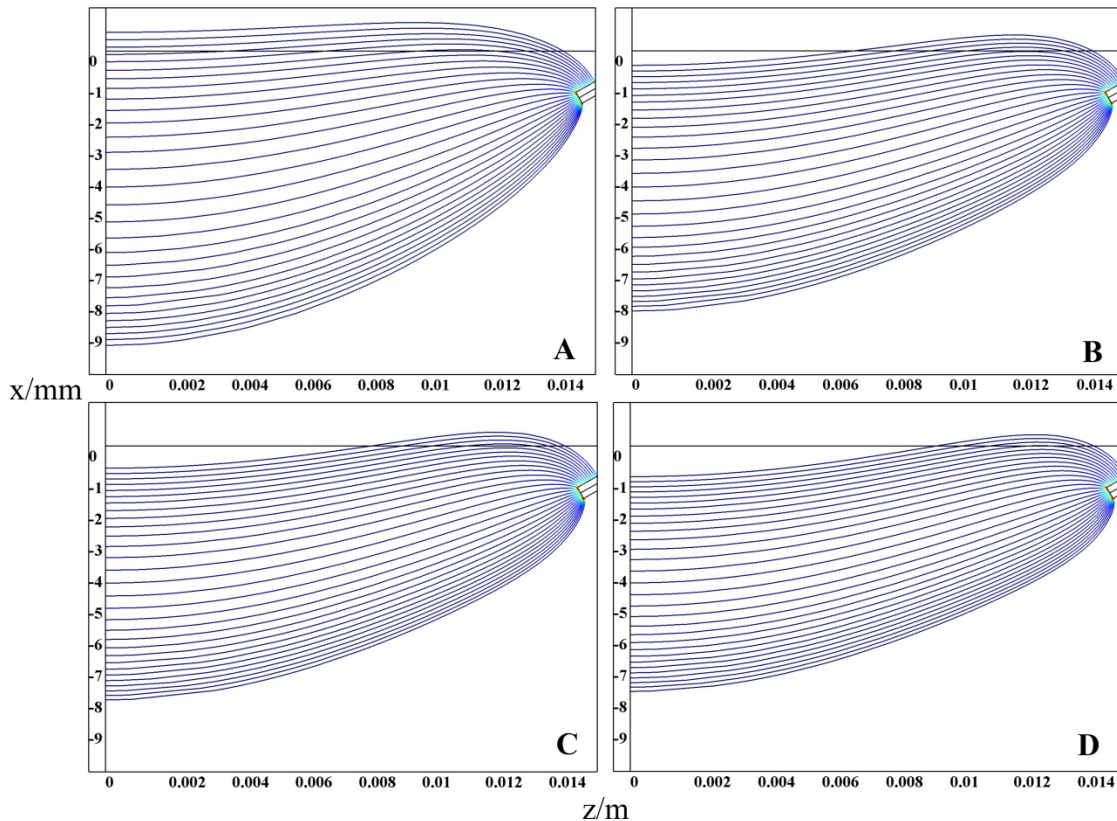


Figure 6.7: Field line distributions for various voltage combinations of the sprayer and ion lens.

Conditions are the same as described in Figure 6.6. (A) sprayer 4000V, ion lens 1000 V; (B) sprayer 4750V, ion lens 2000V; (C) sprayer 5250 V, ion lens 2500 V; and (D) sprayer 5500 V, 3000 V.

6.6 CONCLUSIONS

This work employed numerical methods to simulate the electric field in an ESI source with an atmospheric ion lens. With the help of this powerful tool, the static electric field generated by a complex electrode system can be simulated and the effect understood. Based on experimental data and theoretical calculations, we demonstrate that the atmospheric ion lens has a focusing effect and the sampling efficiency is improved when an appropriate voltage is applied to it. The field intensity is determined by the

local potential gradient, so the magnitude of field intensity close to the sprayer tip is dominated by the voltage difference between the ion lens and the sprayer, while in the larger space further from the tip, the field intensity mainly depends on the voltage difference between the ion lens and the curtain plate. There is always an optimum ion lens voltage to achieve the maximum signal intensity. The calculated results also show that the electric field strengths at the sprayer tip under both the onset and the maximum signal conditions are consistent for different combinations of voltages on the sprayer and ion lens. In the future, this simulation method can be used to design and optimize the geometry of the ESI ion source and atmospheric ion lens to achieve better sampling efficiency.

Chapter 7: Concluding remarks and future work

7.1 CONCLUDING REMARKS

This thesis attempts to improve CE-MS interfacing strategy by using coaxial stainless steel tubing with bevelled tip as both electrospray emitter and CE outlet electrode. The fabrication material provides a robust and long-lasting ESI-MS interface. The flow-through microvial design only requires self alignment of the capillary column and the stainless steel sprayer, and using standard size fittings makes the assembly of the interface simple and fast. The bevelled tip geometry extends the operational flow rate range and decreases the lower limit for a stable spray. The electric continuity of the electrophoresis circuit is guaranteed by the flow-through microvial and modifier supply.

The post-column band broadening effects introduced by this interface and other types of junction-at-the-tip CE-MS interface are investigated by studying the hydrodynamic flow patterns and mass transport process inside the microvial at the end of the CE separation capillary. Simulation results obtained by solving the Navier-Stokes and mass balance equations provide insights into the velocity field and concentration distribution of the analytes while it is going through the microvial. It has been demonstrated that, with a low flow rate of chemical modifier solution, the laminar flow streams confine the analyte molecules to the central part of the microvial and thus maintain major features of the peak shapes. Peaks detected by UV and MS under similar experimental conditions were compared to verify the numerical prediction that the main characteristics of the UV peak can be retained in the MS peak. Experiments also show that band broadening can be minimized when an appropriate chemical modifier flow rate is selected.

Different modes of capillary electrophoresis operations have been applied with this ESI-MS interface, with forward, zero or reversed EOF. Methods for analyzing

metabolites, proteins, peptides and basic drug compounds using this CE-ESI-MS interface were developed. Improvement on sensitivity was demonstrated by side-by-side comparison with commercial sheath flow interface using amino acids under similar conditions. Although the overall detection limit might not reach the region of sheathless interfaces due to the constraints of lowest applicable flow rate, this interface can satisfy the sensitivity requirement in most applications. Furthermore, it is compatible with several special separation modes which could not be achieved with sheathless interfaces, such as cIEF-ESI-MS.

In cIEF-ESI-MS, this interface utilizes the flow-through microvial to supply the catholyte and mobilizer solutions during the isoelectric focusing and mobilization processes. It also allows for complete focusing and mobilization processes to be performed automatically in programmed sequences with commercial CE systems. The flow-through microvial also provides a stable chemical environment and helps to improve the ionization efficiency without significantly diluting the analyte. The interface facilitates the transfer of the mobilized cIEF effluent to the site of electrospray ionization, and the gaseous ions can be detected directly by a mass spectrometer.

Operation strategies developed for the use of bare fused silica capillaries and neutral coated capillaries have been developed, using a part of the capillary or the flow-through microvial of the CE-MS interface as the catholyte reservoir. Reasonable separation efficiency and detection sensitivity was achieved by using proper concentration of carrier ampholytes and suitable strategies of electroosmotic/electrophoretic mobilization.

7.2 FUTURE WORK

7.2.1 Further optimization on cIEF-ESI-MS strategies

Feasibility of online cIEF-ESI-MS with electroosmotic/electrophoretic mobilization has been demonstrated by using the CE-MS interface presented. Further improvements on reproducibility and separation efficiency are still needed for real sample applications. First of all, stability of the capillary surface coatings, and their interaction with the ampholytes and protein samples are important issues to be investigated for improving reproducibility. Neutral surface coatings based on polyacrylamide, polyvinyl alcohol, cellulose derivatives, dimethylpolysiloxane, and fluorocarbons, have been applied in cIEF by other researchers. The one that gives the most consistent forward EOF and interacts least with the ampholytes and proteins should be chosen for further optimization on other factors. Secondly, the synthesis of different brands of ampholytes does not follow the same protocol, so the components differ in several aspects - structures, number of effective species per pH unit, linearity of pH gradient after focusing, buffering capacity, and molecular weight distribution¹⁴⁷⁻¹⁵⁰. Focusing bandwidth and low background noise for ESI-MS detection are two indicators for choosing suitable ampholytes. For specific target proteins, narrow range ampholytes can be used to resolve multiple components that slightly differ in pI. As to the anolyte and catholyte, buffers whose pH are slightly lower or higher than the acidic or basic boundary of the ampholytes, might work better than strong acid or base owing to reduced anodic or cathodic drift. Another problem that needs to be solved is that, proteins tend to aggregate at buffer pH close to their pI values, especially at high concentration after focusing. Adding urea in the focusing media alleviates this problem in applications using optical

detection; however, an ESI-MS compatible protein stabilizer must be chosen for the online cIEF-MS applications. If the problems above could be addressed, we can expect that cIEF-ESI-MS will play an important role in quality control of biopharmaceutical industry and proteomics research.

7.2.2 Incorporation of atmospheric ion lens into the CE-ESI-MS interface

Preliminary work in chapter 6 has demonstrated that the ion lens improves the electrospray ionization and sampling efficiency in the reduced flow rate region. Coupling the ion lens with the presented CE-ESI-MS interface is easy to realize and should give more flexibility on choosing the EOF and chemical modifier flow rate. Additionally, if the two innovations are combined, the sensitivity of this new CE-ESI-MS interface will be substantially improved.

BIBLIOGRAPHY

- (1) Jorgenson, J. W.; Lukacs, K. D. *Analytical Chemistry* **1981**, *53*, 1298.
- (2) *Handbook of capillary and microchip electrophoresis and associated microtechniques*; 3rd ed.; Landers, J. P., Ed.; CRC press: Boca Raton, FL, 2008.
- (3) Giddings, J. C. *Separation Science* **1969**, *4*, 181.
- (4) Peng, X. J.; Chen, D. D. Y. *Journal of Chromatography A* **1997**, *767*, 205.
- (5) Gas, B.; Stedry, M.; Kenndler, E. *Electrophoresis* **1997**, *18*, 2123.
- (6) Huang, X. H.; Coleman, W. F.; Zare, R. N. *Journal of Chromatography* **1989**, *480*, 95.
- (7) Sternberg, J. *Advances in Chromatography* **1966**, *2*, 205.
- (8) Righetti, P. G.; Bossi, A. *Analytica Chimica Acta* **1998**, *372*, 1.
- (9) Hjerten, S.; Zhu, M. D. *Journal of Chromatography* **1985**, *346*, 265.
- (10) Kilar, F. *Electrophoresis* **2003**, *24*, 3908.
- (11) Rilbe, H. *Annals of the New York Academy of Sciences* **1973**, *209*, 11.
- (12) Shimura, K. *Electrophoresis* **2009**, *30*, 11.
- (13) Douglas, D. J. *Mass Spectrometry Reviews* **2009**, *28*, 937.
- (14) March, R. E. *Journal of Mass Spectrometry* **1997**, *32*, 351.
- (15) Hoffmann, E. d.; Stroobant, V. *Mass spectrometry: principles and applications*; 3rd ed.; John Wiley: Chichester, England, 2007.
- (16) Cooks, R. G.; Kaiser, R. E. *Accounts of Chemical Research* **1990**, *23*, 213.
- (17) Douglas, D. J.; Frank, A. J.; Mao, D. M. *Mass Spectrometry Reviews* **2005**, *24*, 1.
- (18) Bailey, A. G. *Electrostatic spraying of liquids*; Wiley: New York 1988.
- (19) Dole, M.; Mack, L. L.; Hines, R. L. *Journal of Chemical Physics* **1968**, *49*, 2240.
- (20) Yamashita, M.; Fenn, J. B. *Journal of Physical Chemistry* **1984**, *88*, 4451.
- (21) Dunn, W. B.; Ellis, D. I. *Trac-Trends in Analytical Chemistry* **2005**, *24*, 285.
- (22) Han, X. L.; Gross, R. W. *Mass Spectrometry Reviews* **2005**, *24*, 367.
- (23) Heck, A. J. R.; van den Heuvel, R. H. H. *Mass Spectrometry Reviews* **2004**, *23*, 368.
- (24) van den Heuvel, R. H. H.; Heck, A. J. R. *Current Opinion in Chemical Biology* **2004**, *8*, 519.
- (25) Cech, N. B.; Enke, C. G. *Mass Spectrometry Reviews* **2001**, *20*, 362.
- (26) Kebarle, P. *Journal of Mass Spectrometry* **2000**, *35*, 804.
- (27) Kebarle, P.; Peschke, M. *Analytica Chimica Acta* **2000**, *406*, 11.
- (28) Iribarne, J. V.; Thomson, B. A. *Journal of Chemical Physics* **1976**, *64*, 2287.
- (29) Thomson, B. A.; Iribarne, J. V. *Journal of Chemical Physics* **1979**, *71*, 4451.
- (30) Nguyen, N. T.; Yonker, C. R.; Smith, R. D. *Analytical Chemistry* **1987**, *59*, 1231.
- (31) Michalke, B.; Schramel, O.; Ketrup, A. *Fresenius Journal of Analytical Chemistry* **1999**, *363*, 456.
- (32) Preisler, J.; Hu, P.; Rejtar, T.; Moskovets, E.; Karger, B. L. *Analytical Chemistry* **2002**, *74*, 17.
- (33) Takada, Y.; Sakairi, M.; Koizumi, H. *Analytical Chemistry* **1995**, *67*, 1474.
- (34) Mol, R.; de Jong, G. J.; Somsen, G. W. *Electrophoresis* **2005**, *26*, 146.
- (35) Maxwell, E. J.; Chen, D. D. Y. *Analytica Chimica Acta* **2008**, *627*, 25.
- (36) Smith, R. D.; Barinaga, C. J.; Udseth, H. R. *Analytical Chemistry* **1988**, *60*, 1948.
- (37) Mokaddem, M.; Gareil, P.; Belgaied, J. E.; Varenne, A. *Electrophoresis* **2009**, *30*, 1692.

- (38) Jussila, M.; Sinervo, K.; Porras, S. P.; Riekkola, M. L. *Electrophoresis* **2000**, *21*, 3311.
- (39) Zhang, B.; Liu, H.; Karger, B. L.; Foret, F. *Analytical Chemistry* **1999**, *71*, 3258.
- (40) Wachs, T.; Sheppard, R. L.; Henion, J. *Journal of Chromatography B-Biomedical Applications* **1996**, *685*, 335.
- (41) Fanali, S.; D'Orazio, G.; Foret, F.; Kleparnik, K.; Aturki, Z. *Electrophoresis* **2006**, *27*, 4666.
- (42) Ramsey, R. S.; McLuckey, S. A. *Journal of Microcolumn Separations* **1995**, *7*, 461.
- (43) Nilsson, S.; Klett, O.; Svedberg, M.; Amirkhani, A.; Nyholm, L. *Rapid Communications in Mass Spectrometry* **2003**, *17*, 1535.
- (44) Chen, Y. R.; Her, G. R. *Rapid Communications in Mass Spectrometry* **2003**, *17*, 437.
- (45) Zamfir, A. D.; Dinca, N.; Sisu, E.; Peter-Katalinic, J. *Journal of Separation Science* **2006**, *29*, 414.
- (46) Bendahl, L.; Hansen, S. H.; Olsen, J. *Rapid Communications in Mass Spectrometry* **2002**, *16*, 2333.
- (47) Nilsson, S.; Wetterhall, M.; Bergquist, J.; Nyholm, L.; Markides, K. E. *Rapid Communications in Mass Spectrometry* **2001**, *15*, 1997.
- (48) Zhu, X. F.; Thiam, S.; Valle, B. C.; Warner, I. M. *Analytical Chemistry* **2002**, *74*, 5405.
- (49) Dahlin, A. P.; Wetterhall, M.; Liljegren, G.; Bergstrom, S. K.; Andren, P.; Nyholm, L.; Markides, K. E.; Bergquist, J. *Analyst* **2005**, *130*, 193.
- (50) Fang, L. L.; Zhang, R.; Williams, E. R.; Zare, R. N. *Analytical Chemistry* **1994**, *66*, 3696.
- (51) Cao, P.; Moini, M. In *Journal of the American Society for Mass Spectrometry* 1997; Vol. 8, p 561.
- (52) Moini, M. *Analytical Chemistry* **2001**, *73*, 3497.
- (53) Moini, M. *Analytical Chemistry* **2007**, *79*, 4241.
- (54) Petersson, M. A.; Hulthe, G.; Fogelqvist, E. *Journal of Chromatography A* **1999**, *854*, 141.
- (55) Whitt, J. T.; Moini, M. *Analytical Chemistry* **2003**, *75*, 2188.
- (56) Figeys, D.; vanOostveen, I.; Ducret, A.; Aebersold, R. *Analytical Chemistry* **1996**, *68*, 1822.
- (57) Severs, J. C.; Smith, R. D. *Analytical Chemistry* **1997**, *69*, 2154.
- (58) Ishihama, Y.; Katayama, H.; Asakawa, N.; Oda, Y. *Rapid Communications in Mass Spectrometry* **2002**, *16*, 913.
- (59) Smyth, W. F. *Electrophoresis* **2005**, *26*, 1334.
- (60) Chalcraft, K. R.; Britz-McKibbin, P. *Analytical Chemistry* **2009**, *81*, 307.
- (61) Ullsten, S.; Danielsson, R.; Backstrom, D.; Sjoberg, P.; Bergquist, J. *Journal of Chromatography A* **2006**, *1117*, 87.
- (62) Haselberg, R.; de Jong, G. J.; Somsen, G. W. *Journal of Chromatography A* **2007**, *1159*, 81.
- (63) Herrero, M.; Ibanez, E.; Cifuentes, A. *Electrophoresis* **2008**, *29*, 2148.
- (64) Monton, M. R. N.; Terabe, S. *Analytical Sciences* **2005**, *21*, 5.
- (65) Metzger, J.; Schanstra, J.; Mischak, H. *Analytical and Bioanalytical Chemistry* **2009**, *393*, 1431.
- (66) Campa, C.; Coslovi, A.; Flamigni, A.; Rossi, M. *Electrophoresis* **2006**, *27*, 2027.

- (67) Zamfir, A.; Peter-Katalinic, J. *Electrophoresis* **2004**, *25*, 1949.
- (68) Amon, S.; Zamfir, A. D.; Rizzi, A. *Electrophoresis* **2008**, *29*, 2485.
- (69) Kolch, W.; Neuss, C.; Peizing, M.; Mischak, H. *Mass Spectrometry Reviews* **2005**, *24*, 959.
- (70) Servais, A. C.; Crommen, J.; Fillet, M. *Electrophoresis* **2006**, *27*, 2616.
- (71) Kele, Z.; Ferenc, G.; Klement, T.; Toth, G. K.; Janaky, T. *Rapid Communications in Mass Spectrometry* **2005**, *19*, 881.
- (72) Chang, Y. Z.; Her, G. R. *Analytical Chemistry* **2000**, *72*, 626.
- (73) Chang, Y. Z.; Chen, Y. R.; Her, G. R. *Analytical Chemistry* **2001**, *73*, 5083.
- (74) Johansson, I. M.; Pavelka, R.; Henion, J. D. *Journal of Chromatography* **1991**, *559*, 515.
- (75) Lewis, K. C.; Opiteck, G. J.; Jorgenson, J. W.; Sheeley, D. M. *Journal of the American Society for Mass Spectrometry* **1997**, *8*, 495.
- (76) Hsieh, F.; Baronas, E.; Muir, C.; Martin, S. A. *Rapid Communications in Mass Spectrometry* **1999**, *13*, 67.
- (77) Chen, Y. R.; Tseng, M. C.; Chang, Y. Z.; Her, G. R. *Analytical Chemistry* **2003**, *75*, 503.
- (78) Tseng, W. C.; Chen, Y. R.; Her, G. R. *Analytical Chemistry* **2004**, *76*, 6306.
- (79) Liu, C. C.; Alary, J. F.; Vollmerhaus, P.; Kadkhodayan, M. *Electrophoresis* **2005**, *26*, 1366.
- (80) Liu, C. C.; Zhang, J. Z.; Dovichi, N. J. *Rapid Communications in Mass Spectrometry* **2005**, *19*, 187.
- (81) Wojcik, R.; Dada, O. O.; Sadilek, M.; Dovichi, N. J. *Rapid Communications in Mass Spectrometry* **2010**, *24*, 2554.
- (82) Maxwell, E. J.; Zhong, X. F.; Zhang, H.; van Zeijl, N.; Chen, D. D. Y. *Electrophoresis* **2010**, *31*, 1130.
- (83) Tetler, L. W.; Cooper, P. A.; Powell, B.; Elsevier Science Bv: 1995, p 21.
- (84) Juraschek, R.; Rollgen, F. W. *International Journal of Mass Spectrometry* **1998**, *177*, 1.
- (85) Maxwell, E. J.; Zhong, X. F.; Chen, D. D. Y. *Analytical Chemistry* **2010**, *82*, 8377.
- (86) Mokaddem, M.; Gareil, P.; Belgaied, J. E.; Varenne, A. *Electrophoresis* **2008**, *29*, 1957.
- (87) Lehninger, A. L.; Nelson, D. L.; Cox, M. M. *Principles of Biochemistry* 2nd ed.; Worth Publishers: New York, NY, 1993.
- (88) Gas, B.; Kenndler, E. *Electrophoresis* **2002**, *23*, 3817.
- (89) Kleparnik, K.; Otevreil, M. *Electrophoresis* **2010**, *31*, 879.
- (90) Cheng, Y. F.; Wu, S. L.; Chen, D. Y.; Dovichi, N. J. *Analytical Chemistry* **1990**, *62*, 496.
- (91) Gebauer, P.; Bocek, P. *Analytical Chemistry* **1997**, *69*, 1557.
- (92) Gallardo, E.; Barroso, M.; Queiroz, J. A. *Drug Testing and Analysis* **2009**, *1*, 109.
- (93) Smyth, W. F. *Electrophoresis* **2006**, *27*, 2051.
- (94) Suntornsuk, L. *Analytical and Bioanalytical Chemistry* **2010**, *398*, 29.
- (95) Servais, A. C.; Crommen, J.; Fillet, M. *Electrophoresis* **2006**, *27*, 2616.
- (96) Santos, B.; Simonet, B. M.; Rios, A.; Valcarcel, M. *Electrophoresis* **2007**, *28*, 1312.
- (97) Hudson, J. C., Personal Communication, **2010**.
- (98) Tang, Q.; Harrata, A. K.; Lee, C. S. *Analytical Chemistry* **1995**, *67*, 3515.

- (99) Jensen, P. K.; Harrata, A. K.; Lee, C. S. *Analytical Chemistry* **1998**, *70*, 2044.
- (100) Wei, J.; Yang, L. Y.; Harrata, A. K.; Lee, C. S. *Electrophoresis* **1998**, *19*, 2356.
- (101) Yang, L. Y.; Tang, Q.; Harrata, A. K.; Lee, C. S. *Analytical Biochemistry* **1996**, *243*, 140.
- (102) Lyubarskaya, Y. V.; Carr, S. A.; Dunnington, D.; Prichett, W. P.; Fisher, S. M.; Appelbaum, E. R.; Jones, C. S.; Karger, B. L. *Analytical Chemistry* **1998**, *70*, 4761.
- (103) Martinovic, S.; Berger, S. J.; Pasa-Tolic, L.; Smith, R. D. *Analytical Chemistry* **2000**, *72*, 5356.
- (104) Yang, L. Y.; Lee, C. S.; Hofstadler, S. A.; Pasa-Tolic, L.; Smith, R. D. *Analytical Chemistry* **1998**, *70*, 3235.
- (105) Tang, Q.; Harrata, A. K.; Lee, C. S. *Analytical Chemistry* **1997**, *69*, 3177.
- (106) Jensen, P. K.; Pasa-Tolic, L.; Anderson, G. A.; Horner, J. A.; Lipton, M. S.; Bruce, J. E.; Smith, R. D. *Analytical Chemistry* **1999**, *71*, 2076.
- (107) Jensen, P. K.; Pasa-Tolic, L.; Peden, K. K.; Martinovic, S.; Lipton, M. S.; Anderson, G. A.; Tolic, N.; Wong, K. K.; Smith, R. D. *Electrophoresis* **2000**, *21*, 1372.
- (108) Zhang, C. X.; Xiang, F.; Pasa-Tolic, L.; Anderson, G. A.; Veenstra, T. D.; Smith, R. D. *Analytical Chemistry* **2000**, *72*, 1462.
- (109) Simpson, D. C.; Smith, R. D. *Electrophoresis* **2005**, *26*, 1291.
- (110) Yang, L. Y.; Lee, C. S.; Hofstadler, S. A.; Smith, R. D. *Analytical Chemistry* **1998**, *70*, 4945.
- (111) Lamoree, M. H.; Tjaden, U. R.; vanderGreef, J. *Journal of Chromatography A* **1997**, *777*, 31.
- (112) Lamoree, M. H.; van der Hoeven, R. A. M.; Tjaden, U. R.; van der Greef, J. *Journal of Mass Spectrometry* **1998**, *33*, 453.
- (113) Chartogne, A.; Tjaden, U. R.; Van der Greef, J. *Rapid Communications in Mass Spectrometry* **2000**, *14*, 1269.
- (114) Mack, S.; Cruzado-Park, I.; Chapman, J.; Ratnayake, C.; Vigh, G. *Electrophoresis* **2009**, *30*, 4049.
- (115) Busnel, J. M.; Varenne, A.; Descroix, S.; Peltre, G.; Gohon, Y.; Gareil, P. *Electrophoresis* **2005**, *26*, 3369.
- (116) Mokaddem, M.; Gareil, P.; Varenne, A. *Electrophoresis* **2009**, *30*, 4040.
- (117) Lecoeur, M.; Gareil, P.; Varenne, A. *Journal of Chromatography A* **2010**, *1217*, 7293.
- (118) Severs, J. C.; Hofstadler, S. A.; Zhao, Z.; Senh, R. T.; Smith, R. D. *Electrophoresis* **1996**, *17*, 1808.
- (119) Tang, Q.; Harrata, A. K.; Lee, C. S. *Analytical Chemistry* **1996**, *68*, 2482.
- (120) Tang, Q.; Harrata, A. K.; Lee, C. S. *Journal of Mass Spectrometry* **1996**, *31*, 1284.
- (121) Martinovic, S.; Pasa-Tolic, L.; Smith, R. D. *Methods in Molecular Biology* **2004**, *276*, 291.
- (122) Clarke, N. J.; Tomlinson, A. J.; Naylor, S. *Journal of American Society for Mass Spectrometry* **1997**, *8*, 743.
- (123) Clarke, N. J.; Naylor, S. *Biomedical Chromatography* **2002**, *16*, 287.
- (124) Kuroda, Y.; Yukinaga, H.; Kitano, M.; Noguchi, T.; Nemati, M.; Shibukawa, A.; Nakagawa, T.; Matsuzaki, K. *Journal of Pharmaceutical and Biomedical Analysis* **2005**, *37*, 423.
- (125) Hjerten, S.; Liao, J. L.; Yao, K. *Journal of Chromatography* **1987**, *387*, 127.

- (126) Wei, J.; Lee, C. S.; Lazar, I. M.; Lee, M. L. *Journal of Microcolumn Separations* **1999**, *11*, 193.
- (127) Martinovic, S.; Pasa-Tolic, L.; Masselon, C.; Jensen, P. K.; Stone, C. L.; Smith, R. D. *Electrophoresis* **2000**, *21*, 2368.
- (128) Zhong, X. F.; Maxwell, E. J.; Chen, D. D. Y. *Analytical Chemistry* **2011**, *83*, 4916.
- (129) Caslavaska, J.; Molteni, S.; Chmelik, J.; Slais, K.; Matulik, F.; Thormann, W. *Journal of Chromatography A* **1994**, *680*, 549.
- (130) Thormann, W.; Zhang, C. X.; Caslavaska, J.; Gebauer, P.; Mosher, R. A. *Analytical Chemistry* **1998**, *70*, 549.
- (131) Thormann, W.; Caslavaska, J.; Mosher, R. A. *Journal of Chromatography A* **2007**, *1155*, 154.
- (132) Steinmann, L.; Mosher, R. A.; Thormann, W. *Journal of Chromatography A* **1996**, *756*, 219.
- (133) Smith, R. D.; Loo, J. A.; Edmonds, C. G.; Barinaga, C. J.; Udseth, H. R. *Analytical Chemistry* **1990**, *62*, 882.
- (134) Wilm, M.; Mann, M. *Analytical Chemistry* **1996**, *68*, 1.
- (135) Schneider, B. B.; Douglas, D. J.; Chen, D. D. Y. *Journal of the American Society for Mass Spectrometry* **2002**, *13*, 906.
- (136) Schneider, B. S.; Douglas, D. J.; Chan, D. D. Y. *Rapid Communications in Mass Spectrometry* **2001**, *15*, 249.
- (137) Thompson, J. W.; Eschelbach, J. W.; Wilburn, R. T.; Jorgenson, J. W. *Journal of the American Society for Mass Spectrometry* **2005**, *16*, 312.
- (138) Sadiku, M. N. O. *Elements of electromagnetics*; Saunders College Pub.: New York, 1989.
- (139) Eyring, C. F.; Mackeown, S. S.; Millikan, R. A. *Physical Review* **1928**, *31*, 0900.
- (140) Smith, D. P. H. *Ieee Transactions on Industry Applications* **1986**, *22*, 527.
- (141) Jones, A. R.; Thong, K. C. *Journal of Physics D-Applied Physics* **1971**, *4*, 1159.
- (142) Heddle, D. W. O. *Electrostatic lens systems*; 2nd ed.; Institute of Physics Publishing: Bristol; Philadelphia, 2000.
- (143) Gupta, O. P. *Finite and boundary element methods in engineering*; A.A. Balkema: Rotterdam, Netherlands; Brookfield, Vt., 1999.
- (144) Dahl, D. A. *International Journal of Mass Spectrometry* **2000**, *200*, 3.
- (145) Evans, G.; Blackledge, J. M.; Yardley, P. *Numerical methods for partial differential equations*; Springer: London; New York, 2000.
- (146) Timmerman, P.; van der Weele, J. P. *American Journal of Physics* **1999**, *67*, 538.
- (147) Righetti, P. G.; Simo, C.; Sebastiano, R.; Citterio, A. *Electrophoresis* **2007**, *28*, 3799.
- (148) Simo, C.; Citterio, A.; Righetti, P. G. *Electrophoresis* **2007**, *28*, 3156.
- (149) Simo, C.; Citterio, A.; Righetti, P. G. *Electrophoresis* **2007**, *28*, 1488.
- (150) Simo, C.; Mendieta, M. E.; Antonioli, P.; Sebastiano, R.; Citterio, A.; Cifuentes, A.; Righetti, P. G. *Electrophoresis* **2007**, *28*, 715.